NORTHWESTERN UNIVERSITY

Defining and Therapeutically Targeting $IDH1^{WT}$ Oncogenicity in GBM

A DISSERTATION

SUBMITTED TO THE GRADUATE SCHOOL

IN PARTIAL FULLFILLMENT OF THE REQUIREMENTS

for the degree

DOCTOR OF PHILOSOPHY

Field of Life Sciences

By

Kevin M. Murnan

EVANSTON, ILLINOIS

March 2022

ABSTRACT

Defining and Therapeutically Targeting IDH1^{WT} Oncogenicity in GBM

Kevin Murnan

Glioblastoma multiforme (GBM) is the most prevalent primary central nervous system tumor, characterized by resistance to therapeutic intervention, inevitable recurrence, and ultimately patient death. The dismal prognosis is due in part to underlying molecular factors that promote an intratumoral cellular state heterogeneity and protect tumor cells from cell death pathways. Our group recently identified that upregulation of IDH1^{WT} is a unique molecular event in the context of GBM which promotes a stem like cellular state while producing NADPH reducing equivalents necessary for fueling de novo lipid biogenesis. Further, we have shown that genetic and pharmacological reduction of IDH1^{WT} function decreases tumor burden while extending survival in a patient-derived xenograft (PDX) mouse model of GBM. Based on these results, we hypothesized that IDH1^{WT} may regulate mechanisms of intratumoral heterogeneity while suppressing cellular death. By performing *in vitro* experiments coupled with TCGA analysis we have uncovered the role of IDH1^{WT} for maintaining GIC stemness and plasticity by promoting an outer radial glia (oRG)-like cellular state capable of contributing to intratumoral heterogeneity. We have further shown that IDH1^{WT} protects glioma cells from ferroptotic cell death by providing precursors and reducing equivalents necessary for master ferroptotic regulator GPX4 cofactor, GSH, production. In an effort to exploit this unique metabolic vulnerability, we have characterized a first-in-class, brain-penetrant IDH1^{WT} inhibitor, IDH1i-13. Treatment with IDH1i-13 resulted in decreased tumor burden and increased survival in a PDX model of GBM. To determine whether

$IDH1^{WT}$ dysregulation is a generalized mechanism of cancer pathogenesis, we performed TCGA analysis identifying a multitude of cancers codified by aberrant $IDH1^{WT}$ expression and associated impact on patient survival. Collectively, our results further our understanding of $IDH1^{WT}$ in GBM pathogenesis while providing a therapeutically viable modality for patient treatment.

ACKNOWLEDGEMENTS

First, I would like to extend a big, special thanks to my advisor Dr. Alexander Stegh for accepting me as a student within his lab. I cannot state enough how much of a positive impact Alex has had on me as both a scientist and person. Alex is an incredibly kind mentor, enthusiastically encouraging me to explore and expand upon any scientific hypotheses we would devise. Due to his patience, understanding, and support these ideas and methodologies have contributed to the genesis of many novel projects and insights regarding cancer biology that I am incredibly proud of. Without Alex's guidance and wisdom, I honestly do not believe I would have been able to achieve my potential as a scientist. I am forever grateful— also if you are reading this and I hope this is the case, you are a much funnier person than you initially let on and I always looked forward to our lab meetings for both scientific and pop cultural related reasons. I cannot thank you enough.

Secondly, I wish to extend my gratitude and thanks towards all the members of Dr. Stegh's lab. You are a lively group of individuals and have been incredibly encouraging and supportive throughout my PhD in Alex's lab. In particular, I owe a great debt to Dr. Serena Tommasini-Ghelfi. Our projects often entwined, and as such I constantly looked towards you for guidance and support—be it experimental design, big picture ideas, or general discussions. I will greatly miss our coffee walks, where we would discuss everything ranging from science to The Americans. I am incredibly grateful for your support and encouragement over the years. You are the best collaborator I could have ever imagined. Similarly, Lisa Hurley is the best lab manager around. She is the glue that kept the lab running, placing orders, assisting with in vivo work, and a plethora

of other tasks that go unaccounted for. I would also like to extend thanks to my fellow PhD students Corey Dussold and Akanksha Mahajan. You two are incredibly kind, intelligent, and funny people and I cannot imagine my time during grad school without you guys by my side. Dr. Timothy Sita, you have been a constant supply of positive energy, encouragement, and insights. I loved our scientific discussions and your overall excitement regarding everyone's projects. Dr. Foteini Kouri, you are one of the smartest and most ambitious persons I have ever met. You and former graduate student Jasmine May were instrumental in helping me feel welcomed in the lab while providing the critical guidance necessary during early stages of my projects. Lastly, I wish to extend a big thank you to Dr. Andrea Calvert. Though we only overlapped briefly, you were a major reason I joined Dr. Stegh's lab. Your excellent $IDH1^{WT}$ studies were the foundation for all of my work and I am incredibly grateful for everything you have done during your PhD and the assistance you have provided beyond.

My thesis committee has been integral in guiding me forward as a scientist. The head of my committee, Dr. Evangelos Kiskinis was instrumental in helping me see my PhD towards completion. He is an incredibly kind, ambitious, and intelligent committee head. Similarly, Dr. Issam Ben-Sahra and Dr. Craig Horbinski have provided their time and expertise towards shaping my ideas and experiments into the best possible projects that could ever be. Each committee members' feedback has shaped my work into exciting, focused projects and I am incredibly grateful. Though not directly affiliated with my work in Dr. Stegh's lab, I need to give special thanks to Dr. Richard Miller, the former head of my thesis committee and an initial interviewer during my recruitment weekend at Northwestern University. Beyond being a constant supply of

support during my time at Northwestern, Dr. Miller first realized my initial thesis lab was not a good fit and encouraged me to find another. Without his encouragement and support, I would have never been fortuitous enough to find Alex.

Each of the collaborators on this work deserve a special thanks. Our collaborator Dr. Daniel Wahl has been instrumental towards furthering our work regarding the $IDH1^{WT}$ inhibitor while Dr. Gary Schiltz spearheaded compound development. Dr. Chian-Yu Peng performed the critical neurosphere differentiation protocol that helped establish our stemness project. Jeannie Marie Camarillo of the Proteomics Center and Kamil Marek Wojdyla of the Mouse Histology and Phenotyping lab similarly provided valuable assistance.

I would like to extend thanks to the Driskill Graduate Program (DGP), in particular Associate Directors Steve Anderson and Pamela Carpentier. During my recruitment weekend, Steve and I were partners during a game of pool where I immediately sunk an 8-ball, causing Steve to lose his first game of pool to recruits in over 20 years. I am incredibly thankful he did not hold this against me and instead allowed me to join DGP. Over the years I constantly went to Steve for guidance and viewed him as a true friend. You have helped shape the trajectory of my career more than you realize. Pam I have similarly known for many years, having really gotten to know her when I was helping run recruitment weekend events. She has been incredibly supportive and was a main driving force towards helping me see this PhD to completion.

My family and the friends I have made during my PhD have been incredibly supportive of me both at Northwestern and in my personal life. Dan Cook and Tania Valez, I appreciate all of your weird jokes and non-sequiturs coupled with surprising insight over the years. Similarly, Jessie Chen you have been a fantastic friend and incredibly helpful person. I'm sorry we wasted so many Sundays watching Game of Thrones for it to end as badly as it did. To my Dad I appreciate all of the encouragement I have received. You are a greater source of inspiration and support than you realize. To my brothers, thanks, I guess.

Lastly, I do not know where I would be without the love and support of my wife. You have been with me ever since we met many, many years ago during our undergraduate years on a bus to a research conference. Since then, you have been by my side, encouraging me at every stage of my life. I am so incredibly happy that I met you that day. I am who I am because of you. Thank you for everything. And thank you for our beautiful daughter, Safiya. What started as a long journey for the two of us has ended with the three of us. I could not be happier.

DEDICATION

This work is dedicated to the memory of my mother, Donna Murnan. She succumbed to Amyotrophic Lateral Sclerosis (ALS) when I was 17. Despite slowly being taken away by ALS, she always remained optimistic and loving. She is my inspiration and the reason I chose to pursue a PhD in biomedical research.

TABLE OF CONTENTS

LIST OF FIGURES

CHAPTER 1: INTRODUCTION

1.1 GLIOBLASTOMA (GBM)

1.1.1 Overview, Clinical Presentation, and Standard of Care

Glioblastoma (GBM) is a devastating brain tumor characterized by poor prognosis and resistance to therapeutic intervention, ultimately culminating in patient death. Manifesting within the brain, GBMs belong to a heterogeneous group of brain tumors known as gliomas which includes astrocytomas and oligodendrogliomas, their names reflecting presumed glial cells of origin (*1*). Presenting as a highly malignant grade IV astrocytoma (graded I-IV), the median survival time for GBM is a mere 14-16 months post diagnosis (*1, 2*). This dismal prognosis is due in part to GBM presenting with significantly heightened rates of cellular division, vascular proliferation, invasion, tumor necrosis, and resistance to therapies relative to grade II and grade III gliomas (*3*). The most critical factor impacting patient survival, however, is the invariable recurrence of the GBM tumor mass following surgical resection (*4*). Unfortunately, in addition to being the deadliest form of central nervous system tumors GBMs are also the most diagnosed with an incidence rate of 3-5 per 100,000 people (*1, 5*). Despite the median age of patients at diagnosis being 65 years old, World Health Organization (WHO) grade IV IDH-mutant astrocytomas (previously identified as IDH-mutant GBM) do arise during early adulthood in approximately 10% of patients (*5-7*) .

Symptomatic onset is non-specific with broadly similar symptoms shared amongst other forms of brain tumors and more benign neurological conditions. The most common early indication shared among GBM patients is headache resulting from increased intracranial pressure (*8*). Motor, sensory, otoneurological, and neuropsychological symptoms may also arise, with any

combinations of these symptoms increasing the likelihood of a GBM tumor being identified within the clinic (*1*). The variety of symptoms a patient presents with are dependent on tumor size, location, and degree of peritumoral edema (*9*). Unfortunately, as these symptoms often overlap with multiple more benign neurological conditions, detecting GBM during the early stages of progression remains challenging. Diagnosis is confirmed based on the presence of prevailing symptoms coupled with gadolinium-enhanced magnetic resonance imaging (MRI) for confirmation (*10*). Immunohistochemistry of resected tissue, assessing for high mitotic index, nuclear atypia, cellular polymorphism, pseudopalisading necrosis, microvascular hyperplasia, further aids in establishing grade and prognosis (*9, 11*).

Following diagnosis, standard of care regimen entails maximal surgical resection with additional steps such as radiation therapy and alkylating agent temozolomide (TMZ) treatment administered depending on the patient's age and performance status (*10*). Surgical resection aims to improve neurological function, wean patients from supportive corticosteroid treatments (such as dexamethasone), and improve quality of life while prolonging survival (*1*). Patients deemed healthy and capable undergo daily fractionated radiation therapy over 6 weeks with concomitant and adjuvant TMZ treatment for a maximum of 6 months (*12*). Of note, heterogeneity between GBMs, as discussed later, may entail stratification of patients into subgroups for specialized treatment. As an example, the promoter methylation status of O^6-methylguanine-DNA methyltransferase (MGMT) influences MGMT expression. When the promoter is unmethylated, MGMT protein reverses the alkylating properties of TMZ, actively preventing TMZ induced DNA

damage and resultant cell death (*13*). Thus, methylation status of the MGMT promoter region can predict a patient's response to standard of care therapy (*14*).

Maximal surgical resection in conjunction with chemoradiation extends survival to approximately 15-16 months whereas the median survival for adults that do not undergo treatment is approximately 3-4.5 months post diagnosis (*15, 16*). Despite surgical resection, GBM invariably recurs with up to 80% of tumors arising within 2-3 cm of the initial tumor site (*17*). This recurrent GBM is often more aggressive and resistant to therapeutic intervention than the initial tumor burden. Due to the potential for adverse effects which impact quality of life (coupled with the incurable nature of GBM) the decision to undergo treatment is often associated with informed counselling (*18*). As such, identifying novel therapeutic modalities with minimal off-target effects is of critical importance.

1.1.2 Heterogeneity Among and Within GBM

1.1.2.1 IDH-wildtype GBM and grade IV IDH-mutant astrocytomas are distinct disease entities

Historically, there have been two major classifications of GBM—primary and secondary GBM. Due to the increasing importance of the IDH family of enzymes in pathogenesis and progression, WHO has recently re-classified these main forms of GBMs as IDH-wildtype GBM and grade IV IDH-mutant astrocytoma, respectively (*11*). IDH-wildtype, or de novo, GBM account for approximately 90% of all grade IV astrocytoma cases and present as a grade IV glioma without previous indication of a lesser lesion (*19*). Though afflicting an older patient population, these

GBMs are more aggressive than grade IV IDH-mutant astrocytomas, with a median survival time of 4.7 months without intervention. Grade IV IDH-mutant astrocytomas, on the other hand, arise from a lower-grade glioma in younger patients and account for the remaining 10% of cases. These grade IV gliomas are less aggressive with a median survival time of 7.8 months without intervention (*19*).

Due to their clinical and pathological presentations IDH-wildtype GBM and grade IV IDH-mutant astrocytoma tumors represent distinct disease entities (*20, 21*) (Fig. 1). IDH-wildtype tumors tend to present later in life, display widespread anatomical distribution, and exhibit the full spectrum of genetic subtypes—classical, mesenchymal, proneural—discussed in detail later (*22-24*). Grade IV

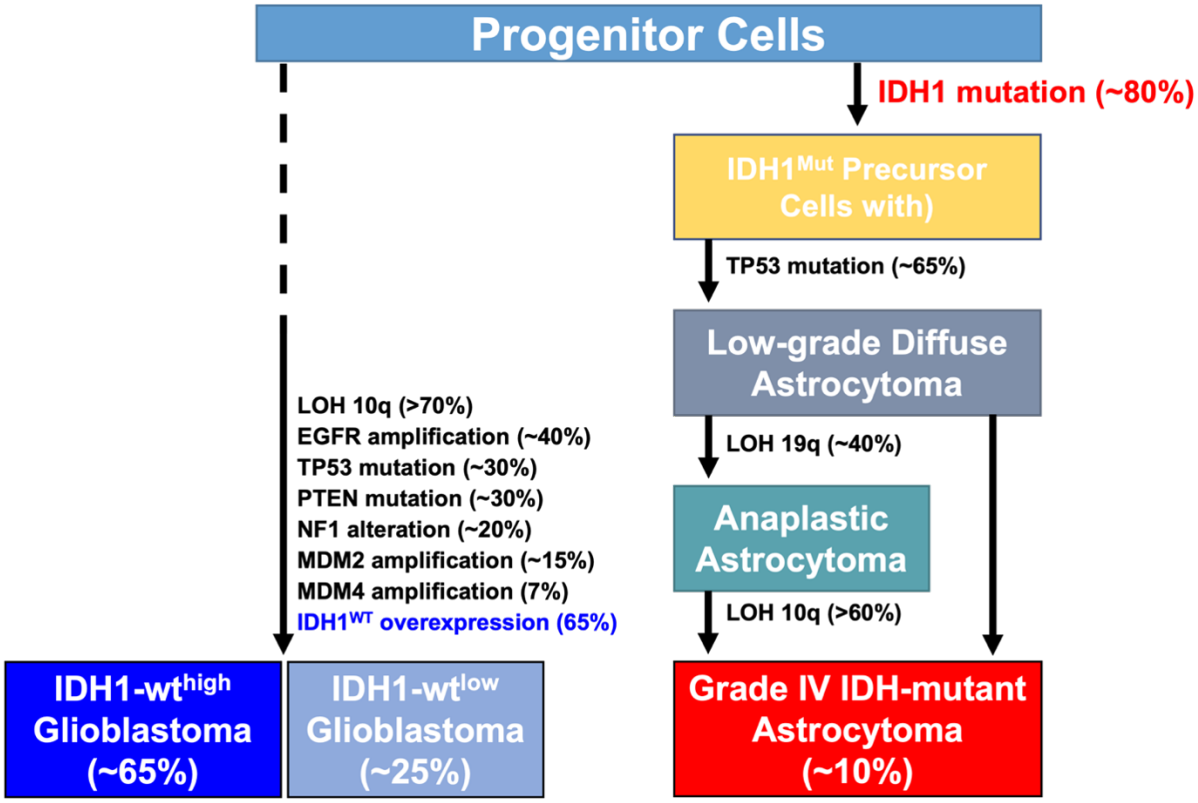

Figure 1. IDH-wildtype GBM and Grade IV IDH-mutant Astrocytoma Development IDH-wildtype GBM and grade IV IDH-mutant astrocytoma are distinct disease entities. IDH-wildtype GBM arise from a neural stem cell (NSC) or multipotent neural progenitor cell (NPC) of origin that progressively accumulates genetic events facilitating presentation as a de novo grade IV astrocytoma. Though a cell of origin for grade IV IDH-mutant astrocytoma is uncertain, IDH mutation is an early initiating event within progenitor cells. Subsequent genetic events progress from low grade glioma to manifestation as grade IV IDH-mutant astrocytoma.

IDH-mutant astrocytomas, on the other hand, arise during early adulthood within frontal lobe structures of the brain (*20*). The spatial, temporal, and genetic differences between these two types

of grade IV astrocytomas may reflect their evolution from distinct progenitor cells of origin. As grade IV IDH-mutant astrocytomas arise during frontal lobe maturation, a period defined by extensive oligodendrocyte development, a lineage restricted oligodendrocyte progenitor cell (OPC) of origin initially appeared likely (*25, 26*). Recent single-cell RNA-seq (scRNA-Seq) studies, however, suggest all IDH-mutant gliomas may arise from neural progenitor cells (NPCs) capable of differentiating into both astrocytes and oligodendrocytes, with progression to grade IV astrocytoma a consequence of distinct genetics (*27*). Variability in anatomical location, histopathological presentation, diverse gene signatures, and molecular resemblance to neural stem cells (NSCs) suggest that IDH-wildtype GBM arise from a NSC or multi-potent NPC cell of origin that, similar to IDH-mutant gliomas, is influenced by underlying genetic factors (*25, 27*). Though precise cells-of-origin are subject to debate, studies found that increasing neural lineage restriction effectively prevents gliomagenesis, thus underscoring stem-like cellular states as most susceptible to tumorigenesis and differentiated cells as least susceptible (*28*).

Further underscoring that despite being histopathologically similar these grade IV astrocytomas are distinct disease entities are the unique molecular dysregulation events. Genetically, the central point of diversion appears to arise from wildtype-IDH1 (IDH^{WT}) and mutant-IDH1 (IDH^{Mut}) functionality. Whereas IDH^{WT} catalyzes the conversion of isocitrate and $NADP^{+}$ into alpha-ketoglutarate (αKG), a neomorphic mutation in IDH^{Mut} results in the conversion of αKG into the oncometabolite 2-hydroxyglutarate (2-HG) at the expense of NADPH (*29*). As a result of aberrant 2-HG production, IDH^{Mut} tumors present with global DNA hypermethylation (*30*). This epigenetic remodeling can in turn enhance expression of oncogenes while limiting expression of tumor

suppressor critical for grade IV IDH-mutant astrocytoma propagation (*31, 32*). In contrast to IDH^{WT} tumors which upregulate IDH1 to enhance NADPH production and facilitate de novo lipid biogenesis, IDH^{Mut} tumors have decreased pools of NADPH (*33, 34*). Beyond IDH mutational status there exists more molecular aberrations that highlight key differences between these two GBMs. For example, EGFR amplification events are prevalent in IDH^{WT} GBM whereas TP53 mutation and 19q loss events occur with heightened frequency in grade IV IDH-mutant astrocytomas (*19*). The role of IDH1 in the context of IDH^{Mut} and IDH^{WT} GBMs is discussed in greater detail later.

1.1.2.2 Subtypes and Cellular States Comprising GBM

In addition to IDH status, GBM tumors can be further classified based on their genetic and associated transcriptional profiles. Presently, there are three molecular subtypes of GBM—classical, mesenchymal, and proneural (*35*). A fourth, neural, subtype was initially identified; however, recent evidence suggests this subtype arose from contamination of the original samples in the study (*23*). Each of these subtypes are enriched for specific genetic events. Classical GBM harbor the most common genetic mutations observed throughout all GBM cases, namely chromosome 10 amplifications and chromosome 7 deletions. These chromosomal events result in significant EGFR amplification and PTEN loss, respectively. This EGFR amplification is coupled with high expression of the neuronal development related Notch and Sonic Hedgehog (SHH) signaling pathways. Intriguingly, the classical subtype may show more pronounced responsiveness to radiation therapy than the other two subtypes (*35*). By comparison, the mesenchymal subtype is associated with high percentage of necrosis and associated inflammation. Frequent

mutation/deletion of NF1 as well as elevated expression of CHI3L1 and MET are associated with the mesenchymal subtype (*35, 36*). Finally, the proneural subtype associates most strongly with a younger patient population than the classical and mesenchymal GBM subtypes. Defining features of proneural GBM include PDGFRA amplification, IDH1 and TP53 mutations, as well as an oligodendrocytic gene signature (*35, 37*). Before reclassification, grade IV IDH-mutant astrocytomas were near universally of the proneural subtype.

While intertumoral heterogeneity between individual patients presents a challenging obstacle for treatment of GBM, intratumoral heterogeneity is more commonly being viewed as the major factor underscoring therapeutic failure. In the context of GBM, a variety of cell types within the same tumor often harbor unique genetic mutations or epigenetic states, influencing a unique cellular phenotype (*38*). For example, despite GBMs being classified into one predominant subtype, multi-regional sampling of GBMs has revealed that each individual tumor is comprised of multiple populations of molecular subtypes within different regions of the tumor (*39*). Moreover, longitudinal studies have shown a propensity for tumor cells to change subtype over time (*23*). Reflecting this, recent studies suggest the classical subtype may itself exist as a blend of mesenchymal and proneural cellular populations (*40*). For these reasons therapeutics targeting one specific GBM subtype are largely ineffective.

Advances in the single cell genomics fields have enhanced our understanding of this intratumoral heterogeneity. In 2019 Neftel et al. performed full length scRNA-Seq on 20 adult and 9 pediatric GBM samples in an effort to identify transcriptional states that drive GBM malignant cell

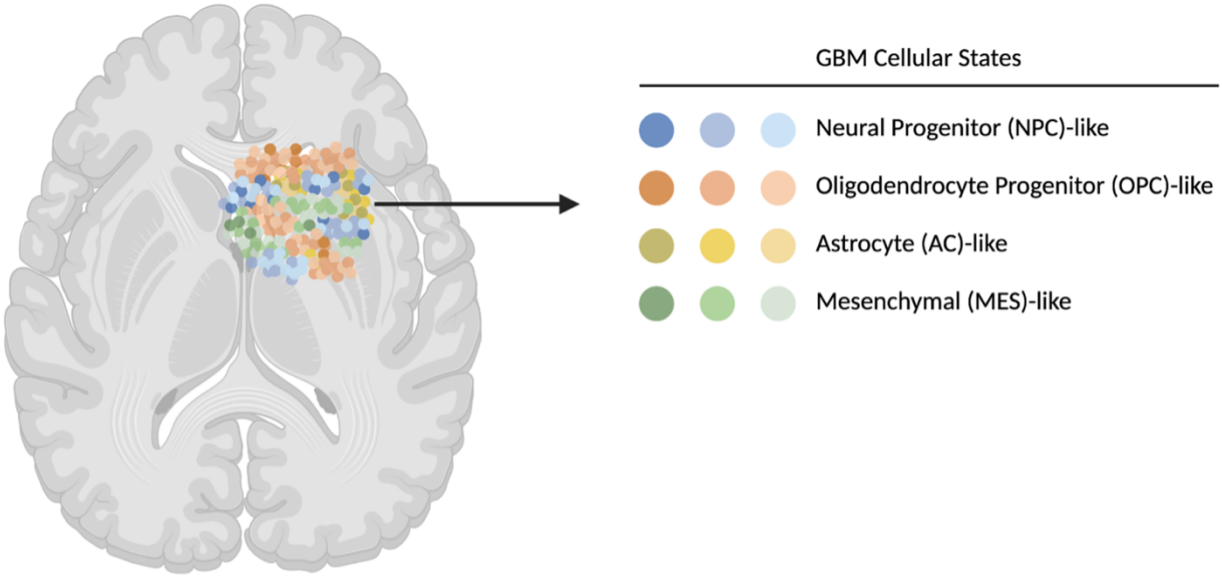

Figure 2. Comprehensive Profiling of Intratumoral Heterogeneity as Revealed by scRNA-Seq
Adapted from *Qazi et al. 2019*. Neftel et al. used scRNA-seq to demonstrate that four cellular states resembling normal neural lineages exist together within a single GBM. Color gradients represent the undifferentiated to differentiated spectrum of cells that can exist within each GBM cellular state.

heterogeneity (*41*). The authors identified that GBM cells exist in four distinct cellular states that reflect distinct gene expression signatures of specific neural cell types (Fig. 2). Further, the distribution of these cell types varied drastically between each sampled tumor. These cell types include NPC-like, OPC-like, astrocyte cell (APC)-like, and mesenchymal cell (MES)-like. Each cell type was associated with an underlying genetic factor—EGFR amplification in APCs, NF1 alterations in MESs, CDK4 amplification in NPCs, and PDGFRA amplifications in OPCs; however, these alterations do not define a state but instead influence it. Most striking, however, is that the authors showed any GBM subpopulation state is capable of giving rise to tumors consisting of all four states, thus highlighting the high plasticity of GBM cells. More recently, single cell proteogenomic and metabolomic investigations have identified four GBM immune subtypes,

characterized by distinct immune cell populations within the tumor (*42*). The identification of these immune subtypes enhances our understanding of GBM heterogeneity in regard to tumor microenvironment interactions.

1.1.3 Reappropriation of the Neurodevelopmental Axis

Establishment of cellular hierarchy in cancer often involves the recapitulation of tissue stem cell and lineage differentiation developmental programs (*27*). The identification of genetic subtypes first hinted at a potential reappropriation of prototypical neurodevelopment pathways in the context of glioblastoma. For example, the proneural subtype of which grade IV IDH-mutant astrocytoma near exclusively exist is characterized by amplification of PDGFRA as previously discussed. PDGFRA is a critical marker that defines the OPC population of cells, responsible for giving rise to the oligodendrocyte populations of the brain, with its ligand Platelet Derived Growth Factor (PDGF) driving OPC proliferation (*43, 44*). The expression of PDGFRA within grade IV IDH-mutant astrocytoma is therefore likely not coincidental, but instead reflects an OPC cell of origin as previously discussed. Contrasting this, classical GBM exhibits heightened upregulation of Nestin (NES), the prototypical marker of neural stem cell (NSC) and neural progenitor cell (NPC) populations. Classical GBM further exhibits activation of the SHH pathway which, in the context of neural development, is responsible for patterning the brain and spinal cord (*45*) while regulating adult NPC populations postnatally (*46*). Similarly activated Notch signaling is essential for the maintenance of NSC populations in the developing and adult brain (*47*). Since the seminal work identifying the molecular subtypes of GBM, our understanding of how GBM repurposes neurodevelopmental pathways for pathogenesis continues to grow stronger.

1.1.3.1 Glioma Initiating Cells (GICs)

A small population of cells, known as glioma initiating cells (GIC)s, that have acquired the stem-like properties of multi-lineage differentiation and self-renewal capabilities drive intratumoral heterogeneity and tumor recurrence following resection in GBM. A population of GICs were first isolated within tumor derived cell fraction via expression of the NSC surface marker CD133 (*48*). GICs are functionally defined by whether orthotopic transplantation into mice generates a tumor that recapitulates hallmarks of the human disease (*49*). In culture, the CD133+ cells could give rise to tumors that recapitulated hallmarks of GBM including cellular subpopulations within the brain underscoring intratumoral heterogeneity (*50*). In addition to seeding the various neural populations present within GBM tumor mass, in vitro culture of GICs in endothelial conditions resulted in transdifferentiation into a cellular population consistent with endothelial cell hallmarks while orthotopic *in vivo* implantation resulted in derivative endothelial cells contributing to vascularization as evidenced by endothelial cell CD133+ expression and chromosomal aberrations (*51*).

Since the initial identification and characterization of GICs, researchers have gained a greater understanding of their functional properties. GICs are profoundly resistance to both chemotherapy and radiation therapy (RT), thus codifying their role in GBM recurrence following resection and therapeutic intervention (*52, 53*). The stemness capabilities of GICs effectively propagate tumor burden. Differentiation along the astroglial axis induced by Bone Morphogenetic Proteins (BMPs) results in GIC astroglial and neuronal differentiation, decrease in proliferation, and suppression of

tumor growth, elegantly showing differentiation reduces GIC tumor propagating potential (*54*). Reprogramming of GICs into induced pluripotent cells alters their tumorigenic potential upon direction to specific cellular lineages, suggesting developmental programs overlaying genetic alterations determine key properties of GICs in gliomas (*55*). Further underscoring the importance of neurodevelopmental reprogramming in GICs, by expressing a core set of neurodevelopmental transcription factors (SOX2, OLIG2, POU3F2, and SALL2), differentiated GBM cells can be fully reprogrammed into GICs (*56*).

Advances in the field of scRNA-seq have furthered our understanding of how GICs contribute to the cellular architecture of GBMs. Initially, GICs were identified within IDH-wildtype GBM via expression of surface markers such as CD133, CD44, CD49f, L1CAM, PDGFRA, EGFR, SSEA1, and A2B5 (*27*). While markers can enrich for GIC populations, it was unclear whether certain markers isolate unique or similar cellular populations. As previously indicated, an emerging model supports GBM malignant cells existing in four cellular states (NPC-like, OPC-like, AC-like, MES-like) (*41*). While proliferation signatures are present in each of the 4 cellular states in IDH^{WT} GBM, only the MES-like, NPC-like, and OPC-like cellular states were capable of propagating tumors *in vivo* (*41, 57*). Cross-referencing published scRNA-seq with expression profiles of aforementioned GIC surface markers, GIC transcription factors, and neural lineage markers revealed that different GIC markers isolate distinct cellular states (*27*). Further, the cell type composition of GBMs reflects GIC cellular states contained within the tumor (*58*).

Recently, a subpopulation of GICs prevalent among the GIC cellular states was identified that recapitulates the hallmarks of outer radial glia (oRG) cells thought absent during adulthood (*58*). During cortical development, radial glia undergo symmetric and asymmetric division, functioning as progenitor cells responsible for giving rise to the majority of neurons and glia that populate the brain (*59*) (Fig 3). In the context of GBM, tumor cell genetic lineages for 11 patient-derived GBM samples were established, identifying presence and absence of copy-number variations originating from an oRG-like cell across all malignant cell types, indicating a precursor oRG-like GIC

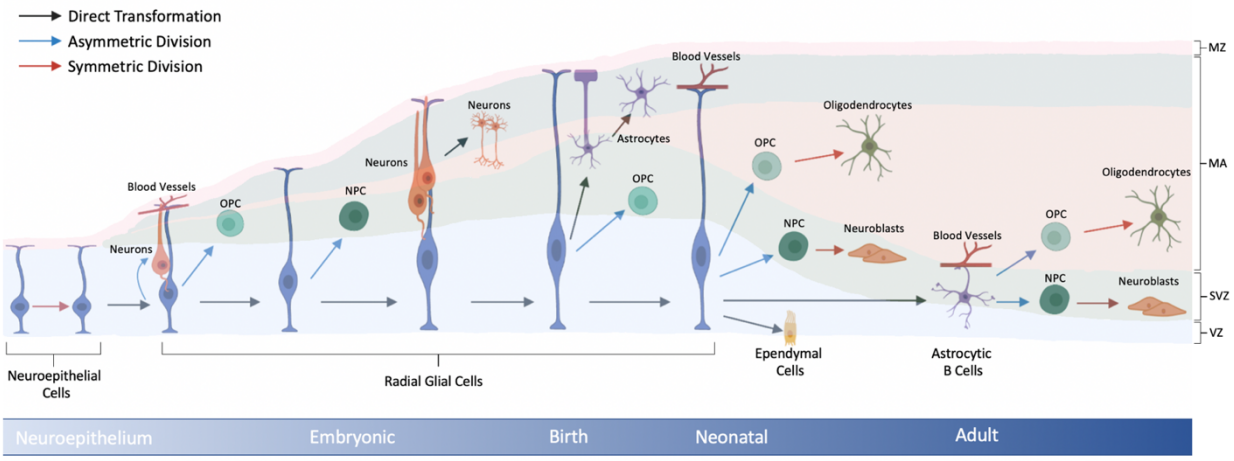

Figure 3. Neural Lineage
Adapted from *Kriegstein et al. 2009*. Glial nature of cells within the brain throughout development and into adulthood. During development as the brain thickens, neuroepithelial cells elongate and become radial glial (RG) cells. These RG cells can divide asymmetrically, giving rise to neurons or neural precursor cells (NPCs) that can further give rise to neurons. RG cells can also divide asymmetrically giving rise to oligodendrocyte progenitor cells (OPCs) that in turn give rise to oligodendrocytes. As RG daughter cells move into mantle for differentiation, with neurons migrating along RG processes, the brain thickens which further elongates RG cells. With an apical/basal polarity, RG cells apically project a single primary cilium into the ventricle; basally, RG contact basal lamina, meninges, and blood vessels. As embryonic development ends, the majority of RG apically detach, converting into astrocytes while remaining RG produce OPCs. A subset of RG remains apically attached, functioning as NSCs in the neonate. Neonatal RG continue producing OPCs and NSCs which in turn generate neurons and oligodendrocytes. Some RG convert into ependymal cells whereas others convert into Type B SVZ astrocytes of the SVZ that function as NSCs within the adult. Apical contact at the ventricle and basal endings in blood cells allows Type B SVZ astrocytes to maintain an epithelial organization while continuing to generate neurons and oligodendrocytes through NSC and OPC intermediaries. Arrow colors represent direct, symmetric, or asymmetric transformation; RG, radial glia; NPC, neural precursor cell; OPC, oligodendrocyte progenitor cell; MA, mantle; MZ, marginal zone; NE neuroepithelium; SVZ, subventricular zone; VZ, ventricular zone.

population is capable of giving rise to each malignant cell type within the tumor (*58*). This oRG-like population's identity was controlled by the expression of canonical oRG cell-surface marker PTPRZ1 (*60*), with knockdown resulting in downregulation of other radial glia markers. In line with a putative role as GICs, orthotopic transplantation of PTPRZ1+ cells resulted in tumors

consisting of neurons and glia (*58*). Further, as a function of mitotic somal translocation, the oRG-like GIC population effectively invaded neighboring brain region. As mitotic somal translocation is not known to occur outside of development, the presence of oRG-like GICs highlights the reactivation of neurodevelopmental pathways normally inactive in adulthood during GBM tumorigenesis.

1.1.3.2 Invasion, Migration, and Infiltration

One of the predominant clinical hallmarks of GBM tumor is extensive infiltration into adjacent brain parenchyma (*61*). These invasive properties of GBM were first described in a 1938 publication by Hans Scherer (*62*). Scherer described in detail gliomas migrating along defined brain structures, infiltrating neighboring tissue. He further noted that glioma cells tend to change morphologically, adapting their physical shape to assume that of the particular brain region they infiltrate. Since his seminal work, investigators have demonstrated that GBM tend to migrate away from tumor bulk hypoxic niches, traveling along white matter tracts and basement membranes of blood vessels into the brain parenchyma (*63, 64*). Contrary to other high-grade cancers which intravasate into blood and lymphatic vessels, GBM cells instead travel along such scaffolding in a manner reminiscent of radial glia asymmetric self-renewal and migration during cortical development (*65, 66*). Indeed, several genes typical for neurodevelopment are repurposed for invasion. Myosin II, for example, plays a critical role during somal translocation within radial glia during brain development by relocating microtubules towards the leading edge of protrusions (*67*). During GBM invasion myosin II is similarly upregulated, facilitating leading edge migration and invasion into neighboring brain regions (*68*). Most striking, however, is the recent identification

of an oRG-like population of cells that persists in adult GBM patients (*58*). This radial glia-like population extends protrusions into neighboring brain regions, facilitating self-renewal of a new population of radial glia-like cells capable of giving rise to tumor bulk. As previously discussed, Bhaduri et al. further showed that this radial glia-like subpopulation of glioma cells is defined and maintained by PTPRZ1 expression. Both the PTPRZ1 receptor and its ligand PTN are necessary for invasion (*69, 70*).

1.2 ISOCITRATE DEHYDROGENASE 1 (IDH1)

1.2.1 Overview of Isocitrate Dehydrogenase Family of Enzymes

Oftentimes altered metabolic states disrupt normal organ physiology and contribute to or cause a wide range of human diseases including cancer and neurodegeneration (*71, 72*). To support unabated tumor growth and progression, for example, cancer cells undergo metabolic rewiring including heightened glutamine catabolism, elevated glucose oxidation through the tricarboxylic acid cycle, and enhanced synthesis of fatty acids (*73, 74*). In fact, more than 90 years ago Otto Warburg observed that even in the presence of abundant oxygen cancer cells rely on enhanced glucose conversion to pyruvate (aerobic) or lactic acid (anaerobic) in order to fuel macromolecular synthesis while generating energy in the form of adenosine 5'-triphosphate (ATP) (*75*). More recently, the identification of neomorphic mutations in $IDH1^{WT}$ and IDH2 nearly a decade ago has helped further fuel the field of cancer metabolism research (*6, 76*). Coupled with their central role in energy metabolism, redox balance, and anaplerosis, metabolism research has begun more comprehensively investigating the IDH family of enzymes in the context of disease pathogenesis and progression.

Eukaryotic cells express three paralogs of IDHs, each differing in structural organization, subcellular localization, allosteric regulation, and catalytic mechanisms (*74*). Ultimately each enzyme catalyzes the oxidative decarboxylation of isocitrate (ICT) into α-ketoglutarate (αKG). Though each paralog's role in cellular metabolism often overlaps, their individual functions are non-redundant. Subcellular localization and the cofactor for catalysis are primary influencers of

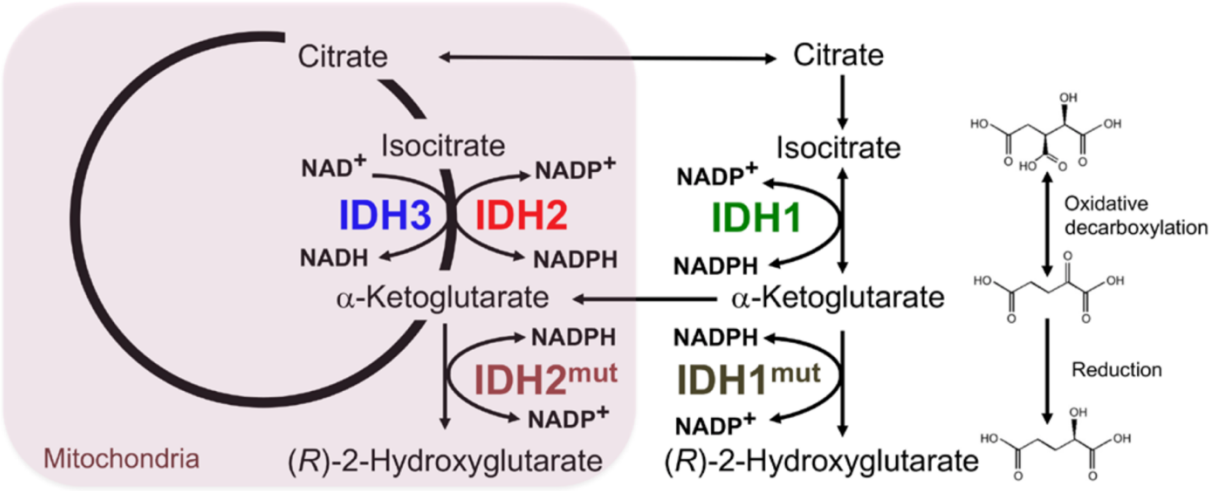

Figure 4. Subcellular localizations and chemical reactions by wild-type IDH and tumor-derived IDH mutant enzymes
Tommasini-Ghelfi, Murnan* et al. 2019.*

metabolic responsibilities for these proteins (Fig 4). While IDH2 and IDH3 are found within the mitochondrial matrix, $IDH1^{WT}$ localizes to the cytosol and peroxisomes. Despite differing localizations, $IDH1^{WT}$ and IDH2 are both homodimers, utilizing nicotinamide adenine dinucleotide phosphate ($NADP^+$) as an electron acceptor (*77, 78*). IDH3, on the other hand, functions as a heterotetramer, catalyzing a rate limiting, irreversible step of the TCA cycle via its substrate nicotinamide dinucleotide (NAD^+) (*79*). Further exemplifying the non-redundancy of these paralogs is their often disparate expression within organs. IDH2, for example, is most highly expressed within the heart, muscle, and activated lymphocytes; $IDH1^{WT}$, on the other hand, shows most prominent expression within the liver while presenting moderate to absent in other tissues (*80*). Aberrant tissue expression of IDH proteins during disease pathogenesis and progression, however, is more widespread (*74*) (Fig 5).

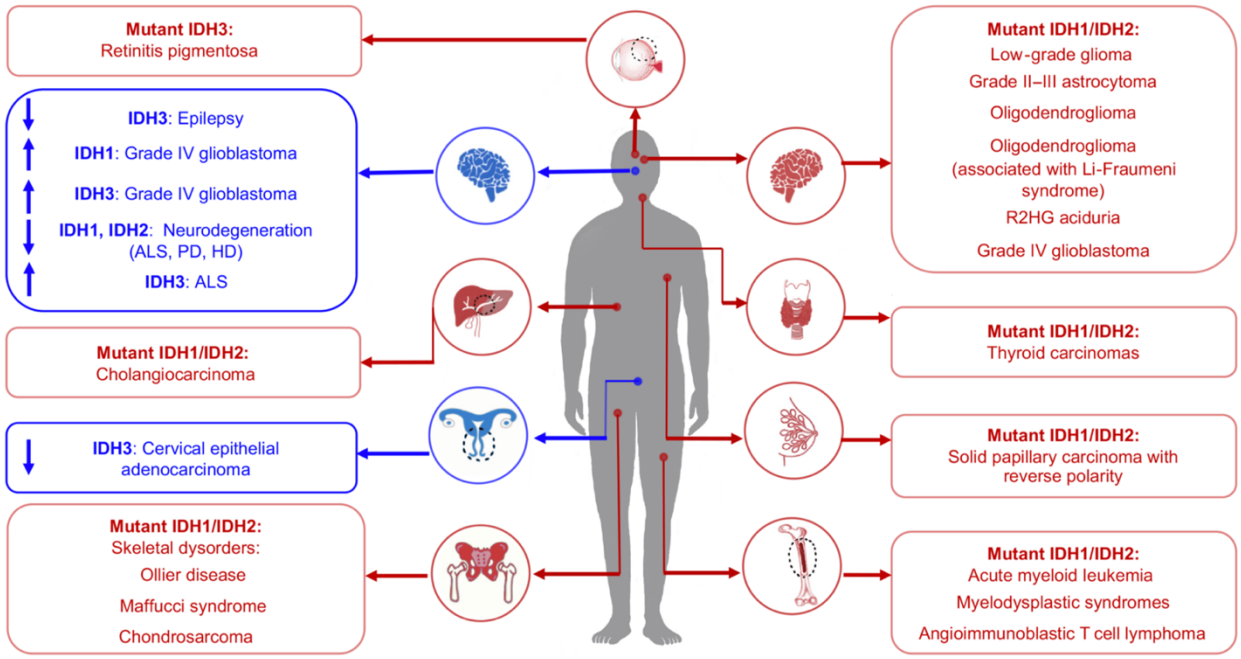

Figure 5. Deregulation of IDH enzymatic activity is associated with human disease. *Tommasini-Ghelfi*, Murnan* et al. 2019*. Upward or downward pointing arrows indicate overexpression or downregulation of wild-type IDHs (shown in blue), respectively.

1.2.2 The Roles of IDH1^{WT} Derived Cytosolic αKG

Through production of αKG, the IDH family of enzymes are capable of exerting influence over a wide variety of cellular processes and pathways. As a key intermediate of the citric acid cycle, oxidative decarboxylation of mitochondrial αKG by αKG dehydrogenase results in the generation of succinyl-CoA and electron donating NADH (*81*). Cytosolic αKG, on the other hand, does not directly participate in the TCA cycle. Under conditions of hypoxia tumor cells can undergo reversion of TCA cycle flux whereby reductive carboxylation of cytosolic αKG to citrate is imported into the mitochondria and serves as a precursor for acetyl-CoA production and lipogenesis (*82*). While this TCA cycle reversion is of importance and worth noting, the primary mechanisms underlying cytosolic αKG's pleiotropic contributions towards cancer progression are

more widespread and common. First, αKG's conversion to glutamate impacts multiple biochemical processes critical for cancer pathogenesis and progression. Perhaps most striking, however, is that by promoting αKG dioxygenase activity αKG exerts epigenetic control over gene expression.

1.2.2.1 Cytosolic αKG Regulation of αKG-Dependent Oxygenases

$IDH1^{WT}$, via its production of αKG, regulates the enzymatic activity of αKG-dependent oxygenases to influence gene expression and function. Molecularly, αKG-dependent oxygenases catalyze a diverse range of biochemical processes and reactions including DNA, RNA, protein, and lipid chemical modifications (*74*). These modifications in turn facilitate a diverse range of cellular processes including maintenance of pluripotency, hypoxic response, angiogenesis, inflammation, among many others (*83-86*). Due to their myriad roles in facilitating cellular homeostasis, disruption in function of αKG-dependent oxygenases often underscore a wide variety of diseases, including grade IV IDH-mutant astrocytoma (*87*). As $IDH1^{WT}$ supplies the necessary cofactor for their function, it appears likely that misregulation of $IDH1^{WT}$ expression may contribute to the pathogenic properties of αKG-dependent oxygenases.

Histone methylation at Lys and Arg residues result in DNA supercoiling, modulating gene expression by diminishing accessibility of transcription factors and enhancers to specific chromatin regions (*88*). Jumonji C (JmjC) catalytic domain containing αKG-dependent oxygenases actively demethylate these histone marks, enhancing chromatin accessibility (*89, 90*). These enzymes have proven critical in the regulation of pluripotency. Jarid2, a Jumonji C domain

protein for example, controls activity of PRC2 which in turn is a key regulator of development genes in embryonic stem cells (*91*). In line with this observation, naïve embryonic stem cells exhibit high levels of intracellular αKG that in turn function to catalyze JmJC dependent histone demethylation (*92*). Dysregulation of JmJC domain containing oxygenase activity has been implicated in a wide variety of cancers ranging from GBM to leukemia, often as a result of IDH mutation (*93, 94*).

DNA methylation is an epigenetic mechanism whereby transfer of a methyl group to the C5 position of cytosine, forming 5-methylcytosine, facilitates the recruitment of proteins that actively inhibit the binding of transcription factors (*95*). Thus, DNA methylation is an efficient and reversible method of regulating transcriptional expression. This epigenetic remodeling is often facilitated by αKG-dependent oxygenases belonging to the Ten-eleven translocation methylcytosine dioxygenase (TET) family of DNA demethylases. One critical cellular process that TET enzymes regulate is the maintenance of pluripotency, with differential tissue and temporal expression influencing non-redundant developmental lineages (*96, 97*). TET1 expression is restricted to non-differentiated cell lines and is involved in maintenance of stemness whereas TET2 is heavily involved in differentiation of embryonic stem cells towards a hematopoietic lineage (*98, 99*). An intracellular pool of αKG is critical for maintaining functional TET activity, as direct manipulation of αKG level results in disrupted TET activity and associated downstream processes (*92, 100, 101*). As with the JmJC domain containing oxygenases, TET family disruption as a result of IDH mutation has been implicated in a variety of cancers including but not limited to GBM, leukemia, and Ollier disease (*93, 102-104*).

1.2.2.2 Cytosolic αKG Production of Glutamate

Recently, the role of glutamate in tumor cell pathogenesis and progression has become a field of heightened interest. Through enzymatic transamination cytosolic αKG may fuel glutamate production within cancer cells. This reversible transamination event can be catalyzed by branched-chain amino acid transaminase 1 (BCAT1) and BCAT2 at the expense of branched-chain α-ketoacids leucine, isoleucine, or valine (*105*). Derivative glutamate itself can in turn fuel nucleotide and fatty acid biosynthesis, control production of alanine, aspartate, and serine, or be imported into the mitochondria to support TCA cycle progression (*106*). Glutamate further plays a key role in neutralizing ROS by supporting synthesis of the potent antioxidant reduced glutathione (GSH). Glutamate contributes to GSH generation via two distinct mechanisms which ultimately are part of the same pathway. First, glutamate and cysteine can be converted into gamma-glutamyl cysteine, the immediate precursor to GSH, via glutamate cysteine ligase (GCL) (*107*). Second, intracellular glutamate can be exported from the cell by antiporter system x_c- at a 1:1 ratio coupled with cystine import (*108*). Cystine in turn is oxidized into cysteine in an NADPH dependent manner, thus fueling GSH synthesis, oxidative stress response, and ferroptosis defense (*109*).

Synaptic glutamatergic signaling in GBM has recently been identified as a critical mechanism for GBM pathogenesis and progression. One of the first studies hinting at the possibility of functional synapses between neurons and tumor revealed GBM tumors release glutamate to facilitate growth whereas inhibition of glutamatergic NMDA receptor signaling attenuates this growth advantage *in*

situ (*110*). A subsequent study identified that GBM also express Ca^{2+} permeable, AMPA receptors (*111*). The authors found that dysregulation of these glutamatergic receptors inhibited tumor cell locomotion while inducing apoptosis (*111*). Recently, investigators identified fully functional glutamatergic synapses between neighboring neurons and GBM tumor cells, thus showing GBMs fully integrate within the neuronal network of the brain (*112, 113*). These neurogliomal synapses exclusively consist of a presynaptic neuron and Ca^{2+}-permeable, AMPA receptor expressing post-synaptic glioma cells. Neuronal excitation results in membrane depolarization and induced post-synaptic currents within recipient GBM tumor cells, in turn evoking secondary messenger Ca^{2+} mediated cellular growth and invasion (*112, 113*). Strikingly, GBM tumor cell release of glutamate into the extracellular environment via aforementioned system x_c- stimulates neuronal excitability, thus facilitating a positive reinforcement feedback loop (*112, 114*). Highlighting the potential importance of $IDH1^{WT}$ in facilitating this glutamatergic synaptic signaling, suppression of the aforementioned amino-acid transaminase BCAT1 effectively blocks glioma cell excretion of glutamate (*115*).

1.2.3 The Effects of $IDH1^{WT}$ Cytosolic NADPH Production

In addition to generating a pool of cytosolic αKG, $IDH1^{WT}$ produces cytosolic NADPH which functions as a reducing equivalent for lipid biogenesis (*74*). During de-novo fatty acid synthesis, the carbon from 8 acetyl-CoA are converted into palmitic acid in a series of reactions which utilize 14 molecules of NADPH (*116*). The saturated fatty acid palmitic acid can in turn be converted into monounsaturated fatty acids (MUFAs) via Stearoyl-CoA desaturase (*117*). Resultant MUFAs can in turn be further processed into polyunsaturated fatty acids (PUFAs) and the phospholipid

phosphatidic acid (*118*). Conversely, elongation of palmitic acid by fatty acid elongases, such as ELOVL6, results in the synthesis of saturated fatty acid stearate, seeding for the production of more complex lipids (*118, 119*). Regardless of the end product, the catalytic progenitor steps in de novo fatty acid synthesis require a vast reservoir of rate-limiting cytosolic NADPH.

Building upon these observations, a direct role for $IDH1^{WT}$ in lipogenesis was uncovered by a series of experiments manipulating $IDH1^{WT}$ expression within murine models. Over-expression of $IDH1^{WT}$ specifically within the liver and adipose tissues of mice resulted in generation of extensive fat pads. These fat pads were characterized by accumulation of lipid droplets, adipocyte hypertrophy, and reduced levels of carbon precursor metabolites required for de novo fatty acid synthesis—acetyl-CoA and malonyl-CoA (*120*). Further supporting a key role for $IDH1^{WT}$ in lipogenesis, ectopic expression of mir-181a directly binds to and downregulates $IDH1^{WT}$ transcript level. Accordingly, there is a substantial decrease in the expression of genes critical for lipid biosynthesis, presumably as a result of reduced αKG dependent dioxygenase activity (*121*). In regard to cancer, our group identified that GBM cells increase $IDH1^{WT}$ to generate a cytosolic pool of NADPH which facilitates growth and proliferation via lipid biogenesis. Depletion of $IDH1^{WT}$ in GBM tumor cells limits this cytosolic pool of NADPH. As a result, acetyl-CoA which can no longer be reduced to palmitic acid accumulates within the cytosol (*33*).

In addition to supporting de novo lipid biogenesis, cytosolic NADPH is a potent antioxidant playing a pivotal role in combatting oxidative stress and radiation damage. While mice homozygously null for $IDH1^{WT}$ undergo normal pre- and postnatal development, upon exposure

to an external stressor induces robust phenotypic response. In contrast to wild-type littermates, $IDH1^{WT}$-deficient mice treated with the endotoxin lipopolysaccharide (LPS) showed enhanced susceptibility to death due to elevated levels of hepatic oxidative stress, pronounced DNA damage leading to apoptosis, and elevated expression of proinflammatory cytokines. These findings correlated with an increase in $NADP^+$/NADPH ratio in comparison to WT mice, suggesting $IDH1^{WT}$'s ability to supply cytosolic NADPH underscored the observed phenotype (*122*). Supporting these findings, $IDH1^{WT}$ depletion in vitro across multiple cell lines revealed that due to a reduced ability to neutralize ROS, cells exhibited heightened sensitivity to UV-radiation and H_2O_2 (*123*). Our group built upon these findings, identifying that IDH-wildtype GBM upregulate $IDH1^{WT}$ to increase and intracellular pool of NADPH, correlating with elevated levels of the critical antioxidant GSH (*33*). Conversely, grade IV IDH-mutant astrocytoma, in which $IDH1^{Mut}$ instead utilizes NADPH in the production of 2-HG, have reduced intracellular NADPH and GSH levels resulting in elevated ROS generation (*34*).

1.2.4 IDH1 In Cancer

A broad spectrum of cancers are characterized by aberrant expression of each of the IDH family members (Fig. 5). Pathogenic over-expression of $IDH1^{WT}$ was initially identified by our group and our collaborator's group in the context of adult and pediatric GBM (*33, 124*). More recently, deleterious over-expression of $IDH1^{WT}$ and $IDH2^{WT}$ has also been reported in the context of prostate cancer (PC) and lung cancer, respectively (*125, 126*). In contrast to the emerging role of IDH^{WT} in cancer progression, IDH mutational events have been extensively documented. While driver or early initiating event mutations within IDH1 and IDH2 are best studied in the context of

brain tumors, such mutations also occur with high prevalence in acute myeloid leukemia (AML), and less frequently within myelodysplastic syndromes (MDSs) and myeloproliferative neoplasms (MPN) (*74, 76*). IDH mutations define a variety of chondrosarcomas including intracranial chondrosarcoma, central chondrosarcoma, and central and periosteal chondromas (*76*). Similarly, IDH mutations further cause Ollier disease and Marfucci syndrome, both of which are characterized by cartilaginous tumors (*104*). IDH mutations have also been identified in angioimmunoblastic T-cell lymphoma, thyroid carcinoma, cholangiocarcinoma and as a hallmark of the unique breast cancer subtype, papillary carcinoma with reverse polarity (*74*). It is worth noting that in nearly every instance, IDH mutations in cancer are heterozygous with retention of a wild-type allele (*76*).

1.2.4.1 Grade IV IDH-mutant Astrocytoma

A single, monoallelic missense mutation at Arg^{132} of IDH1 is the early initiating event that defines approximately 82% of grade IV IDH-mutant astrocytomas, driving evolution of low-grade glioma to grade IV astrocytoma (*6, 127*). This mutation is a gain-of-function, neomorphic mutation, impacting the binding affinity and conformation of the enzyme's active site. As a result, $IDH1^{Mut}$'s affinity for isocitrate is greatly diminished whereas the affinity for NADPH is enhanced. Consequently, the forward reaction is hindered whereas a partial reverse reaction catalyzing the reduction of αKG to (R)-2HG at the expense of NADPH is observed (*29*). Analogous Arg^{172} missense mutation in IDH2 similarly produces (R)-2HG while also defining a subset of grade IV IDH-mutant astrocytomas, albeit production of (R)-2HG is heightened relative to $IDH1^{Mut}$. This elevated production of (R)-2HG by mitochondrial $IDH2^{Mut}$ reflects the necessity for a large αKG

and NADPH reservoir to facilitate the partial reverse reaction, as mitochondrial anaplerosis can readily replenish the substrate and electron donor, respectively (*74*). Targeting $IDH1^{Mut}$ to the mitochondria results in enhanced (R)-2HG production, thus suggesting that $IDH1^{Mut}$ and $IDH2^{Mut}$ have similar intrinsic enzymatic activity and that αKG and NADPH availability greatly influences (R)-2HG production. As $IDH1^{Mut}$ and $IDH1^{WT}$ are localized to the cytosol and peroxisomes, production of (R)-2HG by $IDH1^{Mut}$ enzyme is dependent on the retained wild-type IDH1 allele for the generation of cytosolic NADPH and αKG (*128*). Though grade IV IDH-mutant astrocytoma is codified by the presence of a single mutant allele, loss of wild-type allele has not been observed thus highlighting the possibility of $IDH1^{WT}$ contributing to disease pathogenesis and progression in the context of grade IV IDH-mutant astrocytoma.

Despite being an early initiating event, neomorphic $IDH1^{WT}$ mutation alone appears insufficient for transforming neural cells and promoting gliomagenesis. Expression of $IDH1^{R132}$ promotes proliferation, colony formation, and differentiation inhibition *in vitro*, however, recapitulation of tumorigenesis *in vivo* is more nuanced (*93*). Conditional, heterozygous Cre-mediated knock-in of $IDH1^{R132}$ within NPC or hematopoietic populations fails to recapitulate a glioma phenotype. Embryonic expression within brain progenitors via nestin-Cre resulted in cerebral hemorrhages and perinatal lethality due to high accumulation of (R)-2HG impairing collagen maturation, disrupting brain matter structures and initiating an endoplasmic reticulum stress response (*129*). Conversely, inducible nestin-Cre driven $IDH1^{R132}$ expression within the subventricular zone of adult mice recapitulated early gliomagenesis events such as NSC proliferation, self-renewal, and infiltration; however, the mice failed to develop tumors, instead developing hydrocephalous and

grossly dilated lateral ventricles (*130*). Underscoring the necessity for additional driver events, heterozygous expression of $IDH1^{R132}$ within murine NSCs modified for P53 and ATRX loss (events typical of grade IV IDH-mutant astrocytoma) resulted in low grade astrocytoma (*131*). Expanding upon these findings, viral introduction of $IDH1^{R132}$ in conjunction with PDGFA to a mouse model lacking Cdkn2a, Atrx, and Pten recapitulates a proneural, GBM-like phenotype (*132*).

In grade IV IDH-mutant astrocytoma, (R)-2HG functions as an oncometabolite, eliciting widespread dysregulation that in turn contributes to glioma progression. Supporting a central role of (R)-2HG for disease pathogenesis, cells treated with cell-permeable (R)-2HG mimic the effect of $IDH1^{R132}$ mutation (*93*). More specifically, (R)-2HG treatment elicits a DNA hypermethylation phenotype, a hallmark of grade IV IDH-mutant astrocytoma. While intracellular concentrations of (R)-2HG are maintained via 2HG Dehydrogenase (2HGDH) mediated oxidation of (R)-2HG back into αKG, in the context of grade IV IDH-mutant astrocytoma, production of (R)-2HG appears to exceed the capacity for 2HGDH mediated conversion to αKG (*74*). As a result, astrocytoma tumors have elevated levels of (R)-2HG with intracellular concentrations ranging from 1 mM to 30 mM within the tumor while simultaneously diffusing from the center mass, exposing the tumor microenvironment to low millimolar concentrations of (R)-2HG (*133*).

Competitive inhibition of αKG-dependent enzymes is a core tenet of (R)-2HG's oncogenic capabilities in grade IV IDH-mutant astrocytomas. By competing with αKG, (R)-2HG exerts epigenetic control via modulating the activity of αKG-dependent dioxygenases. Accumulation of

epigenetic disruption results in extensive and irreversible damage to the DNA and histone methylation landscapes (*74, 134*). Targets of interference include the aforementioned JmjC family of histone lysine demethylases and the TET family of DNA demethylators among others previously discussed (*135*). As a functional result of aberrant DNA methylation induced by (R)-2HG, DNA hypermethylation compromises the binding of CCCTC-binding factor (CTCF) with its binding sites, resulting in loss of insulation between topological domains (*136*). This in turn leads to aberrant gene activation and in the context of grade IV IDH-mutant astrocytoma, constitutive activation of PDGFRA, the prototypical oncogene for the proneural GBM subtype of which grade IV IDH-mutant astrocytomas near exclusively existed before reclassification (*35, 136*). Beyond its role in modulating the epigenome, by inhibiting the ALKBH DNA repair enzyme (R)-2HG facilitates the accumulation of DNA damage. While this disruption in DNA repair kinetics can lead to further genomic instability, it also renders grade IV IDH-mutant astrocytomas uniquely sensitive to alkylating agents (*137*). Highlighting another point of susceptibility to therapeutic intervention, (R)-2HG interferes with the activity of aforementioned BCAT1 and BCAT2, abrogating glutamate production via these transaminases. As a result, grade IV IDH-mutant astrocytomas have an increased dependence on Glutaminase (GLS) for the synthesis of glutamate and GSH and are thus susceptible to pharmacological inhibition of GLS (*138*).

1.2.4.2 IDH-wildtype GBM

The functional contributions of $IDH1^{WT}$ to GBM progression is an emerging field of study in comparison to the oncogenic contributions of $IDH1^{Mut}$. The identification of exclusive BCAT1 expression within IDH-wildtype tumors and promoter methylation patterns correlating with this

expression first hinted at the role of $IDH1^{WT}$ in GBM pathogenesis (*115*). The authors identified that BCAT1 expression is contingent on promoter hypomethylation and IDH-wildtype GBM growth is dependent on this expression. Using shRNA targeting BCAT to deplete expression, the authors showed substantial reduction in tumor size without DNA fragmentation, hinting that BCAT's effect is mediated through enhancing proliferation. Mechanistically, $IDH1^{WT}$ produces αKG critical for BCAT mediated branched chain amino acid (BCAA) and fatty acid catabolism. As such, the authors showed shRNA mediated suppression of $IDH1^{WT}$ reduced BCAT1 expression, presumably via modulation of the epigenome as a result of reduced αKG-dependent dioxygenase activity, whereas αKG treatment rescued expression (*115*).

Direct evidence of $IDH1^{WT}$ promoting GBM pathogenesis and progression was later identified. By performing TCGA analysis coupled with immunohistochemistry of patient samples, recent reports indicate that up-regulation of $IDH1^{WT}$ in IDH-wildtype GBM is novel mechanism whereby GBMs increase cytoplasmic NADPH and αKG pools critical for metabolic rewiring (*33, 124*). GBM patient-derived, $IDH1^{WT}$ manipulated orthotopic murine xenografts showed $IDH1^{WT}$ depletion decreases tumor burden while enhancing survival whereas over-expression accelerates tumor growth and decreases survival. Enhanced NADPH production promoted lipid biogenesis whereas elevated cytosolic αKG levels promoted cellular de-differentiation via epigenetic modifications (*33*). Further, researchers have shown elevated NADPH levels contribute to GSH and deoxynucleotide production resulting in decreased ROS production (*33*) and enhanced radiation therapy resistance (*139*), respectively.

1.3 FERROPTOSIS

1.3.1 Overview in the Historical Context

One of the most important factors influencing cell fate is response to oxidative stress. As most living organisms rely on oxygen as an electron acceptor during redox-based metabolism, how cells respond to oxidative stress is of critical importance (*109*). Under most physiological conditions cells have built in defense pathways to curtail accumulation of deleterious reactive oxygen species (ROS). Despite the protective mechanisms, cells may undergo a form of regulated cell death now known as ferroptosis in response to increasing oxidative stress and the ensuing increase in lipid peroxidation (*140*). Unlike apoptosis (characterized by chromatin condensation, disintegration of cytoskeleton, and formation of apoptotic bodies) or necrosis (characterized by cytoplasmic swelling and membrane rupture), ferroptotic cells present with mitochondrial shrinkage, vanishing of mitochondrial cristae as opposed to fragmentation, and increased membrane density (*140-142*). Though the field of ferroptosis research is relatively nascent, ferroptosis is recognized as one of the most evolutionarily conserved and oldest forms of cell death, present throughout many different species (*109, 143-145*).

The term ferroptosis was initially coined in 2012, though the roots of ferroptosis research predate this by more than half a century. During this period researchers identified that deprivation of cysteine results in cellular death whereas supplementation with cysteine prevents this cell death (*140, 146*). For decades the underlying mechanisms remained elusive. In the late 1980s researchers observed similar cellular death in neuroblastoma and hippocampal cells (*147, 148*). This cell death

was associated with glutathione (GSH) depletion, exacerbated by low cystine (oxidized cysteine, the precursor to glutathione) media. Subsequent work in the early 1990s demonstrated that this type of cell death was associated with a substantial increase in ROS as a result of GSH depletion, which in turn allowed for a lethal influx of calcium into the cell (*149*). Though subtle morphological distinctions deviating from early cysteine deprivation studies years prior existed, these works provided valuable insight into how cysteine, GSH, and ROS can contribute to cellular death.

The field of ferroptosis research was more formally solidified in the early 2000s. Via a high-throughput screen to identify novel anti-cancer drugs, a compound known as erastin was discovered that induces cell death without nuclear changes, DNA fragmentation, or caspase activation (*150*). Morphologically, these cells presented with increased lipid bilayer density while the membrane remained intact, reduced mitochondrial volume, and dissipation of mitochondrial cristae (*140, 150*). Counter-screening identified this cell death could be inhibited by iron-chelators (*141*), thus the inspiration for the term ferroptosis (*140*). Further studies showed that promoting activity of cystine transporter system x_c- or GSH-dependent selenoprotein GPX4 activity effectively inhibited oxidative stress and associated ferroptotic death (*151, 152*). Coupled with the cysteine and GSH research decades prior, a much clearer picture of this still relatively undefined form of cell death was beginning to take shape. We now know that ferroptosis is a form of cell death caused by the accumulation of toxic oxidized phospholipids (*109*).

Polyunsaturated fatty acids (PUFAs) of the plasma membrane are converted into phospholipids by Acyl-CoA Synthetase Long Chain Family Member 4 (ACSL4) and Lysophosphatidylcholine Acyltransferase 3 (LPCAT3). These phospholipids in turn are the substrates for lipid peroxidation. Subsequent phospholipid peroxidation can then occur via non-enzymatic or enzymatic pathways. Non-enzymatic lipid peroxidation occurs via the Fenton reaction, a chemical reaction between iron and hydrogen peroxide resulting in cytotoxic free radicals (*153*). These cytotoxic ROS are a result of general cellular maintenance, in particular mitochondrial oxidative metabolism (*154*). Enzymatic lipid peroxidation, on the other hand can be executed by cytochrome P450 oxidoreductase (POR) or iron-dependent lipoxygenases (LOX) (*155-158*). Once peroxidized, these phospholipid hydroperoxides (PLOOHs) can interact with PUFAs or free iron and oxygen, and initiate a cascading chain reaction whereby subsequent phospholipids are converted into PLOOHs while generating more ROS species (*109, 142*).

Though the precise effector mechanisms for ferroptotic cell death remain elusive, several contributing factors have been identified. First, as uncontrolled peroxidation of PUFAs is the most downstream event identified, it stands to reason that elevated membrane damage in conjunction with pore formation disrupts plasma membrane integrity (*109*). Conversely, recent data suggests that cross-linked phospholipids containing two PUFA tails are particularly toxic to cells, likely due to increased susceptibility to peroxidation or decreased membrane fluidity, which in turn disrupts membrane function (*109, 159*). A second scenario exists whereby PLOOHs decompose, generating electrophiles. These deleterious ROS species would in turn elicit further oxidative damage upon macromolecules and cellular structures (*109*). Though the relative contributions of

these factors to ferroptotic death remain to be elucidated, it appears likely they each contribute to lipid peroxidation and the ensuing induction of ferroptosis.

1.3.2 Regulation of Ferroptosis

As a regulated form of cell death, we now know the canonical ferroptosis controlling pathway is the cysteine-GSH-GPX4 axis. The glutamate-cystine antiporter, system x_c^-, imports cystine into the cell at a 1:1 ratio with glutamate. Once imported, cystine is subsequently reduced to cysteine by either thioredoxin reductase 1 (TXNRD1) or glutathione reductase (GR) in an NADPH dependent manner (*160, 161*). Subsequently, cysteine can be converted into GSH via glutathione synthetase (GSS) which then functions as the critical cofactor for GPX4 activity (*162, 163*). Ultimately, GPX4 functions as the master regulator of ferroptosis by catalyzing reduction and detoxification of deleterious lipid peroxides. Mechanistically, GPX4 utilizes GSH as a reducing agent during this detoxification, converting GSH into oxidized glutathione (GSSG). GSSG can then in turn be reduced back to GSH at the expense of NADPH by GR, thus ensuring a steady state reservoir of GSH within the cell. Underscoring the critical importance of GPX4 in protecting cells from oxidative stress, global knockout of GPX4 results in elevated lipid peroxidation and non-apoptotic cell death of mouse embryos (*157*). Similarly, conditional brain specific depletion results in neurodegeneration (*157*).

The role of iron in ferroptosis, as the name suggests, is of critical importance. First, the Fenton reaction responsible for propagating non-enzymatic phospholipid peroxidation utilizes iron (*164*). Second, many redox-based metabolic processes involved in the generation of ROS require iron

(*109*). Finally, many enzymatic executioners of ferroptosis such as the LOX family of proteins rely on iron as an essential component for catalysis (*165*). Thus, cellular regulation of iron homeostasis has a profound effect on sensitizing or desensitizing cells to ferroptosis. For example, when cellular iron storage is increased following autophagic degradation of the iron-containing protein Ferritin, ferroptosis is propagated (*166*). Similarly, the iron-carrier protein Transferrin is a potent inducer of ferroptosis, with the Transferrin Receptor (TfR1) reinforcing cellular import and influencing intracellular iron concentration (*167*). Conversely, iron export has been shown to promote ferroptosis resistance (*168*).

While the cysteine-GSH-GPX4 axis and iron metabolism are most intrinsically entwined with ferroptosis regulation, more regulatory mechanisms exist worth noting. Oxidative-stress defense pathways, such as that regulated by NRF2, oppose ferroptosis (*169*). Similarly, ferroptosis suppressor protein 1 (FSP1) is an NADH:ubiquinone oxidoreductase, effectively suppressing lipid peroxidation and ferroptosis by reducing ubiquinone and lipid radicals (*170*). Hypoxia has recently been identified as an inducer of ferroptosis. Under hypoxic conditions mitochondrial enzyme III increases ROS production which in turn facilitates lipid peroxidation (*109*). Indirect activation of ferroptosis regulating genes can occur in response to mutation or physiological dysregulation. P53, for example, is one of the most highly mutated tumor suppressors in cancer and a key regulator of a large cohort of ferroptosis regulators including FSP1 (*171, 172*). Increased density promoting cell-to-cell contact stimulates the Hippo signaling pathway and activation of Yap, a transcription factor whose targets include aforementioned TfR1 and ACSL4 (*173*). Finally, exogenous monounsaturated fatty acids (MUFAs) incorporate into the plasma membrane, effectively

displacing oxidizable PUFAs and inhibiting ferroptosis (*174*). Thus, plasma membrane lipid composition and ubiquinone supply have a profound effect on ferroptosis regulation.

1.3.3 The Emerging Role of Ferroptosis in Disease Pathogenesis

Though a physiological role for ferroptosis remains elusive, pathological relevance has been extensively documented. In fact, cancer research has been linked to ferroptosis since the studies of the early 2000s which identified the cysteine-GSH-GPX4 axis as a critical regulator. Since then we have learned that cancer cells existing in a mesenchymal state, resistant to chemotherapeutics and apoptosis are uniquely susceptible to ferroptosis induction due to their reliance on GPX4 activity (*175*). This reliance on GPX4 activity reflects the high metabolic rate of cancer cells, producing excess ROS into an environment consisting of elevated intracellular reservoirs of iron relative to normal cells (*176*). Genetic perturbations in critical ferroptosis regulators or pathways controlling the expression of said regulators may also influence cancer cell susceptibility to ferroptosis. Previously discussed Hippo signaling pathway genes, for example, are frequently mutated in cancer, driving a metastatic state while simultaneously sensitizing cells to ferroptosis (*109, 177*). Beyond cancer, ferroptosis has been implicated as a major cause of cell death following ischemic damage (*109, 178*). Similarly, lipid peroxidation, diminished GSH levels and reduced GPX4 activity are hallmarks of a variety of neurodegenerative diseases including Huntington's Disease (AD) and Amyotrophic Lateral Sclerosis (ALS) (*179, 180*). The role of ferroptosis in promoting neurodegeneration underscores the unique susceptibility of neurons, whose membranes are rich PUFAs and undergo high metabolic activity, to oxidative stress and lipid peroxidation (*164, 178*).

Ferroptotic inducing strategies present an attractive avenue for cancer therapy. As the master regulator of ferroptosis, GPX4 presents as an attractive candidate. GPX4 inhibiting compounds such as RSL3 are enticing; however, GPX4 itself is not an ideal candidate for two major reasons. First, GPX4 lacks a small-molecule binding pocket, thus inhibitors such as RSL3 covalently bond with the selenocysteine residue present within GPX4 and other selenoproteins (*181*). This opens the possibility of off-target effects. Second, GPX4 itself is a critical protein essential for the health and maintenance of a wide range of cell types, especially neurons (*157*). Inhibiting system x_c- is another natural candidate. With their elevated levels of metabolism rendering them more susceptible to oxidative stress, tumor cells are more dependent on system x_c- to detoxify ROS than normal cells (*109*). Pharmacological inhibition of system xc- using erastin or FDA approved sulfasalazine was shown to abate tumor growth in lymphoma and glioma murine models, respectively (*182*). Such ferroptosis inducing strategies may further synergize with other therapeutic approaches such as immunotherapy and radiation therapy (RT). Anti-PDL1 antibodies stimulate CD8+ T-cells to secrete IFNγ, an efficient suppressor of system x_c-, thus sensitizing cells towards ferroptosis (*183*). Finally, RT has been shown to both induce ferroptosis and synergize with ferroptotic inducers. Contrary to its perceived canonical role of DNA-damaging effects, cytoplasmic radiation has recently been shown to deplete GSH while inducing lipid peroxidation, triggering ferroptosis itself while further synergizing with ferroptotic inducers (*184*). These findings underscore the exciting promise of exploiting ferroptosis regulation in the context of therapeutic interventions.

CHAPTER 2: MATERIALS AND METHODS

2.1 TCGA *In silico* Analysis

Processed data profiling IDH1^{WT} and associated genes of interest transcript level across 33 unique The Cancer Genome Atlas (TCGA) RNA-Seq datasets were downloaded from the Gene Expression Profiling Interactive Analysis (GEPIA) web-based porta (*185*). Physiologically normal tissue IDH1^{WT} and genes of interest transcriptional data was obtained from the Genotype Tissue Expression (GTEx) project, as accessed via the GEPIA web-based portal. 163 GBM tumors (*186*) and 207 physiologically normal tissue samples (*187*) were profiled, respectively. Processed GBM DNA methylation profiles spanning 543 unique GBMS (*24*) were downloaded from the cBio Cancer Genomics Portal (*188, 189*). Differential, survival, and correlation analysis were performed using GEPIA standardized pipeline. Differential expression was analyzed via one-way ANOVA with ILog_2 FCI Cutoff of 1 and p-value Cutoff of 0.01, matching TCGA disease state data with TCGA normal and GTEx data. Overall survival analysis was performed using Mantel-Cox test with median cutoff for differential groups. Correlation analysis was performed via pair-wise gene expression Pearson analysis. Gene ontology (GO) analysis was performed using PantherDB Fisher's exact statistical overrepresentation test, GO biological process complete, with genes aligned to reference homo sapiens gene database (*190*).

2.2 Cell Culture

Patient derived glioma initiating cell (GIC)-20 and GIC-387 were gifts from Kenneth Aldape (University of M.D. Anderson Cancer Center) and Dr. Jeremy Rich (Cleveland Clinic), respectively. Transformed glioma cell line LN382 was a gift from Dr. Webster Cavenee (University of California, San Diego). Normal human astrocytes (NHA) were a gift from Dr. Russ

Pieper (University of California, San Francisco). GICs were grown as neurospheres within untreated, tissue culture flasks (Corning), in Full Media consisting of DMEM/F12 50:50 with L-glutamine (Corning), supplemented with 1% Pen/Strep antibiotics (Invitrogen), B27 (Invitrogen), N2 (Invitrogen), GlutaMAX (Life Technologies), human-Epidermal Growth Factor (hEGF: Shenandoah Biotech), human-Fibroblast Growth Factor (hFGF- Shenandoah Biotech), Leukemia Inhibitory Factor (LIF: Shenandoah Biotech). LN382 and NHA cell lines were grown in DMEM 1X with 4.5 g/L glucose, L-glutamine and sodium pyruvate (Corning) containing media supplemented with 10% Fetal Bovine Serum (FBS) (Life Technologies) and 1% Pen/Strep antibiotics (Life Technologies). Neurospheres were cultured in Neurosphere Media comprising DMEM/F12 1:1 (Invitrogen), supplemented, B27 (Invitrogen), N2 (Invitrogen), Pen/Strep/Glut 100X mix (Invitrogen). $IDH1^{WT}$ knockdown and over-expression of GIC and LN382 cell lines was previously performed by our lab as detailed in (*33*).

2.3 Cellular Differentiation and Growth curves

GIC-387 cells were seeded at 50,000 cells/well (Day 0) in a 6-well, un-treated or treated plate (Corning) in either Full Media or Full Media supplemented with 10% FBS, respectively. Cells were imaged every 3d, assessing for gross morphological changes. Following imaging, cells were treated with StemPro Accutase Cell Dissociation Reagent (ThermoFisher) to dissociate cells. Cells were counted via Trypan Blue (ThermoFisher) exclusion on a Countess Cell Counter (Invitrogen).

2.4 RT-qPCR

Total RNA was extracted from control and $IDH1^{WT}$-manipulated cultured cells using RNeasy kit (Qiagen) according to manufacturer's protocol. cDNA was reverse transcribed from 500ng total RNA using M-MLV Reverse Transcriptase (Promega) according to manufacturer's instructions. qPCR was performed using Fast SYBR Green Master Mix (Applied Biosystems) and primers specific for IDH1 (forward primer: 5'- GGCGAGCAGCACAGAGAC -3', reverse primer: 5'- TCACCCCAGATACCATCAGA -3'), NES (forward primer: 5'- GGTCTCTTTTCTCTTCCGTCC -3', reverse primer: 5'- CTCCCACATCTGAAACGACTC -3'), PDGFA (forward primer: 5'- GCAAGACCAGGACGGTCATTT -3', reverse primer: 5'- GGCACTTGACACTGCTCGT -3'), PTPRZ1 (forward primer: 5'- ATCCTGGCAGCAGGTGACTCAG -3', reverse primer: 5'- CCTCAGCTAGACCAATACGAGAC -3'), VIM (forward primer: 5'- GACGCCATCAACACCGAGTT -3', reverse primer: 5'- CTTTGTCGTTGGTTAGCTGGT -3'), GAPDH (forward primer: 5'- TGTGGGCATCAATGGATTTGG -3', reverse primer: 5'- ACACCATGTATTCCGGGTCAAT -3'). All reactions were performed via 7900HT Fast Real-Time PCR System (Applied Biosystems) with mRNA quantified and results analyzed using **ΔΔ**Ct method.

2.5 Western Blot Analysis

For all Western analysis, proteins were separated by NuPage 4%-12% Bis-Tris gels via SDS-PAGE (Life Technologies) and transferred to Hybond P PVDF membranes (Genesee Scientific, GE). Membranes were washed for 5 minutes in PBS + 0.05% Tween 20 (PBS/Tween), blocked

with 5% milk in PBS/Tween for 1 hour, and incubated with primary antibodies overnight. Membranes were then washed 3x with PBS/Tween for 10 minutes per wash and developed with secondary goat anti-rabbit, goat anti-mouse, or donkey anti-goat IgG antibodies (Santa Cruz) in 5% milk PBS/Tween. Membranes were then washed 3x more at 10 minutes each wash with PBS/Tween. Following washing, blots were developed with Supersignal West Dura ECL (Pierce) following manufacturer's protocol. Primary antibodies: anti-IDH1 (Invitrogen, PA5-28206), anti-GPX4 (Abcam, ab125066), anti-HSP70 (BD Pharmingen, 610607).

2.6 Murine NSC Isolation and Differentiation

NSCs were isolated from the subventricular zone (SVZ) of postnatal day 1 mice and cultured as neurospheres using established protocols (*191*) and grown in Neurosphere Media containing 20 ng/ml EGF for 3d at 37 °C, 5% CO_2. Neurospheres were then plated at 50,000 cells/ml and 12h later infected with lentivirus containing CSII or CSII-IDH1^{WT} constructs (*33*). Plates were returned to the 37 °C, 5% CO_2 incubator and cultured for 2 additional days. Neurospheres were then collected, pelleted via centrifugation, and virus containing media replaced with fresh Neurosphere Media containing 20 ng/ml EGF, and repeated. Cells were then trypsinized, resuspended in neurosphere media at 1 x 10^7 cells/ml and FACS sorted for GFP+ expression. 2 x 10^4 cells/ml were plated at 1 ml/well onto Poly-D-Lysine (PDL)-coated coverslips within 24-well plate (Corning). Cells were incubated at 37 °C, 5% CO_2 for 3d then neuronal differentiation induced by changing media with Neurosphere Media containing 1 ng/ml EGF and 10 ng/ml BDNF and placed in incubator for 7d. Immunocytochemistry using anti-NeuN and anti-Beta III Tubulin antibodies was

performed following standardized protocols (*192*). Percentage of NeuN+/Beta III Tubulin+ cells was quantified.

2.7 αKG-Quantification

Total αKG was quantified using the αKG Assay Kit (BioVision) according to manufacturer's instructions. $IDH1^{WT}$ and manipulated GICs were grown in 6-well untreated plates (Corning) for 24h. Cells were collected in 50 μl of αKG assay buffer supplied by the aforementioned kit and incubated on ice for 30min. Samples were subsequently deproteinized and neutralized using the Deproteinizing Sample Preparation Kit (BioVision) following manufacturer's instructions. 50 μl of sample was added into triplicate wells of a 96 well plate and 50 μl of Reaction Mix added to each sample. The plate was then incubated in the dark at 37 °C for 30min then read at excitation/emission 535/587 nm.

2.8 Genomic DNA Isolation

Genomic DNA was isolated from $IDH1^{WT}$ and manipulated GICs using the Blood & Cell Culture DNA Kit (Qiagen). GICs were incubated at 37 °C, 5% CO_2 in a 6-well tissue culture plate for 9d in Full Media or Differentiation Media then spun down, washed in PBS, and resuspended in PBS. Following manufacturer's instructions, cells were lysed, spun, and residual debris discarded from nuclear pellet. Nuclear pellet was resuspended and protein degraded via Proteinase K treatment. QIAGEN Genomic-tips (Qiagen) were equilibrated via manufacturer's instructions, and sample applied to Genomic-tips, with the sample moving through resin via gravity flow. Genomic tip was washed 3x with buffer and sample eluted then precipitated by addition of room temp isopropanol.

2.9 DNA Methylation Quantification

Global DNA methylation was quantified using MethylFlash Global DNA 5-mC Quantification Kit (EpiGentek) and MethylFlash according to manufacturer's instructions. In a 96well plate, 100ng of genomic DNA per sample was added to 80ul of binding solution and incubated at 37 °C for 90 min. Binding solution was removed and each well washed 3x with wash buffer. Methylated and hydroxymethylated DNA was captured via addition of provided antibodies, incubated at RT for 30 min. Following incubation wells were washed 4x with wash buffer and incubated with enhancer solution at RT for 30 min. Each well was then washed 5x with wash buffer, incubated with developer for 10 min in dark before stop solution was added. Absorbance at 450nM was then recorded.

2.10 Epigenetic Histone Modification Analysis

Histone modifications as a result of $IDH1^{WT}$ expression were quantified via the Epiproteomic Histone Modification Panel B (Northwestern Proteomics). Biological triplicates of $IDH1^{WT}$ manipulated and control GIC-387 were grown in either Full Media or Differentiation Media for 6d at 37 °C, 5% CO_2. 2 million cells per triplicate were then pelleted, washed in PBS, and pellets flash frozen in liquid nitrogen. Samples were then provided to the Northwestern University Proteomics Core Facility. Nuclei were then isolated and histones acid-extracted. Samples were derivatized via propionylation reaction and digested with trypsin following established protocols (*193*). Each sample was resuspended in 50 μl of 0.1% TFA/mH_2O and 3 μl for each technical triplicate used for liquid chromatography mass spectrometry (LCMS).

2.11 Transwell Invasion Assay

Invasive properties were determined via a transwell invasion assay. Matrigel hESC-Qualified Matrix (Corning) was thawed and liquified on ice. Under sterile conditions, 50 μL of Matrigel was added to 24-well, 12 mm, 8.0 um pore size, polycarbonate transwell inserts (Millipore Sigma) and solidified in a 37 °C incubator for 30 minutes to form a thin gel layer. Transwell inserts were then placed within the wells of a 24 well untreated tissue culture plate (Corning). $IDH1^{WT}$-manipulated and control GIC-387 cells were dissociated with StemPro Accutase Dissociation Reagent (ThermoFisher) and 1 x 10^6 cells / 100μl resuspended in DMEM/F12 50:50 with L-glutamine (Corning), supplemented with 1% Pen/Strep antibiotics (Invitrogen), and 0.1% bovine serum albumin (BSA). 100 μl of cell solution was plated on top of each transwell insert and incubated for 10 minutes at 37 °C and 5% CO_2. 600 μl of Full Media was pipetted to the bottom, lower chamber in each well containing an insert, ensuring Full Media contacted the transwell membrane. Cells were then incubated for 36h at 37 °C and 5% CO_2. Following incubation, migrated cells within the lower chamber were counted via Trypan Blue (ThermoFisher) exclusion on a Countess Cell Counter (Invitrogen).

2.12 Wound Closure Migration Assay

To assess migration capacity, 1 x 10^6 LN382 cells were plated/well in a 6-well tissue culture treated plate (Corning) and placed in an incubator at 37 °C and 5% CO_2. Upon reaching confluency, in a sterile environment, a 200 μl pipette tip was pressed firmly against the top of the tissue culture well and a swift, vertical wound down through the cell monolayer was made for each sample.

Media and debris were aspirated. 2 ml of fresh tissue culture media was slowly added against the wall of each well, avoiding detachment of adherent cells. Following wound generation an image was taken, establishing t= 0 timepoint, and wounding region boundaries established. The tissue culture plate was placed back into the 37 °C and 5% CO_2 incubator. Every 4h the plate was removed from the incubator and images taken of each wound with the Revolve (Echo) microscope. After t= 24h the images were analyzed using the Revolve microscope's software, calculating the total area of each wounding region.

2.13 Oxidative Stress Detection

To determine oxidative stress levels, $IDH1^{WT}$ and manipulated GICs were treated with a final concentration of 5 μM CellROX Reagent (ThermoFisher) and incubated for 30 min at 37 °C. The media was removed and cells washed 3x with PBS and read at emission/excitation 640/665 nm.

2.14 GSH Quantification

Total GSH production was quantified via Glutathione Colorimetric Detection Kit (Invitrogen) following manufacturer's instructions. GIC cell pellets were washed with PBS, resuspended in 5% aqueous 5-sulfo-salicylic acid with 2-vinylpyridine to deproteinize sample, and lysed via vortexing before being incubated for 10 min at 4 °C. Samples were centrifuged and supernatant collected. 50 μl of sample, 25 μl of detection reagent, and 25 μl reaction mixture were added to wells of a 96 well plate. Reaction was incubated at RT for 20 min and absorbance read at 405 nm.

2.15 Lipid Peroxidation Quantification

To determine lipid peroxidation levels, we utilized the Lipid Peroxidation (MDA) Assay Kit (Colorimetric) (Abcam) following manufacturer's instructions. 1 x 10^6 cells/well $IDH1^{WT}$ and manipulated GICs were lysed in 0.5% Triton X-100 lysis buffer containing 10 mM Tris-HCL, pH 8, 150 mM NaCl, and protease inhibitor cocktail. Samples were diluted in Dilution Buffer and 50 μl of samples added to wells of a 96-well clear bottom microplate. 10 μL MDA Color Reagent solution was added to each well and incubated at RT for 10-30 min. 40 μl Reaction Solution was added then incubated at RT for 45 min. Absorbance was read with a microplate reader at 694 nm.

2.16 GSR Activity Assay

To assess GSR enzymatic activity we used the Glutathione Reductase GR Assay Kit (Abcam). 1 x 10^6 $IDH1^{WT}$ and manipulated GICs per biological triplicate were homogenized in Assay Buffer. To 100 μl of sample, 5 μl 3% H_2O_2 was added an incubated at 25 °C for 5 min to destroy GSH. 5 μl Catalase was added and incubated at 25 °C for 5 min before adding 50 μl of samples to a 96-well plate (Corning). 50 μl of reaction mix containing DTNB solution which reacts with GSH to generate TNB2 (yellow, λmax= 405) was added to each well, and absorbance immediately read at 405nm establishing t= 0. Readings were taken every 10 mins until t= 90, with plate incubated at 25 °C between readings.

2.17 GPX4 Activity Assay

To quantify GPX4 activity we used the Glutathione Peroxidase Assay Kit (Abcam). 2 x 10^6 $IDH1^{WT}$ and manipulated cells per biological triplicate were harvested, washed in PBS,

resuspended in 200 μl of Assay Buffer. Supernatant was collected and 50 μl/well added to a 96-well plate. 40 μl of reaction mix containing Assay Buffer, 40nM NADPH solution, GR solution and GSH solution for one set of conditions was added to each well. To assess $IDH1^{WT}$ effect on GPX4 activity independent of supplemental GSH and GR solutions, 40 μl of reaction mix consisting of Assay Buffer and 40nM NADPH solution was added to a second set of samples. Reactions were incubated at RT for 15 min then 10 μl cumene hydroperoxide solution added to each well to start GPX reaction. Absorbance readings at 340 nm were immediately recorded establishing t= 0. Readings were taken every 5 min until t= 120, with the plate stored at 25 °C between readings.

2.18 ^{13}Carbon-Glucose Studies

$IDH1^{WT}$ and manipulated GIC-20s were grown in media supplemented with 10 mM glucose until 90% confluence was achieved. 24h later, media containing 10 mM [U-^{13}C] Glucose was added. After 3h, 24h, and 72h cells were collected, pelleted, washed using 150 mM Ammonium Acetate without disturbing pellet, then snap frozen in liquid nitrogen. Samples were then sent for GC-MS processing. Microtubes containing pellets were removed from -80 °C storage and maintained on wet ice during processing. 0.3 mL chilled 8:2 isopropanol:chloroform (EMD) mixture was added to each sample to initiate protein precipitation and extracted metabolites dried under vacuum at 45 °C. 1 mL BF3/Methanol was added to each sample then samples incubated at 60 °C for 3h. 200 μl LCMS water and 300 μl Hexane were added to cooled samples before being vortexed, sit for 5 min, vortexed again, and centrifuged for 3 min to facilitate layer separation. Organic layer was transferred to autosampler for GC-MS analysis as described (*33*).

2.19 MTS Assay

To assess cellular viability we used the MTS Assay Kit (Abcam). 0.1 x 10^5 cells were seeded per well in a 96-well plate (Corning). Cells were then treated with either vehicle, RSL3 (0.1 μM), or IDH1i-13 (0.1 μM, 0.5 μM, 3 μM, 6 μM, 12 μM) and incubated at 37 °C, 5% CO_2 for 48h and 72h, respectively. For GSH and GSSG rescue studies, 250 μM and 500 μM of GSH and GSSG was added concomitantly to IDH1i-13 treated cells. Following incubation, 20 μl/well of MTS reagent was added and incubated for 2h at 37 °C, 5% CO_2. Plates were then removed from incubator, briefly shaken on a shaker, and absorbance measured at OD= 490nm.

2.20 SYTOX Assay

To determine extent of cell death with membrane rupture, we utilized SYTOX Green Nucleic Acid Stain (Invitrogen). GICs were seeded at 0.1 x 10^5 cells/well in a 96-well, flat, clear bottom black microplate (Corning) and treated with increasing concentrations of IDH1i-13 (0.1 μM, 0.5 μM, 3 μM, 6 μM, 12 μM). For rescue experiments, cells were concomitantly treated with 0 μM and 5 μM N-acetyl L-cysteine (NaC) (Millipore Sigma), 5 mM and 10 mM of membrane permeable Dimethyl 2-oxoglutarate (αKG) (Sigma-Aldrich), or 1 μM and 2 μM of Ferrostatin-1 for 48h and 72h at 37 °C, 5% CO_2. Following incubation, SYTOX Green was added to each well at a final concentration of 500 nM and incubated in the dark at 37 °C, 5% CO_2 for 1h. Absorbance was then read on a fluorescent plate reader with excitation and emission maxima of 504 nm and 523 nm, respectively.

2.21 IDH1i-13 Pharmacokinetics

2.21.1 IDH2 Activity Assay

To determine whether IDH1i-13 inhibits IDH2 we used the Isocitrate Dehydrogenase Activity Kit (Sigma-Aldrich). For each IDH1i-13 concentration, 100 μM, 10 μM, 1 μM, .1 μM, .01 μM, .001 μM, and 0 μM control of IDH1i-13 was added to 50 μl of IDH Assay Buffer in a 96-well plate in triplicate. Master Reaction Mix consisting of 38 μl IDH Assay Buffer, 8 μl Developer, 2 μl IDH Substrate, and 2 μl $NADP^+$ per condition was then added each sample. To start the reactions at the same time, 10 nM of human-rIDH2 (Abcam, ab198082) was added to each well using a multichannel pipette. The plate was incubated at 37 °C in dark and after 3 min absorbance was read at 450 nm on a microplate reader, establishing ($T_{initial}$). The plate was subsequently read every 5 min at 450 nm, with incubation at 37 °C in the dark between readings.

2.21.2 EC_{50} Calculations

EC_{50} value of IDH1i-13 inhibition of IDH2 was determined using Prism. Log concentrations of IDH1i-13 and nmol concentrations of NADPH (readout) datapoints were normalized with 0% defined as smallest mean in each data set and 100% defined as largest mean in each data set. Data was analyzed via nonlinear regression (curve fit); log(inhibitor) vs. normalized response.

2.22 IDH1i-13 Specificity *In Silico* Analysis

Using the Gene Ontology (GO) Browser, a list of proteins associated with the GO term 'NADP binding' was generated (*194*). $IDH1^{WT}$, IDH2, and NADP binding proteins' crystal structures in conformation with cofactor were downloaded from the RCSB Protein Data Bank (rcsb.org) (*77,*

195). Profiled are the stretches of sequences with the most contact with bound cofactor. To determine amino acid sequence specificity of $IDH1^{WT}$ NADPH binding pocket, the $IDH1^{WT}$ 10 amino acid sequence containing His315 was uploaded to Protein Basic Local Alignment Search Tool (BLASTp) (*196*).

2.23 In Vivo Xenograft Model

All animals used in the study were under an approved protocol of the Institutional Animal Care and Use Committee (IACUC) of Northwestern University. Luciferase-expressing GIC-20 cells (1.5×10^5 cells / 3μl) were dissociated via Accutase (Life Technologies) and resuspended in HBSS. 6-8 week old female nude mice (The Jackson Laboratory) were anesthetized and placed within stereotactic frames. Surgical area was cleaned with betadine and 70% ethanol. An incision was made in the scalp of the mice, and subsequently a 0.7 mm Burr hole was created in the skull using a microsurgical drill, 2 mm lateral right of the sagittal suture and 0.5 mm posterior to the bregma. A Hamilton syringe was loaded with 3 μl of GIC-20s and inserted 3.5 mm into the brain. After 1 minute of stabilization, cells were implanted at a rate of 1 μl/min, with 1 minute of stabilization following each μl implanted. The syringe was then withdrawn and skin was closed with sutures. Mice were sacrificed based on observed neurological impairment. 11-13 mice per group were used in each study group. Two weeks following implantation mice were randomized into two groups based on bioluminescence as determined using the Lago (Spectral Instruments Imaging). 11 mice received IDH1i-13 (10 mg/kg) and RT (2GY) x 5 M-F for 2 weeks. 13 mice received vehicle (30% PBS, 20% DMSO, 50% PEG) and RT (2GY) x 5 M-F for 2 weeks. Following 2 weeks treatment, mice rested for 1 week and were treated biweekly with IDH1i-13 or vehicle until week 7 total.

Survival analysis between control and experimental group was determined using the Kaplan-Meier method, with statistical significance determined by the log rank (Mantel-Cox) test.

2.24 In Vivo Bioluminescence Imaging

Tumor growth following orthotopic implantation of luciferase expressing GIC-20s was monitored by bioluminescence imaging (Lago, Spectral Instruments Imaging). Mice were injected with 200 μl luciferin potassium salt (Perkin Elmer), anesthetized, and imaged using the Lago. Bioluminescence was quantified using Aura Imaging Software (Spectral Instruments Imaging), with bioluminescence quantified relative to non-tumor bearing mice.

2.25 Histology

Paraffin embedded mouse brains isolated from patient-derived xenograft (PDX) mouse models were provided to the Mouse Histology and Phenotyping (Laboratory) for sectioning and hematoxylin and eosin (H&E) staining. Gross pathology of brain sections was assessed via light microscopy by pathologist Dr. Craig Horbinski.

2.26 Statistical Analysis

All experimental data are presented as mean ± standard error of the mean, unless otherwise specified. Experimental and control groups were compared for significance by two-tailed Student's t-test. A p-value ≤ 0.05 was considered statistically significant. Sample size estimates were not used. Kaplan-Meier survival curves, cox proportional hazard ratios, and 95% confidence intervals were analyzed by Mantel-Cox and Gehan-Breslow-Wilcoxon tests. Genes with similar

expression pattern were ranked by Pearson correlation coefficient, and gene expression correlation determined using methods including Pearson, Spearman, and Kendall.

CHAPTER 3: IDH1^{WT} PROMOTES A RADIAL GLIA-LIKE, GLIOMA INITIATING CELL IDENTITY

3.1 Abstract

Glioblastoma multiforme (GBM) is a devastating brain cancer characterized by rapid progression, resistance to therapeutic intervention, and inevitable patient mortality. One major hurdle curtailing therapeutic efficacy is the profound interpatient and intratumoral heterogeneity of GBM. GBMs can broadly be classified into three molecular subtypes—classical, proneural, and mesenchymal--based on genetic events within key oncogenic and neurodevelopmental programs. Intratumorally, despite GBMs being primarily represented by one molecular subtype, individual cellular populations of each subtype may exist in different ratios while freely changing from one subtype to another. Thus, understanding molecular events critical for promoting these unique cellular states while maintaining plasticity is of great importance. We recently discovered that IDH-wildtype GBM are characterized by transcriptional upregulation of the non-mutated, wild-type form of IDH1 ($IDH1^{WT}$). Over-expression of $IDH1^{WT}$ in murine P53/PTEN co-deleted NSCs promoted tumorigenesis, whereas genetic and pharmacological inhibition of $IDH1^{WT}$ within patient-derived glioma-initiating cells (GICs) and derivative xenografts reduced growth and tumor progression. Molecularly, $IDH1^{WT}$ depletion in GICs resulted in reduced αKG production that promoted histone hypermethylation, induction of a tumor suppressive gene signature, and cellular differentiation. Building upon these findings, we tested the hypotheses that $IDH1^{WT}$ promotes a stem-like cellular state that influences molecular subtype via unique chromatin modifications.

3.2 Results

3.2.1 IDH1^{WT} is Over-expressed in GBM

Our group previously identified that IDH1^{WT} is upregulated in approximately 2/3 of all high grade gliomas (HGGs) and that this IDH^{WT} upregulation and the occurrence of IDH1 point mutation are mutually exclusive (*33*). We further showed that IDH1^{WT} suppression in glioma initiating cells (GICs) results in decreased αKG production, histone hypermethylation, and a more differentiated glioma cell state (*33, 124*). Our present study sought to expand upon these findings by defining the molecular mechanisms by which IDH1^{WT} promotes the stem like properties of GICs. As the molecular subtypes of GBM are distinguished by dysregulation of non-redundant stemness factors, we performed TCGA-Analysis to assess IDH1^{WT} transcript level across GBM molecular subtypes. IDH1^{WT} was upregulated within each molecular subtype (Fig. 6A) and negatively correlated with patient survival most strongly within the classical subtype (Fig 6B-E). These in silico analyses suggest that enhanced IDH1^{WT} expression is a pathogenic, universal event within IDH-wildtype GBM irrespective of molecular subtype and underlying stemness factors.

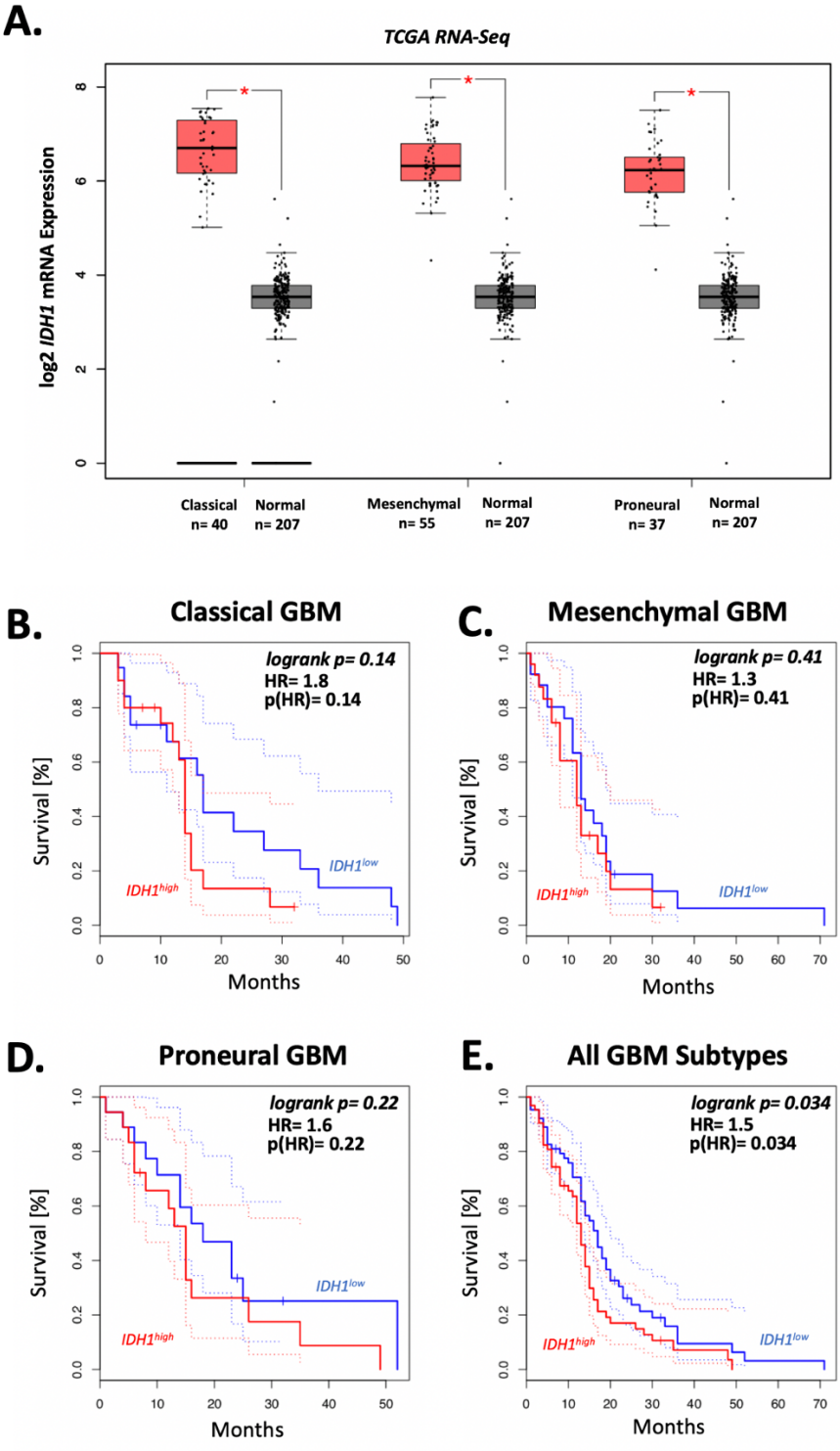
A.
TCGA RNA-Seq
log2 IDH1 mRNA Expression
Classical n= 40
Normal n= 207
Mesenchymal n= 55
Normal n= 207
Proneural n= 37
Normal n= 207
B.
Classical GBM
logrank p= 0.14
HR= 1.8
p(HR)= 0.14
C.
Mesenchymal GBM
logrank p= 0.41
HR= 1.3
p(HR)= 0.41
D.
Proneural GBM
logrank p= 0.22
HR= 1.6
p(HR)= 0.22
E.
All GBM Subtypes
logrank p= 0.034
HR= 1.5
p(HR)= 0.034
Survival [%]
Months
IDH1high
IDH1low

Figure 6. IDH1^{WT} is over-expressed in each GBM molecular subtype, correlating with patient survival
TCGA dataset analysis of IDH1^{WT} transcript levels. IDH1^{WT} mRNA levels in normal tissue (n= 207) vs classical GBM (n= 40), mesenchymal GBM (n= 55), and proneural GBM (n= 37) tumors (**A**). Kaplan-Meier survival analysis of patients expressing high IDH1^{WT} (IDH1^{high}) and low IDH1^{WT} (IDH1^{low}) mRNA levels across classical (**B**), mesenchymal (**C**), proneural (**D**) and all (**E**) GBM subtypes.

3.2.2 IDH1^{WT} Promotes GIC Stemness Via Epigenetic Dysregulation

Previous work by our lab indicated that decreased expression of IDH1^{WT} level within GICs promotes cellular differentiation (*33*). We therefore sought to test the inverse hypothesis, that elevated IDH1^{WT} expression promotes a de-differentiated, stem-like state. Patient-derived GIC-387s genetically modified to stably over-express either IDH1^{WT} (Wt-IDH1) or CSII control plasmid (CSII) were grown in specially formulated media lacking FBS but supplemented with human Epidermal Growth Factor (EGF), basic Fibroblast Growth Factor (bFGF), and Leukemia Initiating Factor (LIF), i.e., conditions that promote neurosphere formation while closely mirroring phenotypic and genotypic properties of primary tumors (*197*). When exposed to fetal bovine serum (FBS), known to induce differentiation in human embryonic stem cells (*198*), we observed that IDH1^{WT} over-expressing GIC-387s resisted adherence to poly-D-lysine/laminin matrix and showed enhanced proliferation in suspension (Fig. 7A, B). By contrast, control GIC-387s readily

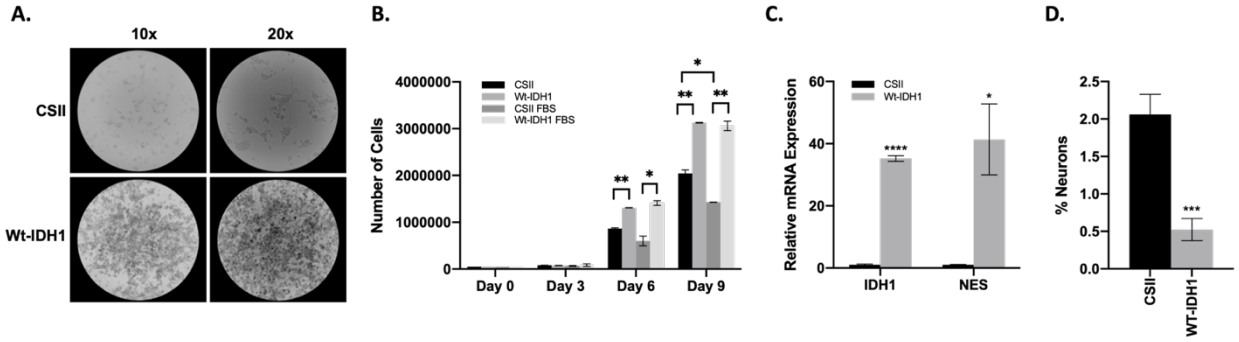

Figure 7. Cellular differentiation is inhibited by IDH1^{WT} expression
(**A**) Gross microscopy of IDH1^{WT}-overexpression (Wt-IDH1) vs control (CSII) GICs 6d post FBS supplementation. (**B**) Cellular growth curve analysis. (**C**) qPCR analysis of IDH1^{WT} and NES transcript levels 6d post FBS supplementation. (**D**) Quantification of FACs sorted NSC populations lentivirally transduced to over-express IDH1^{WT} or control plasmid supplemented with 10 ng/ml BDNF to induce neuronal differentiation. * $p < 0.05$; ** $p < 0.01$; *** $p < 0.001$

adhered and differentiated, with a decreased proliferation rate (Fig. 7A, B) As IDH1^{WT} is most highly upregulated in the classical subtype, and NES expression is elevated within this molecular subtype, we performed qPCR assessing for NES expression. Under differentiation conditions we observed robust upregulation of NES expression in Wt-IDH1 GICs (Fig. 7C). NPCs characterized by NES expression are a presumed cell of origin in the context of IDH-wildtype GBM. Therefore, we investigated whether IDH1^{WT} expression similarly reduces differentiation potential within NSCs. Under differentiation conditions, primary murine NPCs infected with lentivirus containing Wt-IDH1 readily resisted neuronal differentiation relative to CSII control NPCs (Fig. 7D). Together, these results indicate IDH1^{WT} expression is sufficient for promoting stem cell-like properties in patient-derived GICs and murine NPCs.

Due to (R)-2HG competitively inhibiting αKG, αKG-dependent DNA dioxygenase activity is disrupted resulting in a DNA hypermethylation phenotype within IDH-mutant GBMs (*103*). We

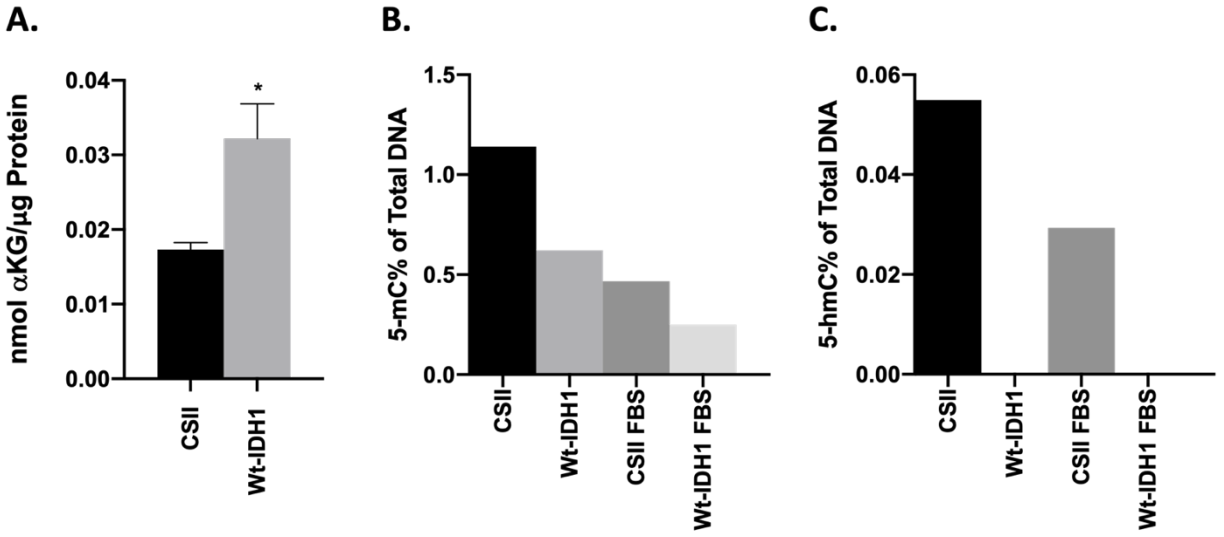

Figure 8. IDH1^{WT} over-expression increases αKG expression, yielding a DNA hypomethylation phenotype

(**A**) Quantification of intracellular αKG levels in cells over-expressing IDH1^{WT} (Wt-IDH1) and control (CSII) GICs. Quantification of total 5-methylcytosine (5-mC) DNA (**B**) and 5-hydroxymethylcytosine (**C**) in Wt-IDH1-GICs and CSII-GICs grown in differentiating (FBS supplementation) and non-differentiating conditions. * $p < 0.05$.

therefore speculated that up-regulation of IDH1^{WT} through increased αKG production regulates DNA methylation in GICs. Stable over-expression of IDH1^{WT} resulted in robust enhancement of αKG production (Fig. 8A). Elevated αKG level in Wt-IDH1 GIC-387s correlated with global decrease in DNA 5-methylcytosine (5-mC) and 5-hydroxymethylcytosine (5-hmC) levels (Fig. 8B, C). Under differentiating conditions, the effect of IDH1^{WT} over-expression on DNA methylation was further enhanced (Fig. 8B, C). Previously we identified disruption of histone modifications upon IDH1^{WT} reduction; however, our approach was limited to H3K4, H3K9, H3K27, and H3K36 marks. To expand upon these results, in an unbiased fashion, we performed liquid chromatography mass spectrometry on CSII and Wt-IDH1 GICs. IDH1^{WT} over-expression resulted in widespread post-translational histone mark dysregulation that was profoundly

exacerbated upon exposure to differentiating conditions (Fig. 9). Collectively, these data highlight IDH1^{WT}'s capacity to drastically remodel the epigenome within GICs.

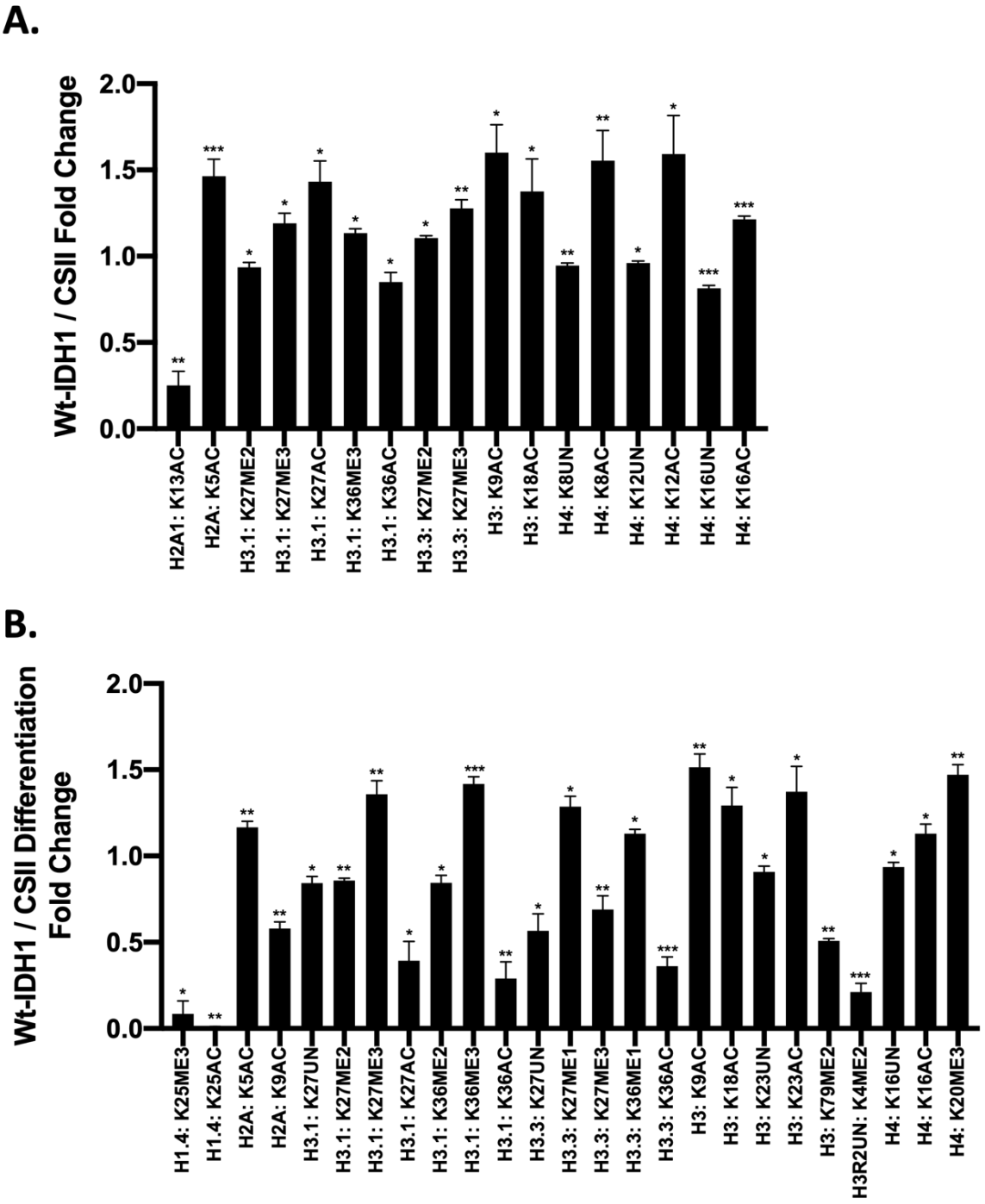

Figure 9. IDH1^{WT} over-expression promotes robust histone mark dysregulation
Quantification of histone marks identified via liquid chromatography mass spectrometry (LCMS) of IDH1^{WT} overexpressing (CSII-IDH1^{WT}) and control (CSII) GICs grown in non-differentiating (**A**) and differentiating (FBS stimulation) conditions (**B**). ** $p < 0.05$; ** $p < 0.01$; *** $p < 0.001$*

Epigenetic disruption often leads to the aberrant activation of genes critical for tumorigenesis. In particular, DNA methylation results in recruitment of repressive complexes to promoter regions, effectively silencing gene expression (*95*). As such, DNA hypomethylation induced by $IDH1^{WT}$ expression may lead to increased expression of genes critical for promoting stemness. Within a brain tumor, GICs are maintained via intrinsic mechanisms as well as exogenous factors derived from their niche, such as hypoxia and eNOS signaling (*49*). In an effort to identify the most clinically relevant $IDH1^{WT}$ regulated stemness candidates, we performed unbiased TCGA correlation analysis to identify the top transcriptional correlates with $IDH1^{WT}$ mRNA expression within human patients (Fig. 10A). Gene ontology pathway analysis of the top 500 $IDH1^{WT}$ correlates identified significant enrichment for pathways involved in neurodevelopmental processes and stem cell maintenance (Fig. 10B). To identify individual genes that may contribute to stemness, we assigned correlation ranks (CRs) to each transcriptional correlate, with the number representing its $IDH1^{WT}$ correlation ranking relative to the entirety of TCGA GBM transcriptome. Strikingly, among the top correlates, we identified stemness factors that underscore the proneural and classical GBM molecular subtypes. Proneural GBM related PDGFA, the ligand for PDGFRA, is sufficient to drive a proneural phenotype (*199*) and had a CR of 2 (Fig. 10A, C). Surprisingly, classical GBM related NES was also highly correlated, with a CR of 149 (Fig. 10A, D). PDGFA and NES gene body methylation negatively correlated with $IDH1^{WT}$ mRNA expression, supporting $IDH1^{WT}$ mediated DNA de-methylation as the mechanism whereby $IDH1^{WT}$ controls their expression (Fig. 10E, F). To confirm that $IDH1^{WT}$ controls the expression of both NES and PDGFA, we performed RT-qPCR on GICs stably transfected with shRNA targeting $IDH1^{WT}$.

Knockdown of $IDH1^{WT}$ resulted in significant reduction in both NES and PDGFA (Fig. 8G). Strikingly this reduction was rescued via treatment with DNA methyltransferase inhibitor and demethylating agent 5-Aza-2'-deoxycytidine (2DE) (Fig. 10G). These results indicate that by

inducing a DNA hypomethylation phenotype, IDH1^{WT} regulates the expression of stemness factors that define classical and proneural tumor cell states.

A.

Gene Symbol	PCC	Correlation Rank
TRIM24	0.6	1
PDGFA	0.57	2
KCNF1	0.56	3
PTN	0.54	4
RNF216P1	0.54	5
SPATA6	0.54	6
RP11-156L14.1	0.53	7
FLOT2	0.52	8
CDK14	0.52	9
SNX6	0.52	10
RAC1	0.52	11
PLEKHF2	0.51	12
DENND2A	0.51	13
PTPRZ1	0.51	14
ETV5	0.51	15
WDR41	0.51	16
ARL4A	0.5	17
RAB8B	0.5	18
COG5	0.5	19

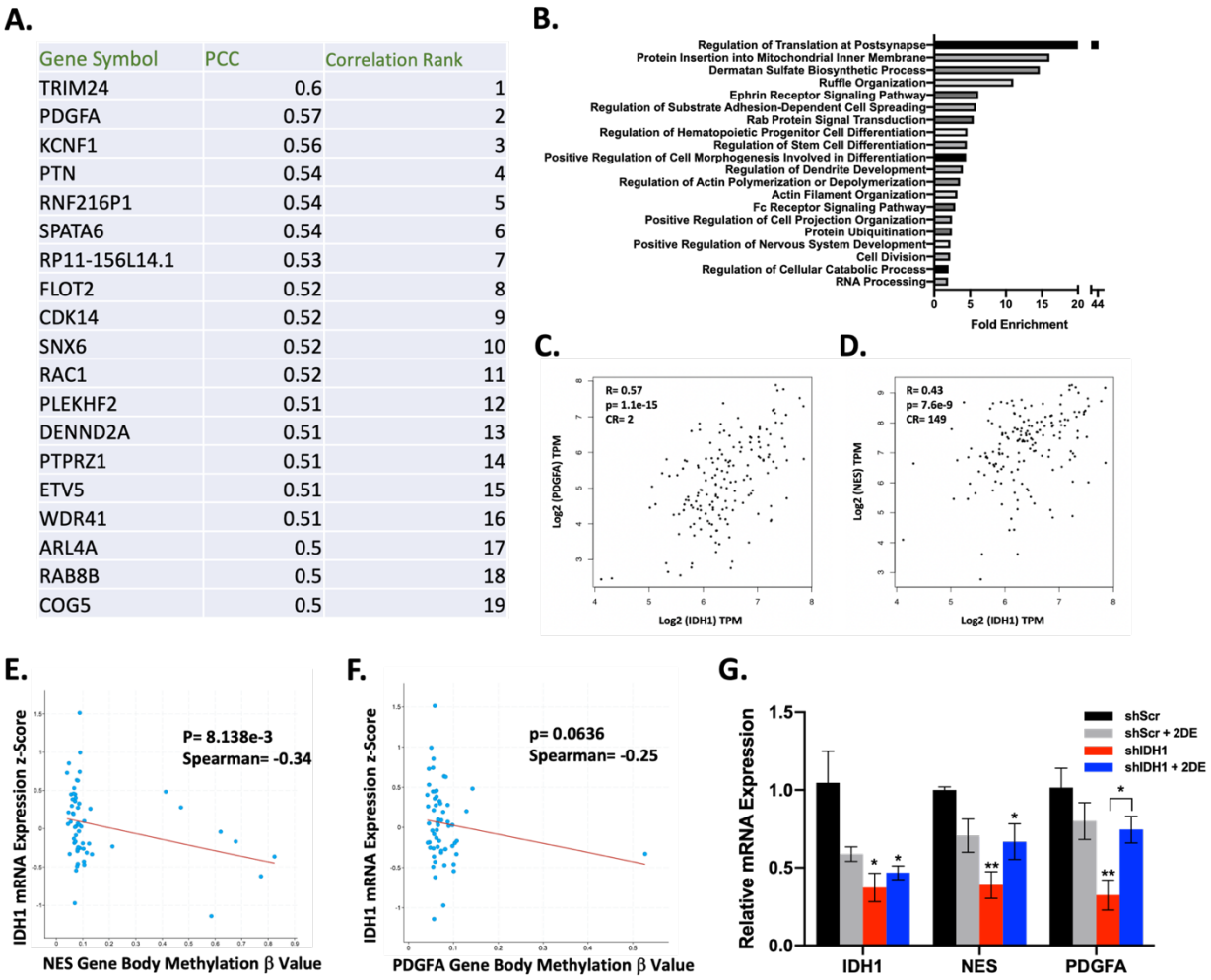

Figure 10. IDH1^{WT} Regulates Expression of Classical and Proneural Driver Genes
(**A**) TCGA dataset analysis profiling top mRNA correlates with IDH1^{WT} transcript level in GBM. (**B**) Gene-ontology analysis of the top 500 TCGA IDH1^{WT} correlates. (**C, D**) TCGA-GBM correlation analysis between IDH1^{WT} transcript level and PDGFA, NES mRNA levels, respectively. (**E, F**) TCGA-GBM correlation analysis between IDH1^{WT} transcript levels and NES, PDGFA, gene body methylation, respectively. (**G**) qPCR analysis of IDH1^{WT}, NES, and PDGFA mRNA levels in GIC-387s stably expressing sh-IDH1^{WT} construct (shIDH1) or sh-scramble (shScr) treated with vehicle or 0.5 μM 5-Aza-2'-deoxycytidine (2DE) for 24h. PCC= pearson correlation coefficient; TPM= transcripts per million; R= correlation coefficient; CR= correlation rank; * $p < 0.05$; ** $p < 0.01$.

3.2.3 IDH1^{WT} Expressing GICs Adopt a Radial Glia-like Identity

Radial glia represent a cellular population that gives rise to the vast majority of neurons and glia within the brain during development. Recently, an outer radial glia (oRG)-like population of GICs was identified that can give rise to each cell type comprising GBM tumor mass (*58*). Of note, the radial glia transcriptome is modulated in a temporal manner in response to ever changing developmental gradients (*59, 200*). Both NES and PDGFA are expressed within radial glia in a temporal manner, with NES expression emerging during radial glia genesis in response to apical-basal Notch gradient levels, before PDGFA expression and glial features are detected during late embryogenesis (*201, 202*). Based on these data we hypothesized that IDH1^{WT} expression induces an oRG-like identity in GICs. Within human patient samples, as assessed through analysis of the TCGA dataset, we observed high correlation between an oRG gene signature [as described in (*60*)] and IDH1^{WT} expression (Fig. 11A). As PTPRZ1 is the master regulator of the oRG-like GIC identity (*58*), we assessed for correlation between IDH1^{WT} and PTPRZ1. These two genes were highly correlated, with a CR of 14 (Fig. 10A, 11B). Gene body methylation, however, was not correlated with IDH1^{WT} mRNA expression (data not shown). We further note that the ligand for PTPRZ1, Pleiotrophin (PTN) exhibited a statistically significant CR of 4 (Fig. 10A). To directly assess whether IDH1^{WT} may be promoting an oRG-like cellular state, we performed RT-qPCR for IDH1^{WT} in GICs modified for stable IDH1^{WT} over-expression and knockdown. Elevated IDH1^{WT} resulted in increased PTPRZ1 and the canonical radial glia marker VIM expression whereas reduced of IDH1^{WT} expression was associated with lower expression of PTPRZ1 and VIM (Fig. 11C, D). Collectively, these data support IDH1^{WT} expression promoting an oRG-like GIC identity.

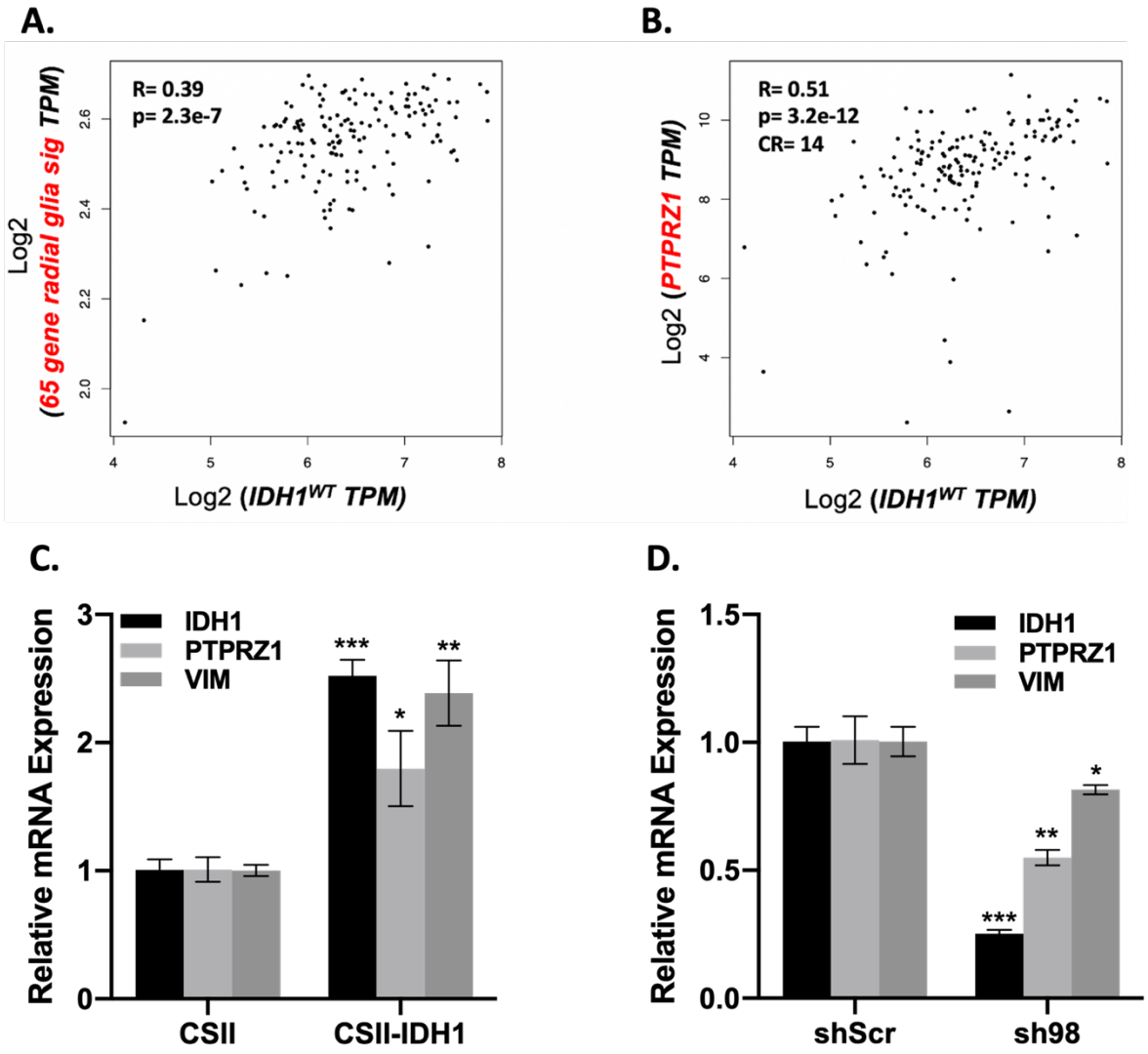

Figure 11. IDH1^{WT} Promotes an oRG-like GIC identity
(**A**) TCGA-GBM dataset analysis of IDH1^{WT} mRNA correlation with outer radial glia gene signature (n= 65 genes). (**B**) TCGA-GBM dataset analysis of IDH1^{WT} transcript correlation with PTPRZ1 mRNA levels. (**C**) qPCR analysis of IDH1, PTPRZ1, and VIM mRNA levels in GICs stably expressing sh-IDH1^{WT} construct (shIDH1) and sh-control (shScr) constructs. (**D**) qPCR analysis of IDH1^{WT}, PTPRZ1, and VIM mRNA levels in GICs stably over-expressing IDH1^{WT} (Wt-IDH1) or control (CSII). TPM= transcripts per million; R= correlation coefficient; CR= correlation rank; * $p < 0.05$; ** $p < 0.01$; *** $p < 0.001$

The oRG gene signature that IDH1^{WT} strongly correlates with is enriched for genes implicated in epithelial to mesenchymal transition and invasive behavior (*58*). Moreover, oRG-like GICs mimic

cortical developmental programs, utilizing mitotic somal transfer in order to invade neighboring tissue within the brain and seeding for future tumor propagation and recurrence (*58*). We therefore tested whether $IDH1^{WT}$ expression within GICs contributes to invasive and migratory properties. In a transwell invasion assay, we found that $IDH1^{WT}$ over-expression significantly enhanced invasion through Matrigel (Fig. 12A). By contrast, $IDH1^{WT}$ knockdown ablated the capability of GICs to migrate through Matrigel (Fig. 12B). To assess whether $IDH1^{WT}$ expression influences migratory behavior, we performed a wound healing assay which mimics in vivo cellular migration using adherent LN382 cells. In line with our invasion assay results, we observed that a reduction in $IDH1^{WT}$ significantly decreased the migratory capacity of glioma cells (Fig. 12C, D). Together our data indicates $IDH1^{WT}$ as regulator of oRG-like identity and phenotypes.

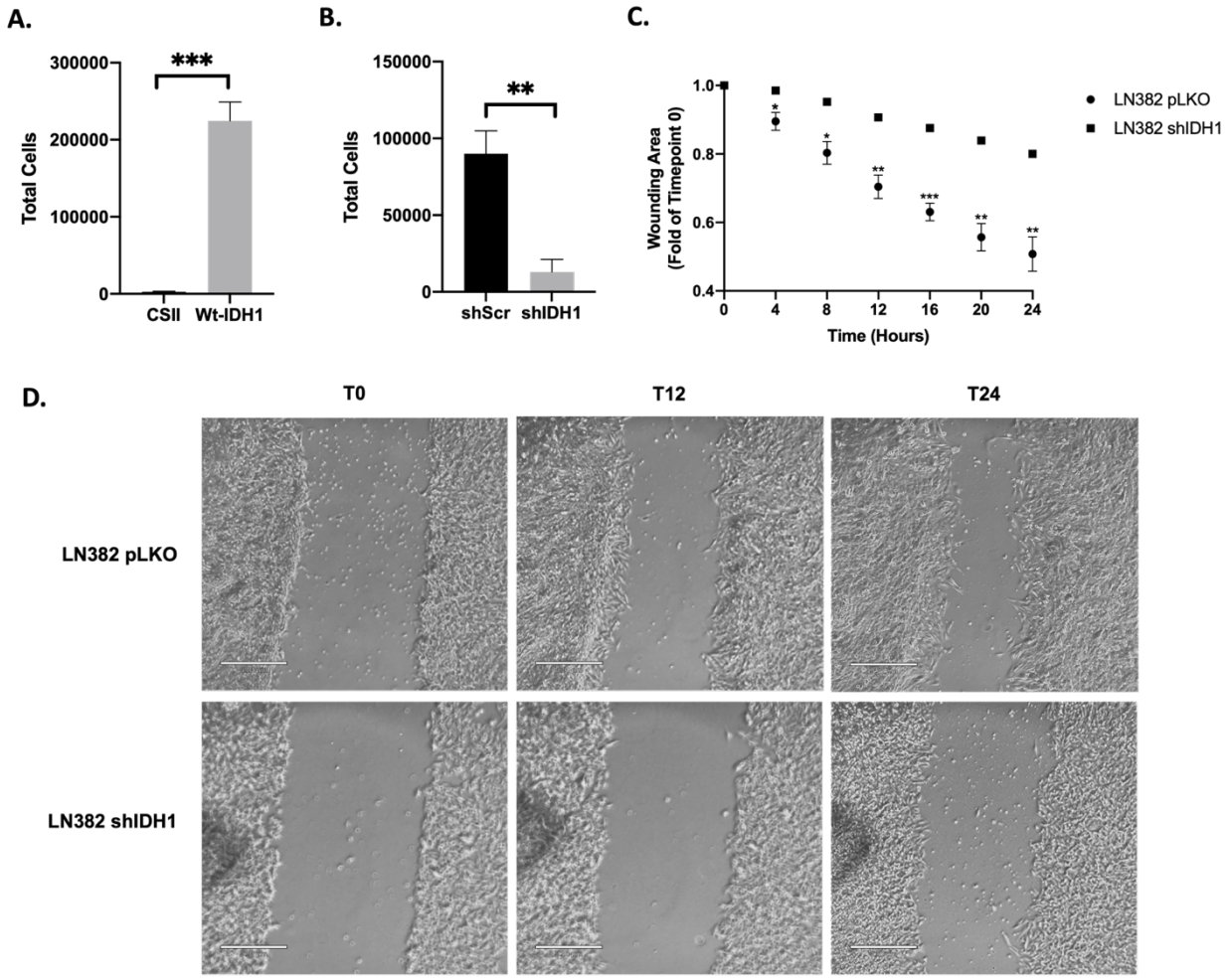

Figure 12. IDH1^{WT} increases invasion and migration in GBM cells
(**A**) Transwell migration assay. Quantification of total number of IDH1^{WT}-overexpressing GIC-387s (Wt-IDH1) vs control GIC-387s (CSII) that invaded through Matrigel after 36h. (**B**) Transwell migration assay. Quantification of total number of shIDH1^{WT} GICs (387 sh98) vs shScr GICs (387 shScr) that invaded through Matrigel after 36h. (**C**) Wound healing assay. Quantification of wounding area closure in patient derived LN382 glioma cells stably expressing sh-IDH1^{WT} knockdown (LN382 shIDH1) or control (LN382 pLKO) constructs. (**D**) Representative images of area quantified during wound healing assay. * $p < 0.05$; ** $p < 0.01$; *** $p < 0.001$

3.3 Discussion

We have demonstrated that IDH1^{WT} is upregulated within each molecular subtype of GBM and that this upregulation promotes GIC stem cell-like properties and marker expression indicative of

an oRG-like cellular state. Underlying transcriptional aberrations were associated with increased αKG production and robust epigenetic dysregulation, including a DNA hypomethylation phenotype. This DNA hypomethylation phenotype underscores how $IDH1^{WT}$ regulates the expression of classical and proneural GBM driver genes NES and PDGFA. Importantly, $IDH1^{WT}$ controls the expression of radial glia master regulator PTPRZ1 and canonical marker VIM through yet to be determined (epigenetic) mechanisms. We have further shown that expression of $IDH1^{WT}$ within GICs is sufficient for promoting a pro-migratory and invasive phenotype, a hallmark of oRG-like GICs. Collectively, these findings support our central hypothesis that $IDH1^{WT}$ promotes a stem-like cellular state that influences molecular subtype at least in part via unique DNA or chromatin modifications.

Our data shows that $IDH1^{WT}$ is capable of evoking widespread epigenetic remodeling via production of αKG. This epigenetic remodeling is associated with an increase in stem-cell like characteristics including elevated proliferation and resistance to differentiation. Moreover, we have shown that the regulation of DNA methylation is the mechanism by which $IDH1^{WT}$ controls expression of stemness factors NES and PDGFA. Whereas IDH-mutant gliomas present with profound CpG Island and DNA hypermethylation (*203*) we observed $IDH1^{WT}$ expression to be correlated with a DNA hypomethylation phenotype. We hypothesize that $IDH1^{WT}$'s effect on DNA methylation is mediated by the Ten-eleven translocation methylcytosine dioxygenase (TET) family of αKG-dependent demethylases. Mechanistically, TET proteins are responsible for oxidation of 5'-methylcytosine to 5'-hydroxymethylcytosine, the first step in the DNA demethylation process (*204*). In the context of grade IV IDH-mutant astrocytoma, however, IDH^{Mut}

derived (R)-2HG actively competes with αKG, resulting in diminished TET activity and associated DNA hypermethylation (*103*). Importantly, the epigenetic modulatory activity of TET proteins is critical for maintaining stem cell state during embryogenesis (*205*). Though our results are preliminary, and an activity assay needs to be performed, it stands to reason that excess αKG production stimulates TET hydroxylase activity resulting in DNA hypomethylation phenotype in the context of IDH-wildtype GBM.

Our finding that $IDH1^{WT}$ can control multiple stemness associated factors, such as NES and PDGFA, is intriguing. While GBM molecular subtypes are a key concept that have been adopted, built upon, and informed therapeutic development since their identification, recent data, however, suggests this ideology should be reevaluated. GBM scRNA-Seq has demonstrated that patient-derived tumors of a specific, predominant subtype, consist of subpopulations of tumor cells with unique cellular states that map to each of the three molecular subtypes, with the highest frequency subpopulation establishing the predominant molecular subtype (*39, 41*). While grade IV IDH-mutant astrocytoma tumors consist of one proliferative, NPC-like cellular state, ~90% of tumor cells exist within non-proliferative, differentiated oligodendrocyte-like (OC-like) and astrocyte-like (AC-like) cellular states. By contrast IDH-wildtype tumor cells are composed of proliferating NPC-like, OPC-like, mesenchymal-like (MES-like), and AC-like cellular states. Importantly, unlike grade IV IDH-mutant astrocytomas, an isolated population of any one IDH-wildtype GBM cellular state can give rise to the diverse spectrum of cellular states upon orthotopic transplantation (*41*). Underlying genetic mutations such as EGFR amplification can influence initial cellular states

and lineage differentiation, however, our knowledge of further intrinsic and environmental cues influencing cellular plasticity is incomplete (*58, 206*).

Here, we propose that IDH1^{WT} is a critical factor for maintaining IDH-wildtype GIC stemness and plasticity by promoting an oRG-like cellular state. While NES and PDGFA are typically markers of adult NPC and OPC populations, respectively, they are temporally expressed within radial glia cells in response to developmental needs and morphogenic gradients during embryogenesis (*201, 202*). Bhaduri et al. recently identified an oRG-like cellular state that becomes reactivated within IDH-wildtype GBM patient samples (*58*). They further demonstrated that this oRG-like GIC population can give rise to genetically diverse cells and therefore may represent a driving force of GBM intratumoral heterogeneity. Our observations that IDH1^{WT} highly correlates with an oRG gene signature within GBM patients, regulates the expression of the oRG master regulator PTPRZ1, the canonical marker VIM, as well as PDGFA and NES, and facilitates an invasive phenotype support IDH1^{WT} as a regulator of the oRG-like GIC state. We speculate that tumors derived from an orthotopic xenograft model overexpressing IDH1^{WT} would consist of the four cellular states identified by Neftel et al. 2019. as tumor cell and stem cell niches provide necessary support for expansion and differentiation (*58, 60*). Thus, our model suggests that by establishing an oRG-like GIC state, IDH1^{WT} promotes a high-level cellular plasticity that facilitates the transition into NPC-like, OPC-like, MS-like and AC-like cellular states in response to physiological stress and developmental cues.

While exciting, our data is preliminary. First, the majority of our in vitro studies were performed

via manipulation of the patient-derived cell line, GIC-387. GIC-387 cells are characterized by EGFR amplification, typical of classical GBM molecular subtype. It will be necessary, in future studies, to expand these experiments by including patient derived GICs of each molecular subtype, to support our central thesis that $IDH1^{WT}$ is eliciting widespread reprogramming to an oRG-like cellular state, and promotes intratumoral heterogeneity in cell and most importantly, in orthotopic tumor models in vivo. Secondly, though we have shown three canonical markers of oRG-like GIC cellular identity (PTPRZ1, VIM, NES) are controlled by $IDH1^{WT}$ expression, we have yet to show that these GICs are capable of undergoing mitotic somal translocation (MST). While our data certainly support an oRG-like identity, future studies are required to identify MST events as the molecular driver of GIC invasion, both in cells *in vitro* and animal models *in vivo*.

Notwithstanding, though, the presented data furthers our understanding of $IDH1^{WT}$'s role in GBM. We have comprehensively documented correlations between $IDH1^{WT}$ expression and the expression and DNA methylation of development genes in the TCGA dataset. We rationalized that highly correlated genes in human patients may be regulated by $IDH1^{WT}$ expression due to the robust epigenetic dysregulation excess αKG elicits. The data presented which identified stemness factors in an unbiased manner regulated by $IDH1^{WT}$ supports our methodology. Our gene set enrichment analysis of top $IDH1^{WT}$ transcriptional correlates revealed a variety of molecular processes beyond stem cell maintenance and will motivate further studies to fully define the impact of $IDH1^{WT}$ on GBM tumor genetics.

CHAPTER 4: PHARMACOLOGICAL INHIBITION OF IDH1^{WT} PROMOTES FERROPTOSIS

4.1 Abstract

Cancer cells maintain elevated levels of nicotinamide adenine dinucleotide phosphate (NADPH) to fuel biosynthetic reactions in support of rapid cellular growth and in powering redox defense mechanisms. Mechanistically, NADPH is a rate-limiting reducing equivalent required for de novo lipid biogenesis, and for maintaining a reservoir of reduced glutathione (GSH)—a key intermediary in redox defense as well as ferroptosis regulation (*207*). Ferroptosis is a programmed cell death pathway driven by the peroxidation of phospholipids and is regulated by the Glutathione peroxidase 4 (GPX4) lipid repair pathway (*208, 209*). Importantly, GSH functions as an indispensable co-factor for GPX4 activity, providing a mechanistic link between NADPH production and ferroptosis regulation (*210*). Due to its role in supporting lipid biosynthesis and maintaining a reservoir of GSH critical for redox and ferroptosis defense, NADPH metabolism has emerged as an enticing metabolic vulnerability and potential point of therapeutic intervention within cancer cells.

Our group has recently identified that IDH-wildtype GBM upregulate wild-type Isocitrate Dehydrogenase 1 ($IDH1^{WT}$) to generate large pools of cytosolic NADPH (*33*). RNAi-mediated knockdown of $IDH1^{WT}$ slows patient derived xenograft tumor growth while over-expression increases tumor burden. We identified that elevated levels of NADPH fuel de-novo lipid biogenesis, supporting rapid growth and proliferation of high grade glioma (HGG) tumor cells. Further, we showed that this excess NADPH generated by $IDH1^{WT}$ associated with reduced reactive oxygen species (ROS) production. These data support $IDH1^{WT}$'s role in HGG pathogenesis and progression via elevating lipid-biosynthesis and enhancing protection from lipid

peroxidation. Based on these findings, **we hypothesize that IDH1^{WT} protects HGG tumors from ferroptotic cell death and is a therapeutically viable drug candidate for ferroptosis induction in GBM tumors**. As IDH1^{WT} global knockout mice present phenotypically normal (*122*), we further hypothesize that inhibition of IDH1^{WT} will have minimal toxicity on healthy tissue.

4.2 Results

4.2.1 IDH1^{WT} Suppresses Ferroptosis via Regulation of the Cysteine/GSH/GPX4 Axis

Enhanced lipid biosynthesis in support of unabated cancer cell growth is a hallmark of tumorigenesis. Our group demonstrated that IDH1^{WT} promotes lipogenesis by providing tumor cells with cytosolic NADPH, which represents a rate- limiting reducing equivalent required for de novo fatty acid synthesis (*33*). Phospholipids of the plasma membrane, however, are susceptible to reactive oxygen species (ROS)-mediated peroxidation which in turn triggers ferroptosis. Ferroptosis is actively inhibited by Glutathione Peroxidase 4 (GPX4) mediated reduction of deleterious peroxides via oxidation of the potent antioxidant reduced glutathione (GSH). The cysteine/GSH/GPX4 lipid repair axis that inhibits ferroptosis has multiple steps that could be regulated by IDH1^{WT} products NADPH and αKG (Fig. 13). As such, we hypothesized that IDH1^{WT} protects glioma cells from ferroptotic death in part through increased GPX4 lipid repair.

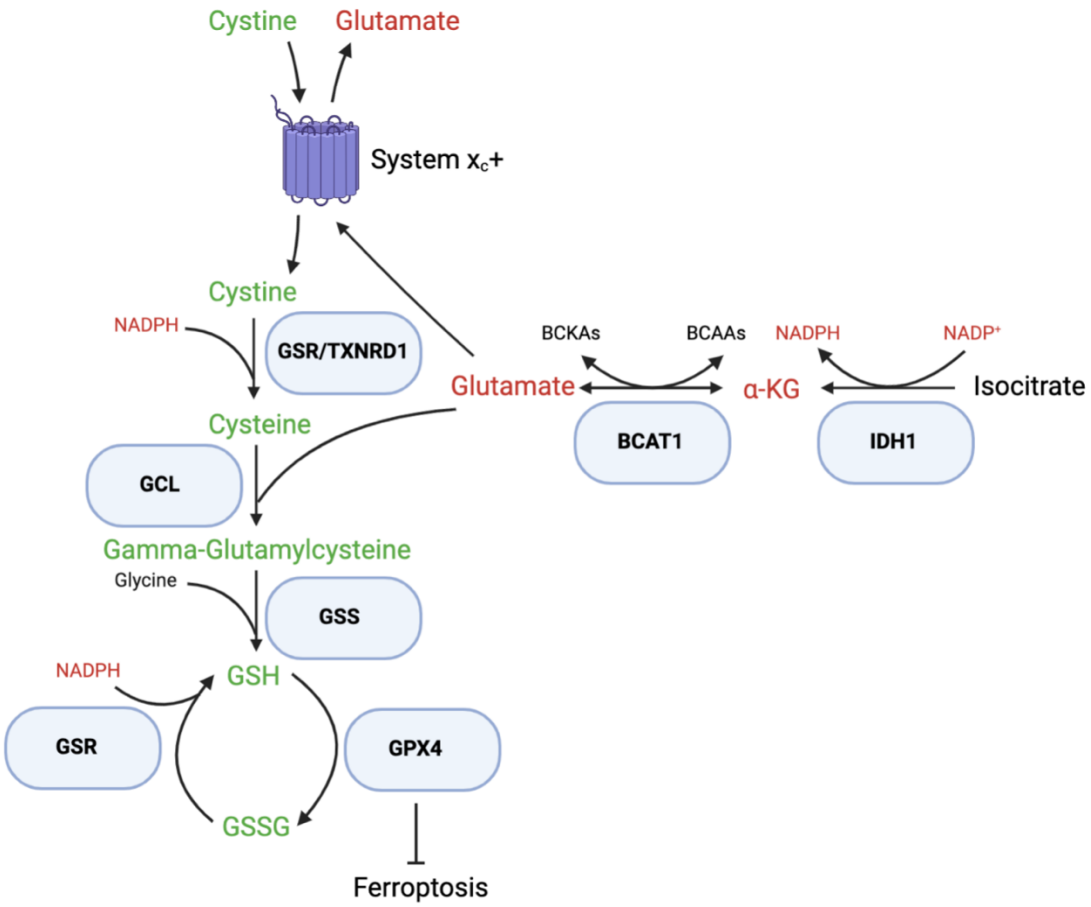

Figure 13. Overview of cysteine/GSH/GPX4 lipid repair axis
Ferroptosis inhibiting cysteine/GSH/GPX4 lipid repair axis and points of potential IDH1^{WT} regulation. Extracellular cystine import is coupled with glutamate efflux at a 1:1 ratio via glutamate/cystine antiporter, System x_c+. Cystine is subsequently reduced to cysteine in an NADPH manner via Glutathione Reductase (GSR) or Thioredoxin Reductase 1 (TXNRD1). Glutamate cysteine ligase (GCL) generates gamma-glutamyl cysteine via ligation of cysteine and glutamate. Glutathione synthetase in turn catalyzes the condensation of gamma-glutamyl cysteine and glycine, forming reduced glutathione (GSH). Glutathione peroxidase 4 (GPX4) converts toxic lipid hydroperoxides to non-toxic peroxide alcohols at the expense of GSH, yielding oxidized glutathione (GSSG). To maintain a reservoir of available GSH within the cell, Glutathione reductase (GSR) utilizes NADPH to reduce GSSG to GSH. Glutamate to fuel the import of cystine and gamma-glutamylcysteine production can be generated from the Branched chain amino transferase 1 (BCAT1) mediated transamination of the IDH1^{WT} product αKG. Red text indicates points of regulation IDH1^{WT} can directly influence via its products. NADPH= nicotinamide adenine dinucleotide phosphate; BKCA= branched chain alphaketo acids; BCAA= branched chain amino acids.

As ferroptosis is initiated in response to unabated oxidative stress which in turn initiates lipid peroxidation we sought to determine whether IDH1^{WT} protects against such cellular stress. Glioma Initiating Cells (GICs) manipulated for stable IDH1^{WT} knockdown (shIDH1) expression showed increased levels of ROS as determined by CellROX Red, a dye that becomes fluorescent in the presence of ROS (Fig. 14A). Because GSH is a potent antioxidant critical for cellular response to

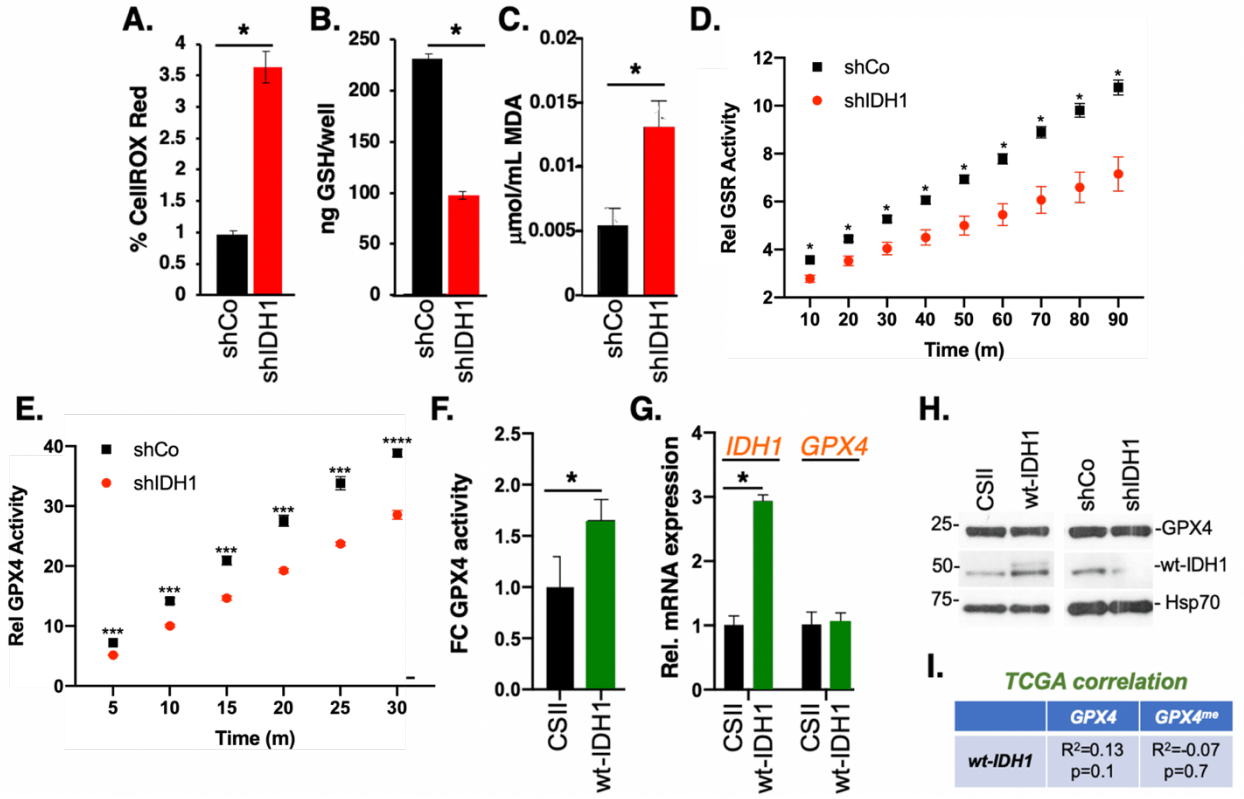

Figure 14. IDH1^{WT} controls lipid repair via regulation of the cysteine/GSH/GPX4 axis
(**A-C**) Quantification of ROS, GSH, and lipid peroxidation levels within GIC cells with stable IDH1^{WT} knock-down (shIDH1) vs control (shCo). (**D**) Relative GSR activity in shIDH1 vs shCo LN382s. (**E**) Relative GPX4 activity in shIDH1 vs shCo LN382. (**F**) Fold change of GPX4 activity in GICs over-expressing IDH1^{WT} (wt-IDH1) vs control (CSII). (**G**) qPCR analysis of relative IDH1^{WT} and GPX4 mRNA expression in CSII and wt-IDH1 GICs. (**H**) Western analysis of GPX4 and IDH1^{WT} protein levels in CSII and wt-IDH1 GICs. Hsp70 serves as loading control. (**I**) TCGA-GBM dataset analysis of IDH1^{WT} transcript correlation with GPX4 mRNA and gene body methylation (GPX4^{me}). ** $p < 0.05$; ** $p < 0.01$; *** $p < 0.001$; **** $p < 0.0001$.*

ROS, we hypothesized that IDH1^{WT} may exert antioxidative effect via enhancement of GSH production. Strikingly, IDH1^{WT} depletion resulted in significant reduction of intracellular GSH levels (Fig. 14B). This reduction in intracellular GSH levels correlated with an increase in malondialdehyde (MDA) detection, a marker for lipid peroxidation (Fig. 14C). During reduction of lipid hydroperoxides and ROS, GPX4 oxidizes GSH into oxidized glutathione (GSSG), which is subsequently reduced by Glutathione Reductase (GSR) to replenish the intracellular pool of GSH necessary for redox defense (Fig. 13). As NADPH is the essential cofactor for GSR, we tested whether IDH1^{WT} expression influences GSR activity. Stable knockdown of IDH1^{WT} expression resulted in a significant decrease in GSR activity (Fig. 14D). Correlating with reduced GSH level, the GPX4 activity was similarly reduced in IDH1^{WT} diminished cells (Fig. 14E). Conversely, over-expression of IDH1^{WT} successfully promoted GPX4 activity (Fig. 14F). The effect of IDH1^{WT} on GPX4 activity was mediated post-translationally, as manipulation of IDH1^{WT} levels failed to elicit an effect on GPX4 mRNA or protein levels (Fig. 14G, H). Similarly, TCGA analysis failed to uncover correlation between IDH1^{WT} transcript expression and GPX4 transcript level or gene body methylation (Fig. 14I). We note, however, that reduction of GPX4 activity in IDH1^{WT} knockdown cells was further exacerbated when the cells were not primed with supplemental GSH, due to GSR being incapable of reducing GSSG to GSH as a result of diminished NADPH levels (Fig. 15). As NADPH is required for inorganic selenate metabolism (*211*), we speculate that NADPH produced by IDH1^{WT} may also influence selenocysteine metabolism, thus impacting the functionality of the selenoprotein GPX4. Together, these data indicate that IDH1^{WT} regulates the cysteine/GSH/GPX4 axis.

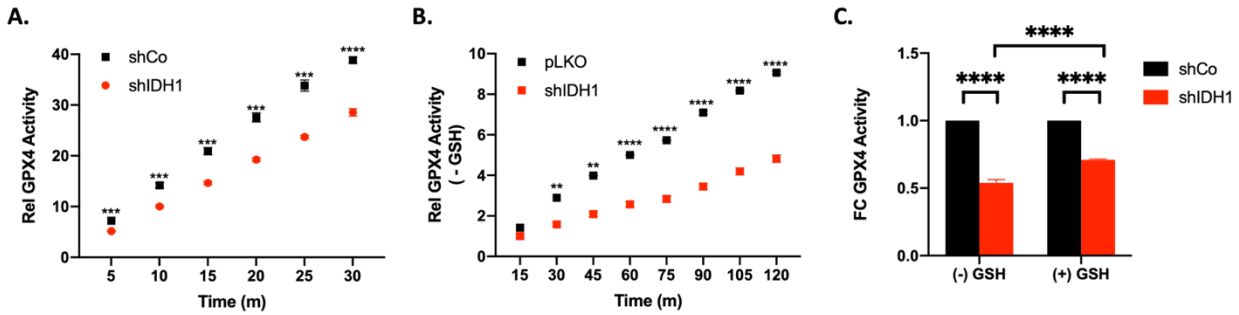

Figure 15. IDH1^{WT} reduces GPX4 activity independent of NADPH production
GPX4 activity assays performed on LN382 cells stably expressing IDH1^{WT} knockdown (shIDH1) and control (shCo). (**A**) nMole of NADPH depleted over time during GPX4 activity assay when assay is primed with supplemental reduced glutathione (GSH). (**B**) nMole of NADPH depleted over time during GPX4 activity assay when assay is not primed with supplemental GSH. (**C**) Relative fold change between LN382 shIDH1 and shCo with and without GSH priming.

Beyond providing reducing equivalents necessary for GSH maintenance, IDH1^{WT} can also provide carbon necessary for GSH biosynthesis via enhanced αKG production. In IDH-wildtype GBM, branched chain amino acid transaminase 1 (BCAT1) is actively upregulated, providing a pathway whereby αKG may be converted to glutamate (*115*). Glutamate, in turn, is converted into gamma-glutamyl cysteine, the immediate precursor to GSH, via glutamate cysteine ligase (GCL) (*107*). We therefore tested the hypothesis that IDH1^{WT} promotes GSH biosynthesis by providing of GSH metabolic precursor (Fig 13). In a GIC cell line modified for stable IDH1^{WT} knockdown, we performed $^{13}C_6$ isotope tracing experiments to quantify label incorporation into glutamate and GSH. In shIDH1 cells, the glucose carbon incorporation into glutamate was reduced compared to vector controls, as determined by LC-MS-based quantification of ^{13}C m+5 glutamate (Fig. 16A). Consistently, the glutamate derived fraction of GSH (carbons m+1 through m+5) was similarly reduced in shIDH1 cells (Fig. 16B), suggesting that depletion of IDH1^{WT} hinders GSH biosynthesis by limiting glutamate.

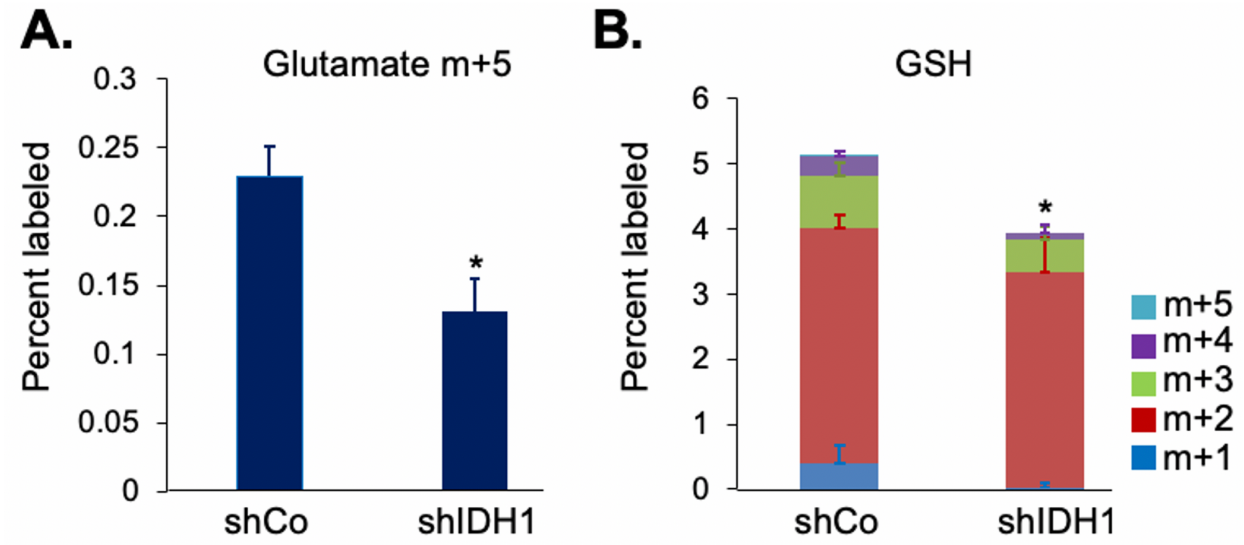

Figure 16. IDH1^{WT}-kd reduces GSH biosynthesis
Levels of $^{13}C_6$ label incorporation in GICs stable expressing IDH1^{WT} knockdown construct (shIDH1) and control (shCo) into glutamate (**A**) and reduced glutathione (GSH) (**B**). * $p < 0.05$.

Our data revealed that IDH1^{WT} regulates GSH biosynthesis, GSSG reduction, as well as overall GPX4 activity. We therefore hypothesized that IDH1^{WT} expression directly protects glioma cells from ferroptosis. Knockdown of IDH1^{WT} sensitized GICs to ferroptotic cell death initiated by RSL3, a potent GPX4 inhibitor and known inducer of ferroptosis (Fig. 17A). Conversely, IDH1^{WT} over-expression effectively protected cells from RSL3- mediated ferroptotic death (Fig. 17B). As radiation therapy (RT) is known to promote lipid peroxidation, priming cells for ferroptosis (*184, 212*), and is an essential component of GBM standard of care, we tested whether IDH1^{WT} expression similarly protects against RT induced cellular death. shIDH1 cells were more sensitive to RT induced cellular death relative to IDH1^{WT}-OE cells (Fig. 17B). Further, concomitant RT and RSL3 greatly enhanced cellular death relative to either treatment alone in control cells whereas

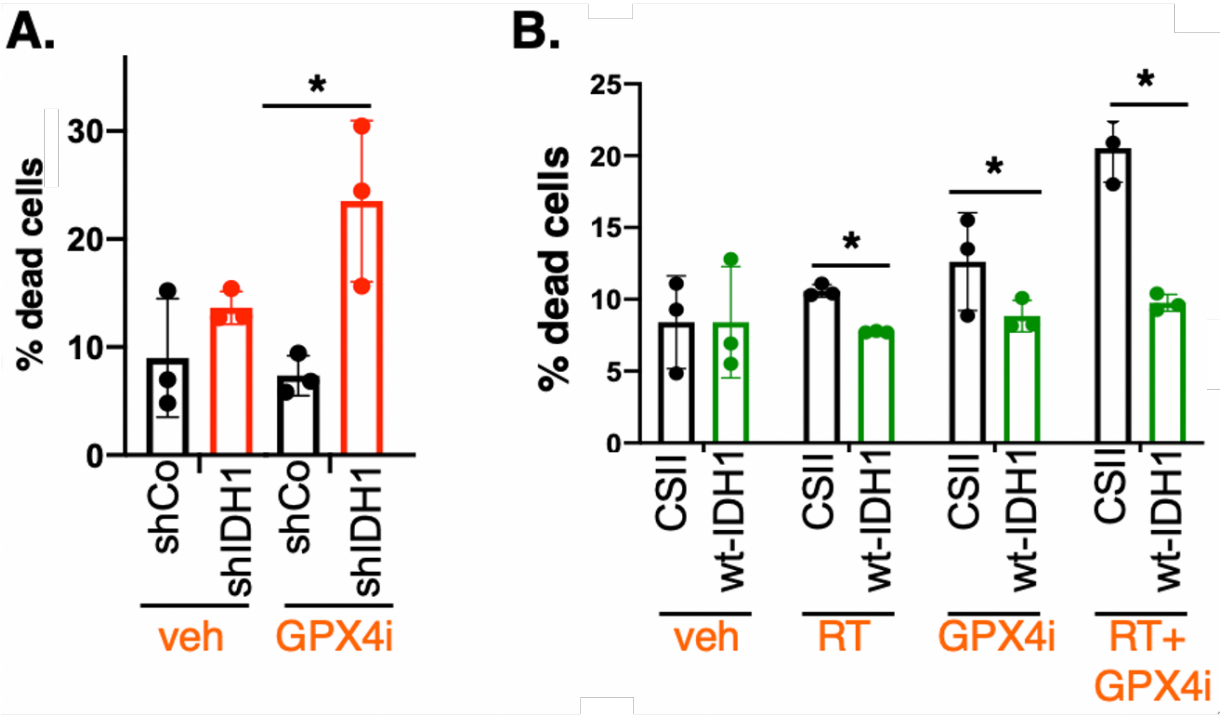

Figure 17. IDH1^{WT} protects from cell death mediated by ferroptosis inducer RSL3 and RT MTS assay quantifying cellular viability. (**A**) GIC cells with stable IDH1^{WT} knock-down (shIDH1) and control (shCo) treated with GPX4 inhibitor, RSL3 (GPX4i) or vehicle (veh). (**B**) GICs over-expressing IDH1^{WT} (wt-IDH1) vs control (CSII) treated with vehicle, radiation therapy (RT), GPX4i, or RT and GPX4i. * $p < 0.05$.

IDH1^{WT}-OE glioma cells were unperturbed (Fig. 17B). Collectively, these data identified IDH1^{WT} as a potent ferroptosis inhibitor in GBM cells.

4.2.2 Pharmacological IDH1^{WT} Inhibition Induces Ferroptosis

Our group has previously shown that treatment of a GBM patient-derived xenograft (PDX) mouse model with GSK864, an IDH1^{Mut} inhibitor with 'off-target' activity against IDH1^{WT} (IC_{50}= 466.5 nM against IDH^{WT}), decreases tumor burden and extends survival (*33*). Mechanistically, GSK864 allosterically modulates both mutant and wild-type IDH1 function by binding to the dimerization domain of IDH1, thereby preventing proper dimer formation required for enzymatic activity (*213*).

While these studies established proof-of-concept that pharmacological inhibition of $IDH1^{WT}$ is feasible and associated with anti-tumor activity, due to the limited potency of GSK864 we sought

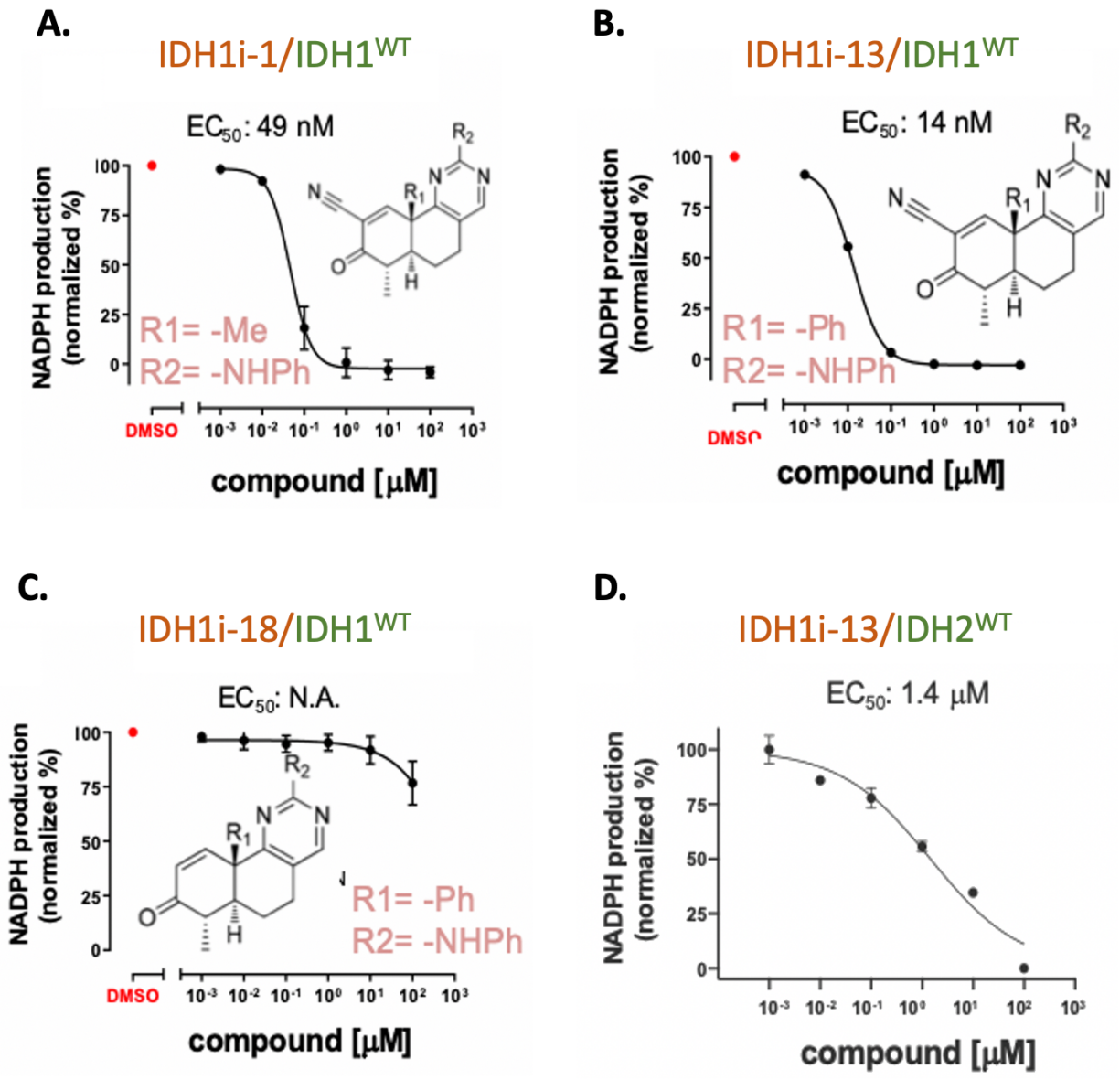

Figure 18. IDH1i-13 is a selective covalent inhibitor of IDH1^{WT}
NADPH production by recombinant IDH1^{WT} as a function of IDH1i-1 (**A**), IDH1i-13 (**B**), and IDH1i-18 (**C**) at indicated inhibitor concentrations. (**D**) NADPH production by recombinant IDH2^{WT} as a function of IDH1i-13 inhibitor concentrations. IDH1^{WT} activity assays performed by Dr. Daniel Wahl's lab at The University of Michigan.

to identify higher potency IDH1^{WT} inhibitors for comprehensive preclinical assessment. To identify such an inhibitor, our group in collaboration with Dr. Daniel Wahl and Sriram Venneti

(University of Michigan) and AbbVie performed high-throughput screening of the AbbVie library consisting of 750,000 proprietary compounds at 30 μM concentration to identify a compound with potent inhibition of $IDH1^{WT}$ NADPH production (*214*). Analysis of the candidate hits revealed a hit series centered around α,β-unsaturated enones that bind to the $IDH1^{WT}$ enzyme by forming a covalent bond with histidine 315 (H315) within the NADP substrate binding pocket, competing with NADPH access. This covalent inhibition yielded robust inhibition of $IDH1^{WT}$ enzymatic activity, with an EC_{50} of 49 nM that, upon further hit-to-lead optimization, led to the identification of IDH1i-13, which showed an EC_{50} of 14 nM (Fig. 18A, B). Of note, a structurally related yet inactive enone (IDH1i-18) failed to inhibit $IDH1^{WT}$ (Fig. 18C). To determine if IDH1i-13 may affect the activity of other known NADPH binding proteins we investigated sequence homology via BLASTp, focusing on the series of amino acids within $IDH1^{WT}$'s NADPH binding pocket surrounding H315. BLASTp revealed NADPH binding pocket sequence homology between $IDH1^{WT}$ and the closely related, mitochondrial NADPH generating Isocitrate Dehydrogenase 2 ($IDH2^{WT}$) (Fig. 19A). Further comparison of $IDH1/2^{WT}$ binding pocket sequence with all other known NADPH binding proteins revealed the sequence is unique among these two Isocitrate Dehydrogenase family members (Fig. 19B, C). For increased potency, the drug candidate was modified during optimization to fill a lipophilic groove between K374/L383/A378. Importantly, within $IDH2^{WT}$ these amino acids and those within the region lack homology with $IDH1^{WT}$, suggesting enhanced specificity (Fig. 19C). Performing an inhibition assay, IDH1i-13 was less efficient at inhibiting recombinant $IDH2^{WT}$, with an EC_{50} 100-fold higher than that of recombinant $IDH1^{WT}$ (Fig. 18D).

A.

Genes	Total Score	Query Cover	E value	Per. Ident	Sequences	Input
					EAAHGTVTRH	Query
IDH1	34.1	100%	0.002	100.00%	EAAHGTVTRH	Subject
					EAAHGTVTRH	Query
IDH2	34.1	100%	0.002	100.00%	EAAHGTVTRH	Subject
					AHGTVT	Query
IgH	21	60%	66	100.00%	AHGTVT	Subject
					AHGTVTRH	Query
IGFLR1	21	80%	96	87.50%	AHGT-TRH	Subject
					AAHGTVT	Query
TNR	20.2	70%	194	85.71%	AVHGTVT	Subject
					AAHGTVTRH	Query
E4F1	19.7	90%	277	66.67%	AEHGTLNRH	Subject
					HGTVTRH	Query
KRTCAP3	19.7	70%	277	85.71%	HGTVLRH	Subject
					EAAHGTV	Query
CSMD2	19.3	70%	395	85.71%	EMAHGTV	Subject
					TVTRH	Query
CYLC1	19.3	50%	395	100.00%	TVTRH	Subject
					TVTRH	Query
HAX1	19.3	50%	396	100.00%	TVTRH	Subject

B.

Symbol	In Complex With	Largetst Pocket Sequence	2nd Largest Pocket Sequence
Akr1b10	NADP+	YSPLGSPD	IPKSVT
Akr1c21	NADPH	YGVLGTQ	LNTSLK
Aspdh	No Data	No Data	No Data
Cat	No Data	No Data	No Data
Cbr3	NADP+	GANRGIC	LDID/NAAV
Cbr4	NADP	PGFIA*TPMT	GA*GSGIG
Crym	NADPH	CAGVQA	VTMAT
Cryz	NADP	HGASGGVG	VVGSR
Decr1	No Data	No Data	No Data
Dhfr	NADPH	IGKNGDLP*W	VGGSSVYK*E
Dpyd	NADPH	LGAGDTA	GMANT
Dus2	No Data	No Data	No Data
Fdxr	NADP	GQGNVAL*D	SIGY/PTGV
FMO	NADPH	VGGASSAN*D	CTGY/LQTN
G6PD	NADP	LALPPTVY	GASGDLA
Gapdh	NADP	NGFGRIGR	GTGVF
Glyr1	No Data	No Data	No Data
Grhpr	No Data	No Data	No Data
Gsr	No Data	No Data	No Data
H6pd	NADP+	NER*KA*EV*R	FQ*YE
Hibadh	NAD+	IGLGNMG	YDVF/MLPT
Hmgcr	NADP+	SGDAMGMNMI*S	VGGG/TSRF
Hsd11b1	NADP+	GASKGIG	LGLID*TE*TA
Hsd17b1	NADP+	GCSSGI	LDVR/NAGL
Idh1	NADP	EAAHGTVTRH	KCATIT
Kcnab1	No Data	No Data	No Data
Lbr	No Data	No Data	No Data
Me1	No Data	No Data	No Data
Me3	No Data	No Data	No Data
Miox	NAD+	IGL*GGNNG	WTANT
Mthfr	NADP	VGRSK*IVG	CHSK/ATGQ/CGIN
Mtrr	NADP+	DAK*NMA*K*D	PGT/GCR/YVQ
Ndor1	No Data	No Data	No Data
Nnt	NADP+	MKRSL*GVGY	PVAGRMP
Nos1	NADP	PGTG	AIV/GCR/YVQ
Nos2	No Data	No Data	No Data
Nos3	No Data	No Data	No Data
Pgd	NADPH	GLAVMG	LVKA
Por	NADPH	PGTG	KV*YVQ
Qdpr	No Data	No Data	No Data
Srd5a1	No Data	No Data	No Data

C.

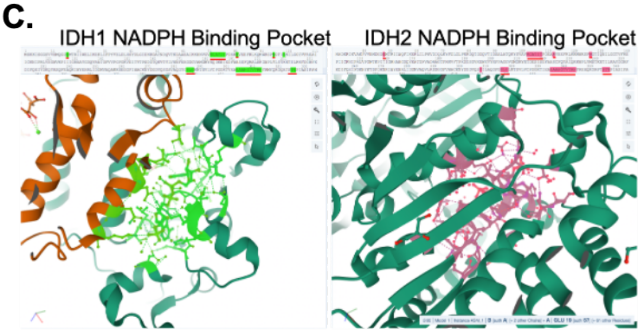

Figure 19. NADPH binding pocket sequence homology between IDH1^{WT} and IDH2^{WT}
(A) BLASTp analysis showing 100% sequence homology of 10 amino acid region around H315 ***(B)*** Binding pocket amino acid sequences of known NADP(H) binding proteins ***(C)*** X-ray crystallography of IDH1^{WT} and IDH2^{WT} NADPH binding pockets, sequence homology underlined in red.

Treatment of a spectrum of patient-derived glioma lines revealed IDH1i-13 decreased cellular viability in a dose dependent manner (Fig. 20A-C). We observed this decrease in cellular viability was accompanied by morphological changes atypical of apoptosis or necrosis. At higher concentrations, despite reduced volume of cells the plasma membranes appeared relative intact, lacking the extensive membrane rupture which is a hallmark of necrosis or the apoptotic bodies

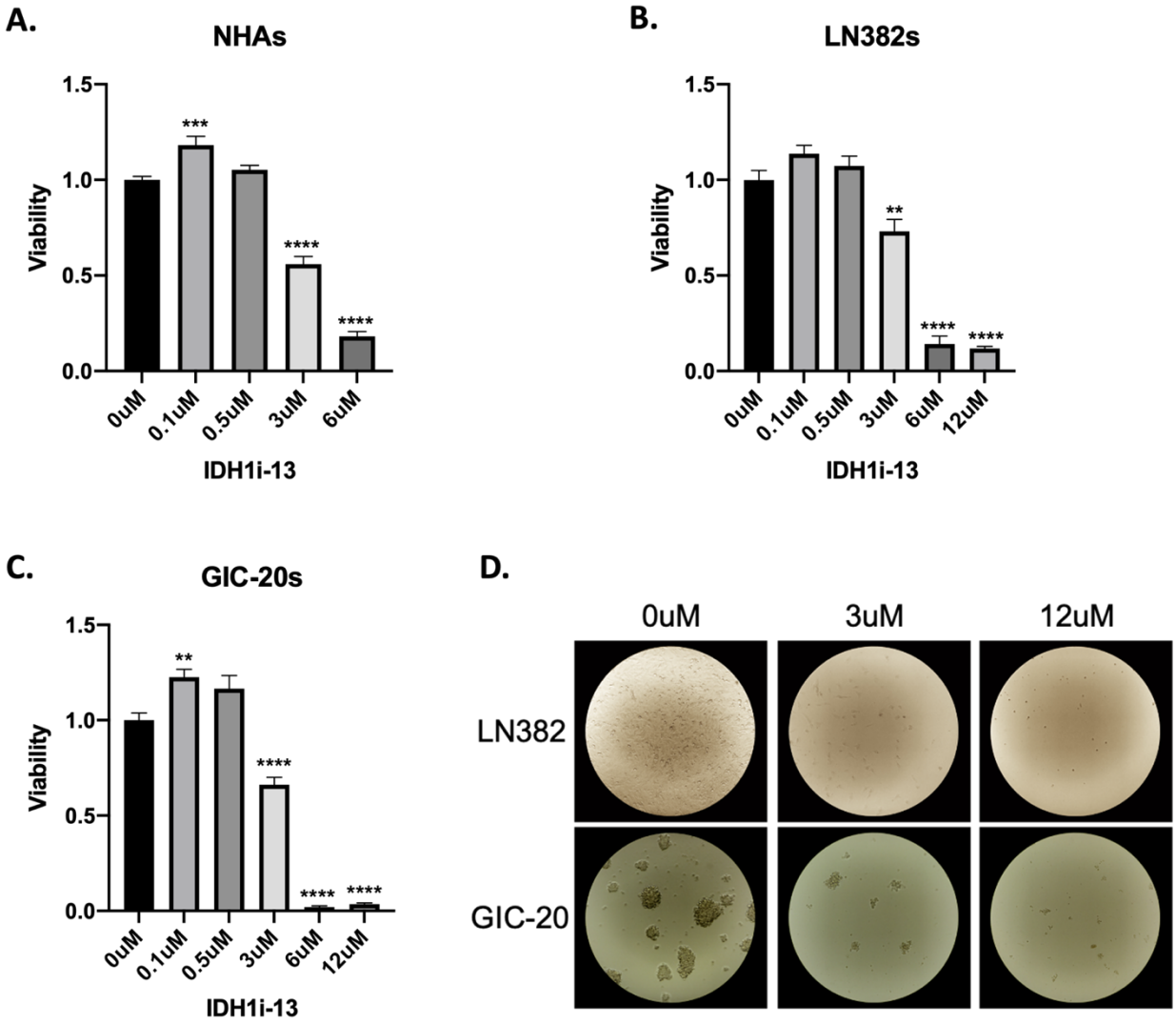

Figure 20. IDH1i-13 decreases glioma cell viability
(**A-C**) MTT assay performed on patient-derived cell lines capable of giving rise to glioma in orthotopic models treated with indicated concentrations of IDH1i-13 for 72h. ***(D)*** Representative microscopic images of LN382 cell IDH1i-13 treatment at indicated concentrations. NHA= immortalized normal human astrocytes. ** $p < 0.01$; *** $p < 0.001$; **** $p < 0.0001$.

that underscore apoptosis (Fig. 20D). To confirm that cell death was mediated by inhibition of $IDH1^{WT}$ enzymatic function, we concomitantly treated cells with IDH1i-13 and αKG, the product of $IDH1^{WT}$ enzymatic activity. Treatment with αKG potently rescued IDH1i-13 induced toxicity in a dose dependent manner suggesting that observed decrease in cellular viability is due to

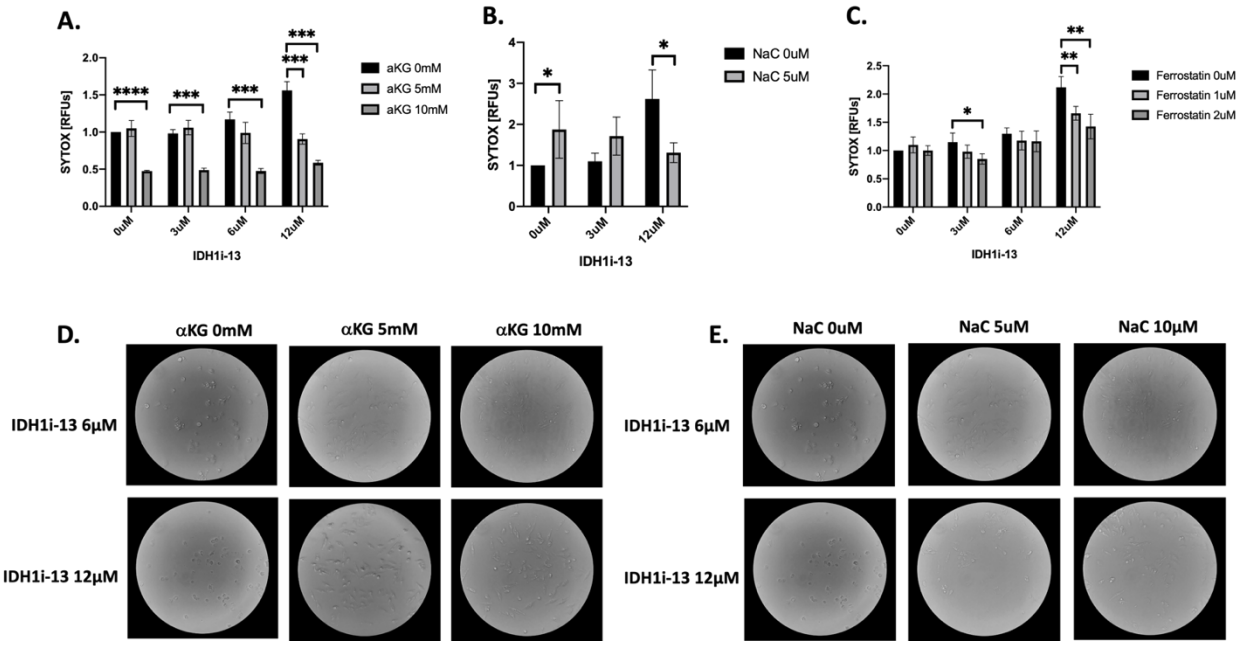

Figure 21. IDH1i-13 promotes ferroptosis
(**A-C**) SYTOX staining assessing non-apoptotic cellular death. Co-treatment of LN382 glioma with indicated concentrations of IDH1i13 and αKG (**A**) for 72h, NaC (**B**) for 48h, and ferrostatin (**C**) for 72h. (**D, E**) Representative microscopy images of αKG and NaC treatments, respectively. NaC= N-acetyl L-cysteine. * $p < 0.05$; ** $p < 0.01$; *** $p < 0.001$; **** $p < 0.0001$.

inhibition of IDH1^{WT} activity (Fig. 21 A, D). Based on our previous results showing IDH1^{WT} suppresses ROS production, we tested whether N-acetyl L-cysteine (NaC), known to increase antioxidant GSH levels, could rescue toxicity. NaC treatment completely abrogated glioma cell death induced by high concentrations of IDH1i-13 (Fig. 21B, E). As we previously showed that IDH1^{WT} protects cells from ferroptotic death, we tested whether a known ferroptosis inhibitor, ferrostatin, could rescue IDH1i-13 mediated cellular death. Ferrostatin was capable of rescuing IDH1i-13 mediated cellular death in a dose dependent manner (Fig. 21 C). Further, GSH was capable of mitigating IDH1i-13 mediated cellular death (Fig. 22A). Likewise, GSSG was similarly capable of mitigating IDH1i-13 toxicity, albeit to a lesser extent than its reduced counterpart (Fig. 22B). We theorize this partial rescue, as opposed to complete rescue, is due in part to depleted

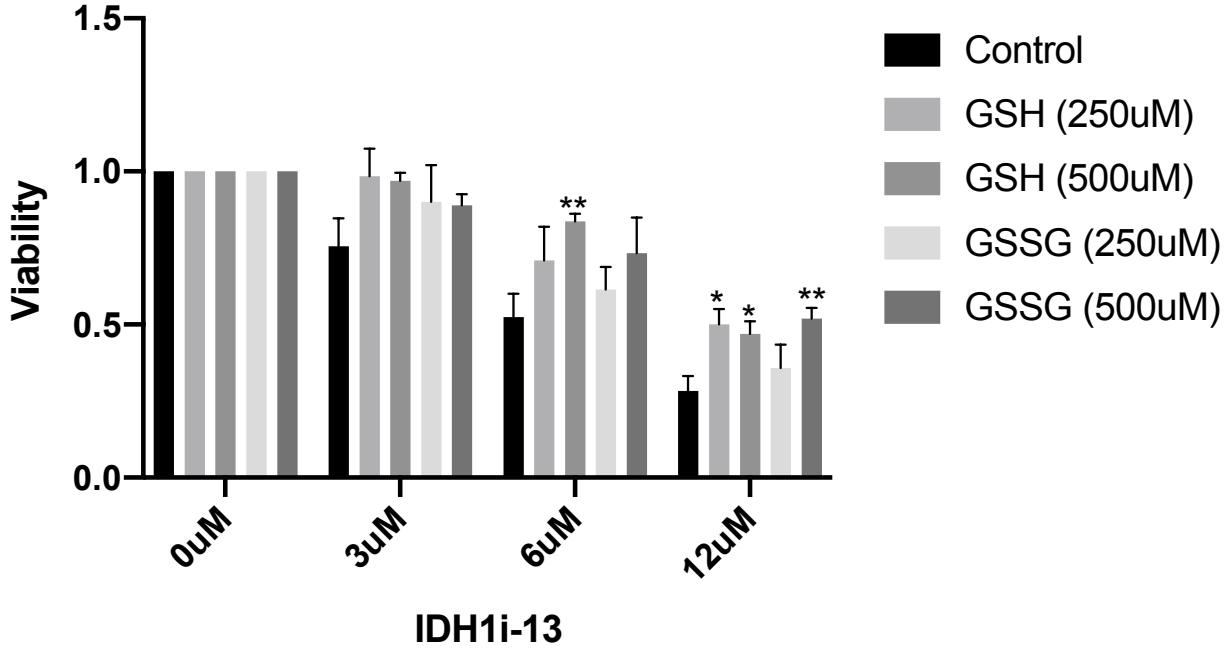

Figure 22. Glutathione partially rescues IDH1i-13 toxicity
MTT assay performed following co-treatment of LN382 with IDH1i13 and GSH or GSSG at indicated concentrations for 72h. * $p < 0.05$; ** $p < 0.01$.

NADPH reservoirs incapable of replenishing the GSH pool necessary to sustain GPX4 activity. Collectively, these data indicate that inhibition of $IDH1^{WT}$ enzymatic function via IDH1i-13 induces ferroptotic cell death.

4.2.3 IDH1i13 as a Viable Therapeutic Modality

To assess whether IDH1i-13 is a viable drug candidate for IDH-wildtype GBM patients, we tested the efficacy of this blood-brain barrier penetrant compound in vivo (*124*). Nude mice were orthotopically implanted with patient derived GICs modified for luciferase expression and upon initial tumor formation were treated to a regiment of radiation therapy (RT) and intraperitoneal IDH1i-13 injection as indicated (Fig. 23A). In conjunction with RT (a known inducer of lipid peroxidation), IDH1i-13 treated mice presented with decreased tumor burden as assessed via

bioluminescence monitoring and prolonged survival when compared to vehicle control mice (Fig. 23B-E). Importantly, we did not observe any toxicity within tumor adjacent regions of the hippocampus, cortex, and cerebellum which presented as pathologically normal (Fig. 23F-H). These data provide critical proof of concept that IDH1i-13 is a promising, therapeutically viable $IDH1^{WT}$ inhibitor.

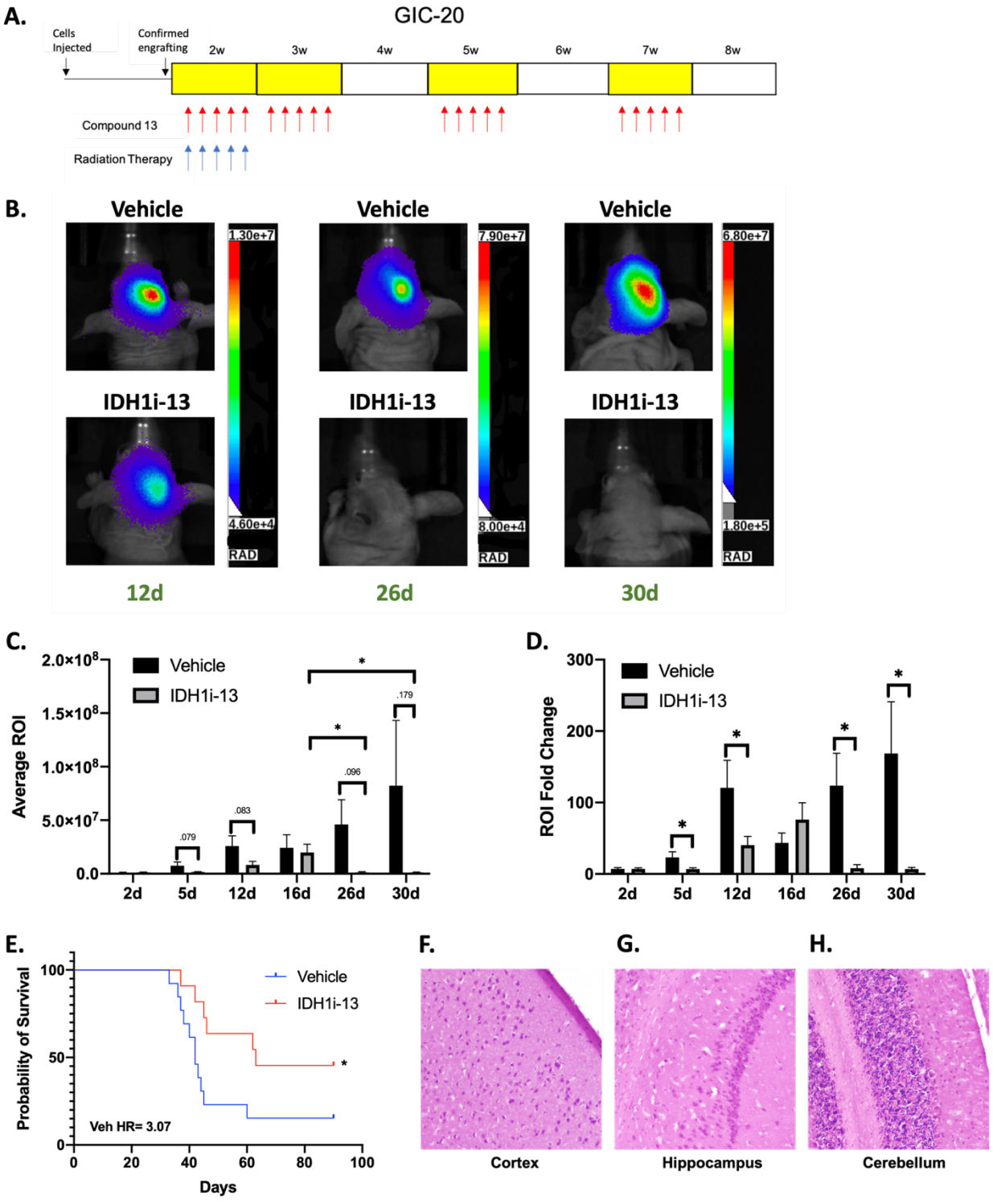

Figure 23. IDH1i-13 decreases tumor burden and extends survival in vivo

Orthotopic intracranial engraftment model of Nude mice with luciferase modified GIC-20 cells. (**A**) Schematic showing treatment regimen, arrows indicating points of treatment. IDH1i-13, 10mg/kg. RT, 2GY x 5 M-F (**B**) Representative In Vivo imaging system (IVIS) of bioluminescence within brain tumor bearing mice at indicated timepoints in days. (**C, D**) Quantification of average bioluminescence radiance within each treatment group at indicated time points in days. (**E**) Kaplan-Meier survival analysis. (**F-H**) Representative microscopy showing H&E staining of tumor adjacent brain region within IDH1i-13, radiation therapy treated mice. ROI= region of interest bioluminescence reading. * $p < 0.05$.

The IDH family of proteins have been implicated in a wide variety of diseases and similarly NADPH and αKG are critical metabolites within cancer cells (*74, 207*). As such, we sought to identify cancers where $IDH1^{WT}$ inhibition via IDH1i-13 treatment may prove effective in curtailing disease pathogenesis and progression. Utilizing the TCGA database we profiled $IDH1^{WT}$ expression across 33 distinct cancer types (Fig. 24A) Similarly, we determined hazard ratios (HR) for $IDH1^{WT}$ within each of these cancers (Fig. 24B). We hypothesize that cancers in which $IDH1^{WT}$ level is elevated while significantly correlating with decreased patient survival may benefit from IDH1i-13 treatment. Our rationale is that in many of these cancers, elevated levels of $IDH1^{WT}$ may function similarly to IDH-wildtype GBM. One cancer of note for future study is prostate cancer where $IDH1^{WT}$ is elevated and has a statistically significant HR of 8.9 (Fig. 24). Further, we identified that only 6 of the 33 profiled cancers did not have upregulation of $IDH1^{WT}$ or mitochondrial IDH2. Whether $IDH1^{WT}$, IDH2, or the pentose phosphate pathway is upregulated to generate NADPH likely reflects distinct metabolic niches of the cancer stem cells and tumor microenvironment. Collectively, these data indicate IDH1i-13 is a therapeutically viable, $IDH1^{WT}$ inhibitor and inducer of ferroptosis in the context of GBM with potential benefit within a wider range of cancers as well.

A.

Cancer	Regulation in Tumor	Significant?
ACC	Down	Y
BLCA	ND	N
BRCA	ND	N
CESC	Up	N
CHOL	Down	N
COAD	Up	Y
DLBC	Up	Y
ESCA	ND	N
GBM	Up	Y
HNSC	ND	N
KICH	Down	Y
KIRC	ND	N
KIRP	Down	N
LAML	Down	N
LGG	Up	Y
LIHC	Up	N
LUAD	Up	N
LUSC	Up	N
MESO	No Data	No Data
OV	ND	N
PAAD	Up	Y
PCPG	Down	Y
PRAD	Up	Y
READ	Up	Y
SARC	Down	N
SKCM	Up	Y
STAD	Up	Y
TGCT	Up	N
THCA	Up	N
THYM	Up	Y
UCEC	Up	Y
UCS	Up	N
UVM	No Data	No Data

B.

Cancer	Median HR	Median p(HR)	Quartile HR	Quartile p(HR)
ACC	3.5	0.0049	6.5	0.016
BLCA	0.08	0.13	0.66	0.062
BRCA	1.2	0.025	1	0.99
CESC	1.3	0.23	1.3	0.42
CHOL	1.1	0.78	1.4	0.66
COAD	0.75	0.23	0.7	0.31
DLBC	1.1	0.89	2.5	0.3
ESCA	1.1	0.68	0.97	0.92
GBM	1.5	0.029	1.3	0.34
HNSC	1.2	0.17	1.4	0.12
KICH	9.1	0.037	2.20E+09	1
KIRC	0.89	0.45	0.99	0.95
KIRP	1.5	0.2	2.4	0.046
LAML	1.3	0.41	2	0.11
LGG	1.7	0.0066	1.9	0.013
LIHC	1.3	0.17	1.7	0.025
LUAD	1.3	0.14	1.4	0.11
LUSC	0.9	0.43	1.2	0.34
MESO	0.67	0.11	0.74	0.37
OV	1.2	0.24	1	0.94
PAAD	1.1	0.51	1.6	0.16
PCPG	0.5	0.42	0.9	0.92
PRAD	1.7	0.43	8.9	0.048
READ	0.58	0.27	0.61	0.43
SARC	0.84	0.38	0.88	0.67
SKCM	1.2	0.21	1.1	0.57
STAD	1.1	0.66	0.81	0.35
TGCT	2.1	0.53	p.5E+08	1
THCA	1.6	0.36	2.9	0.2
THYM	3.2	0.15	4.2	0.2
UCEC	1	0.92	0.5	0.21
UCS	1.3	0.39	1	0.91
UVM	1.5	0.36	1.6	0.49

Figure 24. IDH1 dysregulation is a frequent event across all cancers.
(**A**) TCGA analysis of IDH1^{WT} mRNA expression within indicated cancers relative to GTEX derived transcript level within physiologically normal tissue. (**B**) TCGA Kaplan-Meier survival analysis of 50% of patients with most heightened IDH1^{WT} transcript levels (median) and 25% of patients with most heightened IDH1^{WT} transcript levels (quartile). ACC= adrenocortical carcinoma; BLCA= bladder urothelial carcinoma; BRCA= breast invasive carcinoma; CESC= cervical squamous cell carcinoma and endocervical adenocarcinoma; CHOL= cholangiocarcinoma; COAD= colon adenocarcinoma; DLBC= lymphoid neoplasm diffuse large B-cell lymphoma; ESCA= esophageal carcinoma; GBM= glioblastoma multiforme; HNSC= head and neck squamous cell carcinoma; KICH= kidney chromophobe; KIRC= kidney renal cell carcinoma; KIRP= kidney renal papillary cell carcinoma; LAML= acute myeloid leukemia; LGG= brain lower grade glioma; LIHC= liver hepatocellular carcinoma; LUAD= lung adenocarcinoma; LUSC= lung squamous cell carcinoma; MESO= mesothelioma; OV= ovarian serous cystadenocarcinoma; PAAD= pancreatic adenocarcinoma; PCPG= pheochromocytoma and paraganglioma; PRAD= prostate adenocarcinoma; READ= rectum adenocarcinoma; SARC= sarcoma; SKCM= skin cutaneous melanoma; STAD= stomach adenocarcinoma; TGCT= testicular

germ cell tumors; THCA= thyroid carcinoma; THYM= thymoma; UCEC= uterine corpus endometrial carcinoma; UCS= uterine carcinosarcoma; UVM= uveal melanoma; highlighted yellow denotes $p < 0.05$.

4.3 Discussion

We have discovered a hitherto unknown role for $IDH1^{WT}$ in protecting cancer cells from ferroptotic cellular death. On a molecular level, upregulation of $IDH1^{WT}$ by glioma cells provides NADPH, a critical reductant necessary for the biosynthesis and replenishment of the potent antioxidant GSH. This elevated level of GSH is maintained by reduction of GSSG in an NADPH dependent manner by GSR. As a result of elevated and sustained levels of GSH, enzymatic activity of lipid peroxidase GPX4 is heightened, resulting in decreased levels of ROS and lipid peroxidation thus protecting GBM tumor cells from ferroptotic death. Depletion of $IDH1^{WT}$ enhances ferroptosis induction in response to GPX4 inhibition and RT. This reliance on elevated $IDH1^{WT}$ enzymatic activity to neutralize ROS species provides a unique metabolic vulnerability. As $IDH1^{WT}$ is dispensable within normal tissue (*122*) and its upregulation in the context of IDH-wildtype GBM is critical for disease pathogenesis and progression (*33, 124*), therapeutic modalities targeting $IDH1^{WT}$ could prove highly efficacious. To this end, our group sought out to identify novel drug candidates capable of inhibiting $IDH1^{WT}$ enzymatic function. We have characterized a small molecule inhibitor, IDH1i-13, capable of potently and specifically inhibiting $IDH1^{WT}$ function. We have further shown this molecule induces ferroptosis in glioma cells *in vitro* while decreasing orthotopic xenograft tumor burden *in vivo*. As an adjuvant therapy to RT, this decrease in tumor burden potentiates a substantial survival benefit in tumor bearing mice.

As a recently identified form of regulated cell death our understanding of ferroptosis in the context of cancer is relatively nascent. Nevertheless, ferroptosis regulation is tightly interwoven with cancer cell dynamics due to elevated cancer cell metabolism which leads to heightened oxidative stress. To combat this oxidative stress and potential ferroptotic death, cancer cells require elevated levels of iron to support antioxidant defense (*215*). Similarly, many cancer cells upregulate known genes within the cysteine/GSH/GPX4 axis such as System x_c- component SLC7A11 (*216*). Thus, cancer cells may present with a ferroptotic vulnerability while simultaneously presenting an avenue for targeting apoptosis-resistant persister cells (*217*). Here, we show $IDH1^{WT}$ inhibition promotes ferroptotic death. Mechanistically, $IDH1^{WT}$ production of NADPH provides essential reducing equivalents necessary for the synthesis of GSH. Similarly, $IDH1^{WT}$ production of αKG contributes directly towards GSH synthesis. Upon transamination to glutamate, αKG directly provides a carbon source for the synthesis of GSH independent of NADPH. As IDH-wildtype GBMs are characterized by high secretion of glutamate into the extracellular environment (*218, 219*), we hypothesize that $IDH1^{WT}$ mediated production of glutamate enhances the import of cystine necessary for GSH production via cystine/glutamate antiporter activity.

Whereas several inhibitors targeting IDH-mutant GBM defining $IDH1^{R132H}$ exist, IDH1i-13 is poised as a brain penetrant, first-in-class, therapeutically viable $IDH1^{WT}$ inhibitor. The majority of $IDH1^{Mut}$ inhibitors, including those developed by Bayer, Novartis, Agios and GSK, function via allosteric inhibition, neither directly competing with NADPH for binding pocket access nor engaging the enzyme's active center at Arg^{132} (*74*). While IDH^{Mut} inhibitors have shown high potency in diminishing oncometabolite (R)-2HG, this often comes at the expense of decreased

specificity as evidenced by many compounds showing 'off-target' effects against $IDH1^{WT}$ at higher concentrations (*74*). Unfortunately, studies utilizing the IDH^{R132} allosteric inhibitor GSK864 to target $IDH1^{WT}$ in the context of GBM showed modest results relative to transcriptional reduction and genetic inactivation approaches (*33*). By forming a covalent bond with H315, IDH1i13 actively inhibits NADPH from engaging with the enzymatic binding pocket, resulting in robust inhibition of and specificity towards $IDH1^{WT}$ enzymatic activity. As a treatment modality for GBMs, IDH1i-13 is blood-brain barrier penetrant (*124*) and exhibits no pathological toxicity within neighboring brain tissue.

Whether $IDH1^{WT}$ inhibition suppresses grade IV IDH-mutant astrocytoma pathogenesis is presently unknown. We theorize, however, that IDH1i-13 would prove effective at curbing disease progression in the context of grade IV IDH-mutant astrocytoma. In nearly all instances, IDH1 mutation in cancer (including glioma) is heterozygous with retention of the wild-type allele (*76*). In the context of grade IV IDH-mutant astrocytoma, $IDH1^{R132}$ production of (R)-2HG is αKG substrate dependent. The presence of grade IV IDH-mutant astrocytoma within the frontal lobe suggests that heightened glutamate during frontal lobe development provides a glutamine rich environment, resulting in excess glutamate and derivative αKG necessary for neomorphic activity (*25, 26, 220*). Similarly, IDH^{WT}- containing dimers contribute to the local production of αKG and as such IDH^{R132} neomorphic activity is dependent on IDH^{WT} expression (*128*). We theorize, then, that inhibition of $IDH1^{WT}$ via IDH1i13 would prove efficacious in depleting αKG production and subsequent deleterious (R)-2HG generation. We further speculate the efficacy of IDH1i-13 in

grade IV IDH-mutant astrocytoma would be magnified significantly via concomitant treatment with a glutaminase inhibitor.

Despite an increasing body of literature supporting critical roles for NADPH and αKG in sustaining elevated cancer cell metabolic needs, the role of $IDH1^{WT}$ in cancer cell biology is an emerging field of study. Our TCGA and GTEX analysis has identified 11 cancers whereby $IDH1^{WT}$ transcript expression is significantly elevated in tumor tissue. We have further identified cancers in which $IDH1^{WT}$ expression significantly correlates with overall patient survival. We speculate that $IDH1^{WT}$ upregulation is a mechanism whereby cancer cells enhance production of metabolites critical for lipid biosynthesis, redox defense, and epigenetic remodeling. Importantly, inhibition of $IDH1^{WT}$ increases ROS levels and subsequent lipid peroxidation, thus sensitizing tumor cells to RT which is standard of care for many cancers. As proof of concept, our group has shown genetic inactivation of $IDH1^{WT}$ results in reduced B-cell lymphoma tumor progression *in vivo* (*33*). To this end, we believe $IDH1^{WT}$ inhibition via IDH1i-13 is a generalizable therapeutic modality across a diverse spectrum of cancers characterized by $IDH1^{WT}$ dysregulation.

REFERENCES

1. C. McKinnon, M. Nandhabalan, S. A. Murray, P. Plaha, Glioblastoma: clinical presentation, diagnosis, and management. *BMJ* **374**, n1560 (2021).
2. A. C. Tan *et al*., Management of glioblastoma: State of the art and future directions. *CA Cancer J Clin* **70**, 299-312 (2020).
3. A. Olar, K. D. Aldape, Using the molecular classification of glioblastoma to inform personalized treatment. *J Pathol* **232**, 165-177 (2014).
4. B. Campos, L. R. Olsen, T. Urup, H. S. Poulsen, A comprehensive profile of recurrent glioblastoma. *Oncogene* **35**, 5819-5825 (2016).
5. Q. T. Ostrom *et al*., CBTRUS Statistical Report: Primary Brain and Other Central Nervous System Tumors Diagnosed in the United States in 2011-2015. *Neuro Oncol* **20**, iv1-iv86 (2018).
6. H. Yan *et al*., IDH1 and IDH2 mutations in gliomas. *N Engl J Med* **360**, 765-773 (2009).
7. D. N. Louis *et al*., cIMPACT-NOW update 6: new entity and diagnostic principle recommendations of the cIMPACT-Utrecht meeting on future CNS tumor classification and grading. *Brain Pathol* **30**, 844-856 (2020).
8. A. Behin, K. Hoang-Xuan, A. F. Carpentier, J. Y. Delattre, Primary brain tumours in adults. *Lancet* **361**, 323-331 (2003).
9. B. Oronsky, T. R. Reid, A. Oronsky, N. Sandhu, S. J. Knox, A Review of Newly Diagnosed Glioblastoma. *Front Oncol* **10**, 574012 (2020).

10. R. Stupp *et al*., Radiotherapy plus concomitant and adjuvant temozolomide for glioblastoma. *N Engl J Med* **352**, 987-996 (2005).

11. D. N. Louis *et al*., The 2016 World Health Organization Classification of Tumors of the Central Nervous System: a summary. *Acta Neuropathol* **131**, 803-820 (2016).

12. M. Weller *et al*., EANO guidelines on the diagnosis and treatment of diffuse gliomas of adulthood. *Nat Rev Clin Oncol* **18**, 170-186 (2021).

13. M. E. Hegi *et al*., MGMT gene silencing and benefit from temozolomide in glioblastoma. *N Engl J Med* **352**, 997-1003 (2005).

14. A. L. Rivera *et al*., MGMT promoter methylation is predictive of response to radiotherapy and prognostic in the absence of adjuvant alkylating chemotherapy for glioblastoma. *Neuro Oncol* **12**, 116-121 (2010).

15. R. Stupp *et al*., Effects of radiotherapy with concomitant and adjuvant temozolomide versus radiotherapy alone on survival in glioblastoma in a randomised phase III study: 5-year analysis of the EORTC-NCIC trial. *Lancet Oncol* **10**, 459-466 (2009).

16. L. S. Bjorland, O. Fluge, B. Gilje, R. Mahesparan, E. Farbu, Treatment approach and survival from glioblastoma: results from a population-based retrospective cohort study from Western Norway. *BMJ Open* **11**, e043208 (2021).

17. T. R. Jue, K. L. McDonald, The challenges associated with molecular targeted therapies for glioblastoma. *J Neurooncol* **127**, 427-434 (2016).

18. R. Liu, M. Page, K. Solheim, S. Fox, S. M. Chang, Quality of life in adults with brain tumors: current knowledge and future directions. *Neuro Oncol* **11**, 330-339 (2009).

19. H. Ohgaki, P. Kleihues, Epidemiology and etiology of gliomas. *Acta Neuropathol* **109**, 93-108 (2005).

20. H. Ohgaki, P. Kleihues, The definition of primary and secondary glioblastoma. *Clin Cancer Res* **19**, 764-772 (2013).

21. T. F. Cloughesy, W. K. Cavenee, P. S. Mischel, Glioblastoma: from molecular pathology to targeted treatment. *Annu Rev Pathol* **9**, 1-25 (2014).

22. D. W. Parsons *et al*., An integrated genomic analysis of human glioblastoma multiforme. *Science* **321**, 1807-1812 (2008).

23. Q. Wang *et al*., Tumor Evolution of Glioma-Intrinsic Gene Expression Subtypes Associates with Immunological Changes in the Microenvironment. *Cancer Cell* **33**, 152 (2018).

24. C. W. Brennan *et al*., The somatic genomic landscape of glioblastoma. *Cell* **155**, 462-477 (2013).

25. A. Lai *et al*., Evidence for sequenced molecular evolution of IDH1 mutant glioblastoma from a distinct cell of origin. *J Clin Oncol* **29**, 4482-4490 (2011).

26. S. Sugiarto *et al*., Asymmetry-defective oligodendrocyte progenitors are glioma precursors. *Cancer Cell* **20**, 328-340 (2011).

27. M. L. Suva, I. Tirosh, The Glioma Stem Cell Model in the Era of Single-Cell Genomics. *Cancer Cell* **37**, 630-636 (2020).

28. S. Alcantara Llaguno *et al*., Cell-of-origin susceptibility to glioblastoma formation declines with neural lineage restriction. *Nat Neurosci* **22**, 545-555 (2019).

29. L. Dang *et al*., Cancer-associated IDH1 mutations produce 2-hydroxyglutarate. *Nature* **462**, 739-744 (2009).

30. D. Sturm *et al*., Hotspot mutations in H3F3A and IDH1 define distinct epigenetic and biological subgroups of glioblastoma. *Cancer Cell* **22**, 425-437 (2012).

31. X. Du, H. Hu, The Roles of 2-Hydroxyglutarate. *Front Cell Dev Biol* **9**, 651317 (2021).

32. C. Horbinski, What do we know about IDH1/2 mutations so far, and how do we use it? *Acta Neuropathol* **125**, 621-636 (2013).

33. A. E. Calvert *et al*., Cancer-Associated IDH1 Promotes Growth and Resistance to Targeted Therapies in the Absence of Mutation. *Cell Rep* **19**, 1858-1873 (2017).

34. J. Shi *et al*., An IDH1 mutation inhibits growth of glioma cells via GSH depletion and ROS generation. *Neurol Sci* **35**, 839-845 (2014).

35. R. G. Verhaak *et al*., Integrated genomic analysis identifies clinically relevant subtypes of glioblastoma characterized by abnormalities in PDGFRA, IDH1, EGFR, and NF1. *Cancer Cell* **17**, 98-110 (2010).

36. H. S. Phillips *et al*., Molecular subclasses of high-grade glioma predict prognosis, delineate a pattern of disease progression, and resemble stages in neurogenesis. *Cancer Cell* **9**, 157-173 (2006).

37. E. L. Jackson *et al*., PDGFR alpha-positive B cells are neural stem cells in the adult SVZ that form glioma-like growths in response to increased PDGF signaling. *Neuron* **51**, 187-199 (2006).

38. M. A. Qazi, D. Bakhshinyan, S. K. Singh, Deciphering brain tumor heterogeneity, one cell at a time. *Nat Med* **25**, 1474-1476 (2019).

39. A. P. Patel *et al*., Single-cell RNA-seq highlights intratumoral heterogeneity in primary glioblastoma. *Science* **344**, 1396-1401 (2014).

40. L. Wang *et al*., The Phenotypes of Proliferating Glioblastoma Cells Reside on a Single Axis of Variation. *Cancer Discov* **9**, 1708-1719 (2019).

41. C. Neftel *et al*., An Integrative Model of Cellular States, Plasticity, and Genetics for Glioblastoma. *Cell* **178**, 835-849 e821 (2019).

42. L. B. Wang *et al*., Proteogenomic and metabolomic characterization of human glioblastoma. *Cancer Cell* **39**, 509-528 e520 (2021).

43. N. P. Pringle, W. D. Richardson, A singularity of PDGF alpha-receptor expression in the dorsoventral axis of the neural tube may define the origin of the oligodendrocyte lineage. *Development* **117**, 525-533 (1993).

44. A. R. Calver *et al*., Oligodendrocyte population dynamics and the role of PDGF in vivo. *Neuron* **20**, 869-882 (1998).

45. N. Dahmane, A. Ruiz i Altaba, Sonic hedgehog regulates the growth and patterning of the cerebellum. *Development* **126**, 3089-3100 (1999).

46. K. Lai, B. K. Kaspar, F. H. Gage, D. V. Schaffer, Sonic hedgehog regulates adult neural progenitor proliferation in vitro and in vivo. *Nat Neurosci* **6**, 21-27 (2003).

47. I. Imayoshi, M. Sakamoto, M. Yamaguchi, K. Mori, R. Kageyama, Essential roles of Notch signaling in maintenance of neural stem cells in developing and adult brains. *J Neurosci* **30**, 3489-3498 (2010).

48. S. K. Singh *et al*., Identification of a cancer stem cell in human brain tumors. *Cancer Res* **63**, 5821-5828 (2003).

49. J. D. Lathia, S. C. Mack, E. E. Mulkearns-Hubert, C. L. Valentim, J. N. Rich, Cancer stem cells in glioblastoma. *Genes Dev* **29**, 1203-1217 (2015).

50. S. K. Singh *et al*., Identification of human brain tumour initiating cells. *Nature* **432**, 396-401 (2004).

51. L. Ricci-Vitiani *et al*., Tumour vascularization via endothelial differentiation of glioblastoma stem-like cells. *Nature* **468**, 824-828 (2010).

52. S. Bao *et al*., Glioma stem cells promote radioresistance by preferential activation of the DNA damage response. *Nature* **444**, 756-760 (2006).

53. J. Chen *et al*., A restricted cell population propagates glioblastoma growth after chemotherapy. *Nature* **488**, 522-526 (2012).

54. S. G. Piccirillo *et al*., Bone morphogenetic proteins inhibit the tumorigenic potential of human brain tumour-initiating cells. *Nature* **444**, 761-765 (2006).

55. S. H. Stricker *et al*., Widespread resetting of DNA methylation in glioblastoma-initiating cells suppresses malignant cellular behavior in a lineage-dependent manner. *Genes Dev* **27**, 654-669 (2013).

56. M. L. Suva *et al*., Reconstructing and reprogramming the tumor-propagating potential of glioblastoma stem-like cells. *Cell* **157**, 580-594 (2014).

57. M. G. Filbin *et al*., Developmental and oncogenic programs in H3K27M gliomas dissected by single-cell RNA-seq. *Science* **360**, 331-335 (2018).

58. A. Bhaduri *et al*., Outer Radial Glia-like Cancer Stem Cells Contribute to Heterogeneity of Glioblastoma. *Cell Stem Cell* **26**, 48-63 e46 (2020).

59. A. Kriegstein, A. Alvarez-Buylla, The glial nature of embryonic and adult neural stem cells. *Annu Rev Neurosci* **32**, 149-184 (2009).

60. A. A. Pollen *et al*., Molecular identity of human outer radial glia during cortical development. *Cell* **163**, 55-67 (2015).

61. A. Claes, A. J. Idema, P. Wesseling, Diffuse glioma growth: a guerilla war. *Acta Neuropathol* **114**, 443-458 (2007).

62. H. J. Scherer, Structural Development in Gliomas. *The American Journal of Cancer* **34**, 333-351 (1938).

63. M. Westphal, K. Lamszus, The neurobiology of gliomas: from cell biology to the development of therapeutic approaches. *Nat Rev Neurosci* **12**, 495-508 (2011).

64. V. A. Cuddapah, S. Robel, S. Watkins, H. Sontheimer, A neurocentric perspective on glioma invasion. *Nat Rev Neurosci* **15**, 455-465 (2014).

65. A. Hatoum, R. Mohammed, O. Zakieh, The unique invasiveness of glioblastoma and possible drug targets on extracellular matrix. *Cancer Manag Res* **11**, 1843-1855 (2019).

66. D. V. Hansen, J. H. Lui, P. R. Parker, A. R. Kriegstein, Neurogenic radial glia in the outer subventricular zone of human neocortex. *Nature* **464**, 554-561 (2010).

67. J. W. Tsai, K. H. Bremner, R. B. Vallee, Dual subcellular roles for LIS1 and dynein in radial neuronal migration in live brain tissue. *Nat Neurosci* **10**, 970-979 (2007).

68. M. Osswald *et al*., Brain tumour cells interconnect to a functional and resistant network. *Nature* **528**, 93-98 (2015).

69. Y. Shi *et al*., Tumour-associated macrophages secrete pleiotrophin to promote PTPRZ1 signalling in glioblastoma stem cells for tumour growth. *Nat Commun* **8**, 15080 (2017).

70. E. Y. Qin *et al*., Neural Precursor-Derived Pleiotrophin Mediates Subventricular Zone Invasion by Glioma. *Cell* **170**, 845-859 e819 (2017).

71. D. Hanahan, R. A. Weinberg, Hallmarks of cancer: the next generation. *Cell* **144**, 646-674 (2011).

72. F. Yin, J. Yao, R. D. Brinton, E. Cadenas, Editorial: The Metabolic-Inflammatory Axis in Brain Aging and Neurodegeneration. *Front Aging Neurosci* **9**, 209 (2017).

73. M. G. Vander Heiden, R. J. DeBerardinis, Understanding the Intersections between Metabolism and Cancer Biology. *Cell* **168**, 657-669 (2017).

74. S. Tommasini-Ghelfi *et al*., Cancer-associated mutation and beyond: The emerging biology of isocitrate dehydrogenases in human disease. *Sci Adv* **5**, eaaw4543 (2019).

75. O. Warburg, On the origin of cancer cells. *Science* **123**, 309-314 (1956).

76. H. Yang, D. Ye, K. L. Guan, Y. Xiong, IDH1 and IDH2 mutations in tumorigenesis: mechanistic insights and clinical perspectives. *Clin Cancer Res* **18**, 5562-5571 (2012).

77. X. Xu *et al*., Structures of human cytosolic NADP-dependent isocitrate dehydrogenase reveal a novel self-regulatory mechanism of activity. *J Biol Chem* **279**, 33946-33957 (2004).

78. Y. Xu *et al*., Studies on the regulatory mechanism of isocitrate dehydrogenase 2 using acetylation mimics. *Sci Rep* **7**, 9785 (2017).

79. K. P. Bzymek, R. F. Colman, Role of alpha-Asp181, beta-Asp192, and gamma-Asp190 in the distinctive subunits of human NAD-specific isocitrate dehydrogenase. *Biochemistry* **46**, 5391-5397 (2007).

80. K. Smolkova, P. Jezek, The Role of Mitochondrial NADPH-Dependent Isocitrate Dehydrogenase in Cancer Cells. *Int J Cell Biol* **2012**, 273947 (2012).

81. L. Tretter, V. Adam-Vizi, Alpha-ketoglutarate dehydrogenase: a target and generator of oxidative stress. *Philos Trans R Soc Lond B Biol Sci* **360**, 2335-2345 (2005).

82. F. V. Filipp, D. A. Scott, Z. A. Ronai, A. L. Osterman, J. W. Smith, Reverse TCA cycle flux through isocitrate dehydrogenases 1 and 2 is required for lipogenesis in hypoxic melanoma cells. *Pigment Cell Melanoma Res* **25**, 375-383 (2012).

83. B. Keith, M. C. Simon, Hypoxia Inducible Factors, stem cells and cancer. *Cell*, (2007).

84. F. J. Gonzalez, C. Xie, C. Jiang, The role of hypoxia-inducible factors in metabolic diseases. *Nat Rev Endocrinol*, (2018).

85. P. Büchler *et al*., Hypoxia-Inducible Factor 1 Regulates Vascular Endothelial Growth Factor Expression in Human Pancreatic Cancer. *Pancreas*, (2003).

86. A. Palazon, A. W. Goldrath, V. Nizet, R. S. Johnson, HIF transcription factors, inflammation, and immunity. *Immunity* **41**, 518-528 (2014).

87. G. Joberty *et al*., Interrogating the Druggability of the 2-Oxoglutarate-Dependent Dioxygenase Target Class by Chemical Proteomics. *ACS Chem Biol* **11**, 2002-2010 (2016).

88. B. A. Sullivan, G. H. Karpen, Centromeric chromatin exhibits a histone modification pattern that is distinct from both euchromatin and heterochromatin. *Nat Struct Mol Biol* **11**, 1076-1083 (2004).

89. L. J. Walport *et al*., Arginine demethylation is catalysed by a subset of JmjC histone lysine demethylases. *Nat Commun* **7**, 11974 (2016).

90. Y. Tsukada *et al*., Histone demethylation by a family of JmjC domain-containing proteins. *Nature* **439**, 811-816 (2006).

91. J. C. Peng *et al*., Jarid2/Jumonji coordinates control of PRC2 enzymatic activity and target gene occupancy in pluripotent cells. *Cell* **139**, 1290-1302 (2009).

92. B. W. Carey, L. W. Finley, J. R. Cross, C. D. Allis, C. B. Thompson, Intracellular alpha-ketoglutarate maintains the pluripotency of embryonic stem cells. *Nature* **518**, 413-416 (2015).

93. C. Lu *et al*., IDH mutation impairs histone demethylation and results in a block to cell differentiation. *Nature* **483**, 474-478 (2012).

94. P. S. Ward *et al*., The common feature of leukemia-associated IDH1 and IDH2 mutations is a neomorphic enzyme activity converting alpha-ketoglutarate to 2-hydroxyglutarate. *Cancer Cell* **17**, 225-234 (2010).

95. L. D. Moore, T. Le, G. Fan, DNA methylation and its basic function. *Neuropsychopharmacology* **38**, 23-38 (2013).

96. J. Yang, N. Bashkenova, R. Zang, X. Huang, J. Wang, The roles of TET family proteins in development and stem cells. *Development* **147**, (2020).

97. P. Melamed, Y. Yosefzon, C. David, A. Tsukerman, L. Pnueli, Tet Enzymes, Variants, and Differential Effects on Function. *Front Cell Dev Biol* **6**, 22 (2018).

98. K. P. Koh *et al*., Tet1 and Tet2 regulate 5-hydroxymethylcytosine production and cell lineage specification in mouse embryonic stem cells. *Cell Stem Cell* **8**, 200-213 (2011).

99. K. Moran-Crusio *et al*., Tet2 loss leads to increased hematopoietic stem cell self-renewal and myeloid transformation. *Cancer Cell* **20**, 11-24 (2011).

100. T. TeSlaa *et al*., alpha-Ketoglutarate Accelerates the Initial Differentiation of Primed Human Pluripotent Stem Cells. *Cell Metab* **24**, 485-493 (2016).

101. I. Y. Hwang *et al*., Psat1-Dependent Fluctuations in alpha-Ketoglutarate Affect the Timing of ESC Differentiation. *Cell Metab* **24**, 494-501 (2016).

102. M. E. Figueroa *et al*., Leukemic IDH1 and IDH2 mutations result in a hypermethylation phenotype, disrupt TET2 function, and impair hematopoietic differentiation. *Cancer Cell* **18**, 553-567 (2010).

103. W. Xu *et al*., Oncometabolite 2-hydroxyglutarate is a competitive inhibitor of alpha-ketoglutarate-dependent dioxygenases. *Cancer Cell* **19**, 17-30 (2011).

104. M. F. Amary *et al*., Ollier disease and Maffucci syndrome are caused by somatic mosaic mutations of IDH1 and IDH2. *Nat Genet* **43**, 1262-1265 (2011).

105. T. R. Hall, R. Wallin, G. D. Reinhart, S. M. Hutson, Branched chain aminotransferase isoenzymes. Purification and characterization of the rat brain isoenzyme. *J Biol Chem* **268**, 3092-3098 (1993).

106. B. J. Altman, Z. E. Stine, C. V. Dang, From Krebs to clinic: glutamine metabolism to cancer therapy. *Nat Rev Cancer* **16**, 749 (2016).

107. Y. Chen, H. G. Shertzer, S. N. Schneider, D. W. Nebert, T. P. Dalton, Glutamate cysteine ligase catalysis: dependence on ATP and modifier subunit for regulation of tissue glutathione levels. *J Biol Chem* **280**, 33766-33774 (2005).

108. S. Bannai, Exchange of cystine and glutamate across plasma membrane of human fibroblasts. *J Biol Chem* **261**, 2256-2263 (1986).

109. X. Jiang, B. R. Stockwell, M. Conrad, Ferroptosis: mechanisms, biology and role in disease. *Nat Rev Mol Cell Biol* **22**, 266-282 (2021).

110. T. Takano *et al*., Glutamate release promotes growth of malignant gliomas. *Nat Med* **7**, 1010-1015 (2001).

111. S. Ishiuchi *et al*., Blockage of Ca(2+)-permeable AMPA receptors suppresses migration and induces apoptosis in human glioblastoma cells. *Nat Med* **8**, 971-978 (2002).

112. H. S. Venkatesh *et al*., Electrical and synaptic integration of glioma into neural circuits. *Nature* **573**, 539-545 (2019).

113. V. Venkataramani *et al*., Glutamatergic synaptic input to glioma cells drives brain tumour progression. *Nature* **573**, 532-538 (2019).

114. S. A. Lyons, W. J. Chung, A. K. Weaver, T. Ogunrinu, H. Sontheimer, Autocrine glutamate signaling promotes glioma cell invasion. *Cancer Res* **67**, 9463-9471 (2007).

115. M. Tonjes *et al*., BCAT1 promotes cell proliferation through amino acid catabolism in gliomas carrying wild-type IDH1. *Nat Med* **19**, 901-908 (2013).

116. G. Carta, E. Murru, S. Banni, C. Manca, Palmitic Acid: Physiological Role, Metabolism and Nutritional Implications. *Front Physiol* **8**, 902 (2017).

117. H. G. Enoch, A. Catala, P. Strittmatter, Mechanism of rat liver microsomal stearyl-CoA desaturase. Studies of the substrate specificity, enzyme-substrate interactions, and the function of lipid. *J Biol Chem* **251**, 5095-5103 (1976).

118. N. Koundouros, G. Poulogiannis, Reprogramming of fatty acid metabolism in cancer. *Br J Cancer* **122**, 4-22 (2020).

119. T. Matsuzaka *et al*., Crucial role of a long-chain fatty acid elongase, Elovl6, in obesity-induced insulin resistance. *Nat Med* **13**, 1193-1202 (2007).

120. H. J. Koh *et al*., Cytosolic NADP+-dependent isocitrate dehydrogenase plays a key role in lipid metabolism. *J Biol Chem* **279**, 39968-39974 (2004).

121. B. Chu, T. Wu, L. Miao, Y. Mei, M. Wu, MiR-181a regulates lipid metabolism via IDH1. *Sci Rep* **5**, 8801 (2015).

122. M. Itsumi *et al*., Idh1 protects murine hepatocytes from endotoxin-induced oxidative stress by regulating the intracellular NADP(+)/NADPH ratio. *Cell Death Differ* **22**, 1837-1845 (2015).

123. S. M. Lee *et al*., Cytosolic NADP(+)-dependent isocitrate dehydrogenase status modulates oxidative damage to cells. *Free Radic Biol Med* **32**, 1185-1196 (2002).

124. C. Chung *et al*., Integrated Metabolic and Epigenomic Reprograming by H3K27M Mutations in Diffuse Intrinsic Pontine Gliomas. *Cancer Cell* **38**, 334-349 e339 (2020).

125. K. Gonthier, R. T. K. Poluri, C. Weidmann, M. Tadros, E. Audet-Walsh, Reprogramming of Isocitrate Dehydrogenases Expression and Activity by the Androgen Receptor in Prostate Cancer. *Mol Cancer Res* **17**, 1699-1709 (2019).

126. J. Li *et al*., Wild-type IDH2 promotes the Warburg effect and tumor growth through HIF1alpha in lung cancer. *Theranostics* **8**, 4050-4061 (2018).

127. T. Watanabe, S. Nobusawa, P. Kleihues, H. Ohgaki, IDH1 mutations are early events in the development of astrocytomas and oligodendrogliomas. *Am J Pathol* **174**, 1149-1153 (2009).

128. P. S. Ward *et al*., The potential for isocitrate dehydrogenase mutations to produce 2-hydroxyglutarate depends on allele specificity and subcellular compartmentalization. *J Biol Chem* **288**, 3804-3815 (2013).

129. M. Sasaki *et al*., D-2-hydroxyglutarate produced by mutant IDH1 perturbs collagen maturation and basement membrane function. *Genes Dev* **26**, 2038-2049 (2012).

130. C. Bardella *et al*., Expression of Idh1(R132H) in the Murine Subventricular Zone Stem Cell Niche Recapitulates Features of Early Gliomagenesis. *Cancer Cell* **30**, 578-594 (2016).

131. A. S. Modrek *et al*., Low-Grade Astrocytoma Mutations in IDH1, P53, and ATRX Cooperate to Block Differentiation of Human Neural Stem Cells via Repression of SOX2. *Cell Rep* **21**, 1267-1280 (2017).

132. B. Philip *et al*., Mutant IDH1 Promotes Glioma Formation In Vivo. *Cell Rep* **23**, 1553-1564 (2018).

133. A. Linninger *et al*., Modeling the diffusion of D-2-hydroxyglutarate from IDH1 mutant gliomas in the central nervous system. *Neuro Oncol* **20**, 1197-1206 (2018).

134. D. Ye, K. L. Guan, Y. Xiong, Metabolism, Activity, and Targeting of D- and L-2-Hydroxyglutarates. *Trends Cancer* **4**, 151-165 (2018).

135. J. A. Losman, W. G. Kaelin, Jr., What a difference a hydroxyl makes: mutant IDH, (R)-2-hydroxyglutarate, and cancer. *Genes Dev* **27**, 836-852 (2013).

136. W. A. Flavahan *et al*., Insulator dysfunction and oncogene activation in IDH mutant gliomas. *Nature* **529**, 110-114 (2016).

137. P. Wang *et al*., Oncometabolite D-2-Hydroxyglutarate Inhibits ALKBH DNA Repair Enzymes and Sensitizes IDH Mutant Cells to Alkylating Agents. *Cell Rep* **13**, 2353-2361 (2015).

138. S. K. McBrayer *et al*., Transaminase Inhibition by 2-Hydroxyglutarate Impairs Glutamate Biosynthesis and Redox Homeostasis in Glioma. *Cell* **175**, 101-116 e125 (2018).

139. D. R. Wahl *et al*., Glioblastoma Therapy Can Be Augmented by Targeting IDH1-Mediated NADPH Biosynthesis. *Cancer Res* **77**, 960-970 (2017).

140. S. J. Dixon *et al*., Ferroptosis: an iron-dependent form of nonapoptotic cell death. *Cell* **149**, 1060-1072 (2012).

141. N. Yagoda *et al*., RAS-RAF-MEK-dependent oxidative cell death involving voltage-dependent anion channels. *Nature* **447**, 864-868 (2007).

142. J. Li *et al*., Ferroptosis: past, present and future. *Cell Death Dis* **11**, 88 (2020).

143. A. M. Distefano *et al*., Heat stress induces ferroptosis-like cell death in plants. *J Cell Biol* **216**, 463-476 (2017).

144. M. Bogacz, R. L. Krauth-Siegel, Tryparedoxin peroxidase-deficiency commits trypanosomes to ferroptosis-type cell death. *Elife* **7**, (2018).

145. T. Hirschhorn, B. R. Stockwell, The development of the concept of ferroptosis. *Free Radic Biol Med* **133**, 130-143 (2019).

146. H. Eagle, Nutrition needs of mammalian cells in tissue culture. *Science* **122**, 501-514 (1955).

147. T. H. Murphy, A. T. Malouf, A. Sastre, R. L. Schnaar, J. T. Coyle, Calcium-dependent glutamate cytotoxicity in a neuronal cell line. *Brain Res* **444**, 325-332 (1988).

148. T. H. Murphy, M. Miyamoto, A. Sastre, R. L. Schnaar, J. T. Coyle, Glutamate toxicity in a neuronal cell line involves inhibition of cystine transport leading to oxidative stress. *Neuron* **2**, 1547-1558 (1989).

149. T. H. Murphy, R. L. Schnaar, J. T. Coyle, Immature cortical neurons are uniquely sensitive to glutamate toxicity by inhibition of cystine uptake. *FASEB J* **4**, 1624-1633 (1990).

150. S. Dolma, S. L. Lessnick, W. C. Hahn, B. R. Stockwell, Identification of genotype-selective antitumor agents using synthetic lethal chemical screening in engineered human tumor cells. *Cancer Cell* **3**, 285-296 (2003).

151. S. J. Dixon *et al*., Pharmacological inhibition of cystine-glutamate exchange induces endoplasmic reticulum stress and ferroptosis. *Elife* **3**, e02523 (2014).

152. W. S. Yang *et al*., Regulation of ferroptotic cancer cell death by GPX4. *Cell* **156**, 317-331 (2014).

153. N. A. Porter, S. E. Caldwell, K. A. Mills, Mechanisms of free radical oxidation of unsaturated lipids. *Lipids* **30**, 277-290 (1995).

154. D. B. Zorov, M. Juhaszova, S. J. Sollott, Mitochondrial reactive oxygen species (ROS) and ROS-induced ROS release. *Physiol Rev* **94**, 909-950 (2014).

155. Y. Zou *et al*., Cytochrome P450 oxidoreductase contributes to phospholipid peroxidation in ferroptosis. *Nat Chem Biol* **16**, 302-309 (2020).

156. M. K. Ghosh, M. Mukhopadhyay, I. B. Chatterjee, NADPH-initiated cytochrome P450-dependent free iron-independent microsomal lipid peroxidation: specific prevention by ascorbic acid. *Mol Cell Biochem* **166**, 35-44 (1997).

157. A. Seiler *et al*., Glutathione peroxidase 4 senses and translates oxidative stress into 12/15-lipoxygenase dependent- and AIF-mediated cell death. *Cell Metab* **8**, 237-248 (2008).

158. H. Kuhn, S. Banthiya, K. van Leyen, Mammalian lipoxygenases and their biological relevance. *Biochim Biophys Acta* **1851**, 308-330 (2015).

159. V. A. N. Kraft *et al*., GTP Cyclohydrolase 1/Tetrahydrobiopterin Counteract Ferroptosis through Lipid Remodeling. *ACS Cent Sci* **6**, 41-53 (2020).

160. G. Powis, W. R. Montfort, Properties and biological activities of thioredoxins. *Annu Rev Pharmacol Toxicol* **41**, 261-295 (2001).

161. D. P. Jones *et al*., Cysteine/cystine couple is a newly recognized node in the circuitry for biologic redox signaling and control. *FASEB J* **18**, 1246-1248 (2004).

162. R. Njalsson, S. Norgren, Physiological and pathological aspects of GSH metabolism. *Acta Paediatr* **94**, 132-137 (2005).

163. M. Maiorino, M. Conrad, F. Ursini, GPx4, Lipid Peroxidation, and Cell Death: Discoveries, Rediscoveries, and Open Issues. *Antioxid Redox Signal* **29**, 61-74 (2018).

164. M. Conrad, D. A. Pratt, The chemical basis of ferroptosis. *Nat Chem Biol* **15**, 1137-1147 (2019).

165. E. K. Pistorius, B. Axelrod, Iron, an essential component of lipoxygenase. *J Biol Chem* **249**, 3183-3186 (1974).

166. W. Hou *et al*., Autophagy promotes ferroptosis by degradation of ferritin. *Autophagy* **12**, 1425-1428 (2016).

167. M. Gao, P. Monian, N. Quadri, R. Ramasamy, X. Jiang, Glutaminolysis and Transferrin Regulate Ferroptosis. *Mol Cell* **59**, 298-308 (2015).

168. C. W. Brown *et al*., Prominin2 Drives Ferroptosis Resistance by Stimulating Iron Export. *Dev Cell* **51**, 575-586 e574 (2019).

169. A. Anandhan, M. Dodson, C. J. Schmidlin, P. Liu, D. D. Zhang, Breakdown of an Ironclad Defense System: The Critical Role of NRF2 in Mediating Ferroptosis. *Cell Chem Biol* **27**, 436-447 (2020).

170. K. Bersuker *et al*., The CoQ oxidoreductase FSP1 acts parallel to GPX4 to inhibit ferroptosis. *Nature* **575**, 688-692 (2019).

171. S. J. Wang *et al*., Acetylation Is Crucial for p53-Mediated Ferroptosis and Tumor Suppression. *Cell Rep* **17**, 366-373 (2016).

172. N. Horikoshi, J. Cong, N. Kley, T. Shenk, Isolation of differentially expressed cDNAs from p53-dependent apoptotic cells: activation of the human homologue of the Drosophila peroxidasin gene. *Biochem Biophys Res Commun* **261**, 864-869 (1999).

173. J. Wu *et al*., Intercellular interaction dictates cancer cell ferroptosis via NF2-YAP signalling. *Nature* **572**, 402-406 (2019).

174. L. Magtanong *et al*., Exogenous Monounsaturated Fatty Acids Promote a Ferroptosis-Resistant Cell State. *Cell Chem Biol* **26**, 420-432 e429 (2019).

175. V. S. Viswanathan *et al*., Dependency of a therapy-resistant state of cancer cells on a lipid peroxidase pathway. *Nature* **547**, 453-457 (2017).

176. B. Spangler *et al*., A reactivity-based probe of the intracellular labile ferrous iron pool. *Nat Chem Biol* **12**, 680-685 (2016).

177. C. G. Hansen, T. Moroishi, K. L. Guan, YAP and TAZ: a nexus for Hippo signaling and beyond. *Trends Cell Biol* **25**, 499-513 (2015).

178. H. F. Yan *et al*., Ferroptosis: mechanisms and links with diseases. *Signal Transduct Target Ther* **6**, 49 (2021).

179. S. Agrawal, J. Fox, B. Thyagarajan, J. H. Fox, Brain mitochondrial iron accumulates in Huntington's disease, mediates mitochondrial dysfunction, and can be removed pharmacologically. *Free Radic Biol Med* **120**, 317-329 (2018).

180. A. B. Chaves-Filho *et al*., Alterations in lipid metabolism of spinal cord linked to amyotrophic lateral sclerosis. *Sci Rep* **9**, 11642 (2019).

181. Y. Chen *et al*., Quantitative Profiling of Protein Carbonylations in Ferroptosis by an Aniline-Derived Probe. *J Am Chem Soc* **140**, 4712-4720 (2018).

182. W. J. Chung *et al*., Inhibition of cystine uptake disrupts the growth of primary brain tumors. *J Neurosci* **25**, 7101-7110 (2005).

183. H. Sato, K. Fujiwara, J. Sagara, S. Bannai, Induction of cystine transport activity in mouse peritoneal macrophages by bacterial lipopolysaccharide. *Biochem J* **310 (Pt 2)**, 547-551 (1995).

184. L. F. Ye *et al*., Radiation-Induced Lipid Peroxidation Triggers Ferroptosis and Synergizes with Ferroptosis Inducers. *ACS Chem Biol* **15**, 469-484 (2020).

185. Z. Tang *et al*., GEPIA: a web server for cancer and normal gene expression profiling and interactive analyses. *Nucleic Acids Res* **45**, W98-W102 (2017).

186. N. Cancer Genome Atlas Research, Comprehensive genomic characterization defines human glioblastoma genes and core pathways. *Nature* **455**, 1061-1068 (2008).

187. G. T. Consortium, The Genotype-Tissue Expression (GTEx) project. *Nat Genet* **45**, 580-585 (2013).

188. J. Gao *et al*., Integrative analysis of complex cancer genomics and clinical profiles using the cBioPortal. *Sci Signal* **6**, pl1 (2013).

189. E. Cerami *et al*., The cBio cancer genomics portal: an open platform for exploring multidimensional cancer genomics data. *Cancer Discov* **2**, 401-404 (2012).

190. H. Mi *et al*., PANTHER version 16: a revised family classification, tree-based classification tool, enhancer regions and extensive API. *Nucleic Acids Res* **49**, D394-D403 (2021).

191. M. A. Bonaguidi *et al*., LIF and BMP signaling generate separate and discrete types of GFAP-expressing cells. *Development* **132**, 5503-5514 (2005).

192. J. Chen *et al*., BMP-Responsive Protease HtrA1 Is Differentially Expressed in Astrocytes and Regulates Astrocytic Development and Injury Response. *J Neurosci* **38**, 3840-3857 (2018).

193. B. A. Garcia *et al*., Chemical derivatization of histones for facilitated analysis by mass spectrometry. *Nat Protoc* **2**, 933-938 (2007).

194. H. Mi, A. Muruganujan, D. Ebert, X. Huang, P. D. Thomas, PANTHER version 14: more genomes, a new PANTHER GO-slim and improvements in enrichment analysis tools. *Nucleic Acids Res* **47**, D419-D426 (2019).

195. H. M. Berman *et al*., The Protein Data Bank. *Nucleic Acids Res* **28**, 235-242 (2000).

196. S. F. Altschul *et al*., Gapped BLAST and PSI-BLAST: a new generation of protein database search programs. *Nucleic Acids Res* **25**, 3389-3402 (1997).

197. J. Lee *et al*., Tumor stem cells derived from glioblastomas cultured in bFGF and EGF more closely mirror the phenotype and genotype of primary tumors than do serum-cultured cell lines. *Cancer Cell* **9**, 391-403 (2006).

198. E. Bettiol *et al*., Fetal bovine serum enables cardiac differentiation of human embryonic stem cells. *Differentiation* **75**, 669-681 (2007).

199. T. Ozawa *et al*., Most human non-GCIMP glioblastoma subtypes evolve from a common proneural-like precursor glioma. *Cancer Cell* **26**, 288-300 (2014).

200. F. Del Bene, A. M. Wehman, B. A. Link, H. Baier, Regulation of neurogenesis by interkinetic nuclear migration through an apical-basal notch gradient. *Cell* **134**, 1055-1065 (2008).

201. M. Gotz, Y. A. Barde, Radial glial cells defined and major intermediates between embryonic stem cells and CNS neurons. *Neuron* **46**, 369-372 (2005).

202. H. J. Yeh *et al*., PDGF A-chain gene is expressed by mammalian neurons during development and in maturity. *Cell* **64**, 209-216 (1991).

203. H. Noushmehr *et al*., Identification of a CpG island methylator phenotype that defines a distinct subgroup of glioma. *Cancer Cell* **17**, 510-522 (2010).

204. Y. F. He *et al*., Tet-mediated formation of 5-carboxylcytosine and its excision by TDG in mammalian DNA. *Science* **333**, 1303-1307 (2011).

205. C. E. Senner *et al*., TET1 and 5-Hydroxymethylation Preserve the Stem Cell State of Mouse Trophoblast. *Stem Cell Reports* **15**, 1301-1316 (2020).

206. A. S. Venteicher *et al*., Decoupling genetics, lineages, and microenvironment in IDH-mutant gliomas by single-cell RNA-seq. *Science* **355**, (2017).

207. H. Q. Ju, J. F. Lin, T. Tian, D. Xie, R. H. Xu, NADPH homeostasis in cancer: functions, mechanisms and therapeutic implications. *Signal Transduct Target Ther* **5**, 231 (2020).

208. B. R. Stockwell, X. Jiang, W. Gu, Emerging Mechanisms and Disease Relevance of Ferroptosis. *Trends Cell Biol* **30**, 478-490 (2020).

209. B. R. Stockwell, X. Jiang, The Chemistry and Biology of Ferroptosis. *Cell Chem Biol* **27**, 365-375 (2020).

210. F. Ursini, M. Maiorino, Lipid peroxidation and ferroptosis: The role of GSH and GPx4. *Free Radic Biol Med* **152**, 175-185 (2020).

211. D. Kang *et al*., The role of selenium metabolism and selenoproteins in cartilage homeostasis and arthropathies. *Exp Mol Med* **52**, 1198-1208 (2020).

212. X. Lang *et al*., Radiotherapy and Immunotherapy Promote Tumoral Lipid Oxidation and Ferroptosis via Synergistic Repression of SLC7A11. *Cancer Discov* **9**, 1673-1685 (2019).

213. U. C. Okoye-Okafor *et al*., New IDH1 mutant inhibitors for treatment of acute myeloid leukemia. *Nat Chem Biol* **11**, 878-886 (2015).

214. C. G. Jakob *et al*., Novel Modes of Inhibition of Wild-Type Isocitrate Dehydrogenase 1 (IDH1): Direct Covalent Modification of His315. *J Med Chem* **61**, 6647-6657 (2018).

215. S. V. Torti, F. M. Torti, Iron and cancer: more ore to be mined. *Nat Rev Cancer* **13**, 342-355 (2013).

216. M. Rojo de la Vega, E. Chapman, D. D. Zhang, NRF2 and the Hallmarks of Cancer. *Cancer Cell* **34**, 21-43 (2018).

217. M. J. Hangauer *et al*., Drug-tolerant persister cancer cells are vulnerable to GPX4 inhibition. *Nature* **551**, 247-250 (2017).

218. S. C. Buckingham *et al*., Glutamate release by primary brain tumors induces epileptic activity. *Nat Med* **17**, 1269-1274 (2011).

219. Z. C. Ye, H. Sontheimer, Glioma cells release excitotoxic concentrations of glutamate. *Cancer Res* **59**, 4383-4391 (1999).

220. M. J. Seltzer *et al*., Inhibition of glutaminase preferentially slows growth of glioma cells with mutant IDH1. *Cancer Res* **70**, 8981-8987 (2010).

CURRICULUM VITAE

Kevin Murnan

(614) 795-1218 | KevinMurnan2013@u.northwestern.edu

EDUCATION

Northwestern University | Chicago, IL | 2013 – present | GPA 3.82
Ph.D. Candidate in Driskill Graduate Program at Feinberg School of Medicine
NIH T32 Carcinogenesis Training Grant Fellow
Thesis Advisor: Alexander Stegh

The Ohio State University | Columbus, OH | 2007 – 2011
Bachelor of Science in Molecular Genetics
Honors: Biological Science Scholar, Pelotonia Fellow, Dean's List, Cum Laude

EXPERIENCE

Northwestern University, Feinberg School of Medicine | Chicago, IL | 2013 – present
Ph.D. Candidate, Departments of Neurology and Medicine

- Conducted research investigating metabolic mediated mechanisms of glioblastoma multiforme (GBM) initiation, propagation, and progression utilizing immunoblotting, qRT-PCR, IHC/ICC, stem cell culture, genomic analysis and other techniques
- Designed and tested novel drug candidates targeting deleterious IDH1 gene product in GBM patient derived cell lines and recipient xenograft mouse models
- Presented research findings to faculty, peers, academics and non-technical audience
- Prior laboratory work included identifying a protein interactome in degenerating motor neurons and investigating the role of lncRNAs in cerebellar function

The Ohio State University, Comprehensive Cancer Center | Columbus, OH | 2011 – 2013
Research Assistant, Department of Cancer Biology and Genetics

- Researched the role of microvessicles and circulating miRNA in facilitating multiple myeloma pathogenesis and progression
- Investigated biochemical mechanisms of trimeric protein complex formation during mismatch repair

Indian Institute of Science and Education Research (IISER) Pune | Pune, India | 2011
Summer Intern, Laboratory of Chromatin Biology and Epigenetics

- Awarded one of two collaborative international internships between OSU and IISER Pune
- Worked to construct an interactome of nuclear lamina associated with progeria and aging via cloning and tagging

The Ohio State University, Comprehensive Cancer Center | Columbus, OH | 2008 – 2011
Student Research Assistant, Department of Molecular Immunology, Virology, and Medical Genetics

- Investigated the role of DNA repair protein, BLM, in suppression of colorectal cancer tumorigenesis
- Wrote research proposal resulting in Pelotonia fellowship, presentations, and publication
- Managed mouse colony through weaning, breading, maintenance and dissection

PUBLICATIONS

Serena Tommasini-Ghelfi*, **Kevin Murnan***, Fotini M. Kouri, Akanksha S. Mahajan, Jasmine L. May, and Alexander H. Stegh. "Cancer-associated mutation and beyond: The emerging biology of isocitrate dehydrogenases in human disease." *Science advances* 5, no. 5 (2019): eaaw4543.

Dervishi, Ina, Oge Gozutok, **Kevin Murnan**, Mukesh Gautam, Daniel Heller, Eileen Bigio, and P. Hande Ozdinler. "Protein-protein interactions reveal key canonical pathways, upstream regulators, interactome domains, and novel targets in ALS." *Scientific reports* 8, no. 1 (2018): 1-19.

McIlhatton, Michael A., **Kevin Murnan**, Daniel Carson, Gregory P. Boivin, Carlo M. Croce, and Joanna Groden. "Genetic manipulation of homologous recombination in vivo attenuates intestinal tumorigenesis." *Cancer Prevention Research* 8, no. 7 (2015): 650-656.

PRESENTATIONS

Society For Neuro-Oncology Annual Meeting | Boston, MA | Nov 17-21, 2021 (Tentative)

- *Molecular characterization and preclinical development of novel small molecule inhibitor specific for wild-type IDH1 for ferroptosis induction in Glioblastoma*

27th International Symposium on ALS/MND | Dublin, Ireland | December 7-9, 2016

- *Human mutations connect genes to pathways and networks, offering mechanistic insight for selective motor neuron vulnerabilities*

6th Annual Les Turner Symposium on ALS and Neurorepair | Chicago, IL | Nov 7, 2016

- *Human Mutations Help Connect Genes To Pathways And Networks, And Offer A Mechanistic Insight For Selective Motor Neuron Vulnerabilities*

Denman Undergraduate Research Forum | Columbus, OH | May 11, 2011

- *Over-expression of the DNA repair protein BLM decreases tumor number in a mouse model of intestinal tumorigenesis.*

NMS Undergraduate Research Forum | Columbus, OH | April 9, 2011
- *Over-expression of the DNA repair protein BLM in a mouse model of intestinal tumor formation dramatically decreases tumor number.*

National Conference on Undergraduate Research | Ithaca, NY | Mar 30-April 2, 2011
- *Over-expression of the DNA repair protein BLM in a mouse model of intestinal tumor formation dramatically decreases tumor number.*

13th Annual Scientific Meeting | Columbus, OH | Feb 18, 2011
- *DNA repair protein BLM over-expression in a mouse model of intestinal tumor formation dramatically decreases tumor number.*

LEADERSHIP AND TEACHING EXPERIENCES

Northwestern University Brain Awareness Outreach | Chicago, IL | 2013 – Present
- Designed and delivered neuroscience demonstrations at events throughout Chicago including Museum of Science and Industry and Adler Planetarium

Northwestern University Science Club | Chicago, IL | 2015 – 2019
- Mentored 8 middle school students in STEM once a week at the Boys and Girls Club in Chicago's Uptown neighborhood

Driskill Graduate Program Student Council | Chicago, IL | 2014 – 2016
- Represented Ph.D. students in the Driskill Graduate Program at Northwestern University and led research, mentoring, and social initiatives

Student Assisted Mentoring Program (STAMP) | Chicago, IL | 2015 – 2016
- Developed events, presentations and demonstrations fostering communication and mentoring skills
- Served as a mentor for first- and second- year PhD graduate students

Northwestern University Feinberg School of Medicine | Chicago, IL | 2015
- Teaching assistant for *Topics in Drug Discovery* graduate level course

Walter Peyton Seminar Series | Chicago, IL | 2014
- Created and presented neural development lecture for seniors in high school

AWARDS

- **NIH T32 Carcinogenesis Training Grant** (2019-2021) – Full tuition, stipend, discretionary funds for laboratory supplies, travel allowance
- **International Internship, IISER Pune** (2011) – Stipend, travel, research, and housing expenses paid for
- **Pelotonia Fellowship** (2010-2011) – $12,000 stipend
- **OSU College of Arts and Sciences** – One of twelve proposals funded for presentation at the National Conference on Undergraduate Research
- **Cum Laude** (2011)
- **Dean's List** (2007-2011)
- **Trustees Scholarship** (2007-2011)

LABORATORY SKILLS

- Mouse weaning, breeding, tagging, genotyping, dissecting. IP, IV, IM injections. Orthotopic xenograft implantation, *in vivo* imaging, monitoring.
- Cell culture, transfection, transduction, drug treatment. Growth, survival, invasion, migration, differentiation assays. MTS/MTT/SYTOX assays.
- Primary cortical, neural stem cell isolation and culture.
- Cloning, PCR, DNA purification, primer design, antisense-oligonucleotide design.
- Protein purification, SDS-PAGE, Western blot, cryostat sectioning. IHC, ICC, ELISA.
- RNA isolation, RT-qPCR.
- Microvesicle isolation, cellular microvesicle treatment.
- Computational analysis including TCGA analysis, gene ontology analysis.

PROFESSIONAL SKILLS

- Navigate both Microsoft OS and Mac OS
- Proficient in Microsoft Office Suite, Adobe Photoshop, PRISM
- Highly experienced with NCBI databases—PubMed, GeneBank, OMIM, etc.
- Capable of utilizing molecular biology software—BLAST, CLUSTAL, PANTHERdb, IPA, Primer 3, STRING, GEPIA, cBioPortal, etc.
- Highly proficient in data analysis and interpretation, statistical analysis
- Capable of learning new software quickly